

NASA CR-143837

RELATIONSHIPS BETWEEN STRATOSPHERIC CLEAR AIR TURBULENCE AND
SYNOPTIC METEOROLOGICAL PARAMETERS OVER THE WESTERN
UNITED STATES BETWEEN 12-20 KM ALTITUDE


James R. Scoggins, Terry L. Clark, and Norman C. Possiel

Texas A & M University
College Station, Texas 77843

December 1975

Prepared for

NATIONAL AERONAUTICS AND SPACE ADMINISTRATION
Flight Research Center
Edwards, Calif. 93523



**U.S. AIR FORCE
VAFB TECHNICAL LIBRARY**

1. Report No. NASA CR-143837	2. Government Accession No.	3. Recipient's Catalog No.	
4. Title and Subtitle RELATIONSHIPS BETWEEN STRATOSPHERIC CLEAR AIR TURBULENCE AND SYNOPTIC METEOROLOGICAL PARAMETERS OVER THE WESTERN UNITED STATES BETWEEN 12-20 KM ALTITUDE		5. Report Date December 1975	6. Performing Organization Code H-919
		8. Performing Organization Report No.	10. Work Unit No.
7. Author(s) James R. Scoggins, Terry L. Clark, and Norman C. Possiel		11. Contract or Grant No. NGR-44-001-081	13. Type of Report and Period Covered Contractor Report - Final
9. Performing Organization Name and Address Texas A & M University College Station, Texas 77843		14. Sponsoring Agency Code	
		12. Sponsoring Agency Name and Address National Aeronautics and Space Administration Washington, D. C. 20546	
15. Supplementary Notes NASA Technical Monitor: L. J. Ehernberger, NASA Flight Research Center			
16. Abstract <p>Procedures for forecasting clear air turbulence in the stratosphere over the western United States from rawinsonde data are described and results presented. Three approaches were taken to relate meteorological parameters to regions of turbulence and nonturbulence encountered by the XB-70 during 46 flights at altitudes between 12-20 km, viz., empirical probabilities, discriminant function analysis, and mountain-wave theory. Results from these techniques were combined into a procedure to forecast regions of clear air turbulence with an accuracy of 70-80 percent. A computer program was developed to provide an objective forecast directly from the rawinsonde sounding data.</p>			
17. Key Words (Suggested by Author(s)) Stratospheric turbulence Clear air turbulence Mountain waves Discriminant functions Forecasting		18. Distribution Statement Unclassified - Unlimited	
19. Security Classif. (of this report) Unclassified	20. Security Classif. (of this page) Unclassified	21. No. of Pages 161	22. Price*

*For Sale by the National Technical Information Service, Springfield, Virginia 22151

FOREWORD

Because of the length of this report and the extensiveness of the subject matter included, the authors decided to organize it in such a manner that it could be read in part or in total without loss of perspective. The first two chapters and the portion of Chapter III dealing with computational procedures and statistical distributions are common to all which follows. After reading this portion of the report, the reader may continue to the end of Chapter III or read Chapters IV or V independently. Chapters VI and VII would be meaningful only after having read Chapters I through V.

TABLE OF CONTENTS

	Page
ABSTRACT	ii
FOREWORD	iii
TABLE OF CONTENTS	iv
LIST OF TABLES	viii
LIST OF FIGURES	x
SUMMARY	1
CHAPTER I. INTRODUCTION	2
CHAPTER II. BACKGROUND TO PRESENT RESEARCH	4
CHAPTER III. STATISTICS OF METEOROLOGICAL VARIABLES VERSUS CLEAR AIR TURBULENCE (CAT) IN THE STRATOSPHERE	6
A. COMPUTATION OF SYNOPTIC METEOROLOGICAL PARAMETERS	6
B. SPECIFICATION OF TURBULENT AND NON-TURBULENT AREAS FOR EACH FLIGHT	7
C. FREQUENCY DISTRIBUTIONS OF SYNOPTIC METEOROLOGICAL PARAMETERS ASSOCIATED WITH TURBULENT AND NON-TURBULENT AREAS	7
D. RANGE(S) OF SYNOPTIC METEOROLOGICAL PARAMETERS OBTAINED FROM EMPIRICAL FREQUENCY DISTRIBUTIONS ASSOCIATED WITH CAT AND NON-CAT AREAS	8
E. EMPIRICAL AND JOINT PROBABILITIES OF CAT FOR SELECTED RANGES AND LIMITS OF SYNOPTIC METEOROLOGICAL VARIABLES BASED ON FREQUENCY DISTRIBUTIONS	13
F. VERIFICATION OF RESULTS AND A SUGGESTED PROCEDURE FOR FORECASTING CAT	20
CHAPTER IV. FORECASTING CLEAR-AIR TURBULENCE WITHIN SUB- LAYERS OF THE STRATOSPHERE BY DISCRIMINANT FUNCTION ANALYSIS	23

TABLE OF CONTENTS (Continued)

	Page
A. ABSTRACT	23
B. INTRODUCTION	24
1. <u>Statement of the problem</u>	24
2. <u>Objectives</u>	24
C. BACKGROUND TO RESEARCH	25
1. <u>Previous studies</u>	25
2. <u>Theory</u>	28
D. DATA	32
1. <u>Aircraft</u>	32
2. <u>Meteorological</u>	33
E. ANALYSIS OF DATA	34
1. <u>Stratification</u>	34
2. <u>Determination of variables used</u>	34
3. <u>Determination of linear discriminant functions</u>	35
4. <u>Determination of non-linear discriminant functions</u>	36
5. <u>Determination of predictive procedure for turbulence</u>	36
6. <u>Procedure for predicting the intensity of turbulence</u>	37
F. RESULTS	41
G. SUMMARY	48
H. CONCLUSIONS	50
CHAPTER V. THE CURVATURE OF THE WIND PROFILE AS A FACTOR IN THE FORMATION OF CLEAR AIR TURBULENCE	52
A. ABSTRACT	52
B. INTRODUCTION	52
1. <u>Statement of the problem</u>	53
2. <u>Objectives</u>	53

TABLE OF CONTENTS (Continued)

	Page
C. BACKGROUND TO PRESENT RESEARCH	54
1. <u>Theoretical influence of curvature upon mountain waves</u>	54
2. <u>Large-amplitude mountain waves in the stratosphere</u>	55
3. <u>Influence of wave motions upon energy transfer and the generation of turbulence</u>	57
D. DESCRIPTION OF DATA	60
1. <u>Meteorological data</u>	60
2. <u>Aircraft data</u>	60
E. ANALYSIS OF DATA	63
1. <u>Grouping of the turbulence encounters</u>	63
2. <u>The areal distribution of expected mountain waves</u>	64
3. <u>Evaluation of the vertical gradient of curvature</u>	67
F. RESULTS	70
G. SUMMARY AND CONCLUSIONS	74
CHAPTER VI. COMPOSITE CAT FORECASTING PROCEDURE	75
A. INTRODUCTION	75
B. APPROACH	75
1. <u>Method of analysis</u>	75
a. <u>Data input</u>	75
b. <u>Determination of synoptic fields</u>	76
c. <u>Application of the techniques</u>	80
2. <u>Development of the composite CAT forecasting procedure</u>	81
C. VERIFICATION PROCEDURE	84
D. RESULTS	86
CHAPTER VII. SUMMARY AND COMMENTS	92
REFERENCES	94

TABLE OF CONTENTS (Continued)

	Page
APPENDIX A	99
APPENDIX B	116
APPENDIX C	135

LIST OF TABLES

Table		Page
1	Limits of variables at 300 mb within which empirical frequency distributions differ for turbulent (T) and non-turbulent (NT) areas and the percentage of occurrence of turbulent and non-turbulent areas within the specified limits	9
2	Same as Table 1 except for 200 mb	10
3	Same as Table 1 except for 100 mb	11
4	Same as Table 1 except obtained from 100- and 200-mb data	12
5	Empirical probabilities expressed in percent of CAT associated with selected variables and combinations of variables over ranges where frequency distributions differed for CAT and No-CAT encountered by the XB-70 airplane in the stratosphere	14
6	The five discriminant functions selected for each sub-layer	42
7	Verification percentages of the turbulent (T) and non-turbulent (NT) regions for the functions presented in Table 6	45
8	Summary of results obtained by Cox (1973)	47
9	Verification percentages (VP) of the turbulent and non-turbulent regions in the sub-layers of the XB-70 (dependent) and YF-12A (independent) samples for the turbulence forecasting procedure	48
10	The sign of $\Delta(U''/U)$ for the turbulent and non-turbulent regions occurring within and outside of expected mountain-wave areas	71
11	List of parameters required in forecasting procedure	79
12	Critical values that distinguish between CAT and non-CAT for each technique	83
13	Examples of forecasts from various combinations of the three techniques	83
14	Extreme values of the numerical results from the three techniques	84

LIST OF TABLES (Continued)

Table		Page
15	Verification rates of the forecasting procedure for the first sample of 23 flight tracks	87
16	Verification rates of the forecasting procedure for the second sample of 13 flight tracks	88
17	Verification rates of the forecasting procedure for the non-CAT portions of the first sample excluding the non-CAT portions above 18.3 km (60,000 ft)	89
18	Same as Table 17 except for the second sample	90
19	CAT verification rates for the five, 2.1-km (7000-ft) thick sub-layers of the first sample	91

LIST OF FIGURES

Figure		Page
1	Grid used in analyzing data from constant-pressure charts	6
2	An example of the classification of turbulent or non-turbulent areas for a flight made on November 2, 1965	8
3	Analysis of the number of parameters exceeding specified limits for October 16, 1965	21
4	Analysis of the number of parameters exceeding specified limits for January 3, 1966	22
5	Illustration of the stages of breaking gravity waves resulting in the formation of clear-air turbulence	26
6	Illustration of the discrimination of two events by an ideal, linear discriminant function . . .	31
7	Illustration of the discrimination of two events by an ideal, non-linear discriminant function	31
8	Subjective discrimination of the intensities of the turbulence encountered by the XB-70 and YF-12A aircraft within the 16.8-18.9-km (55,000-62,000-ft) sub-layer	39
9	Logarithmic plots of the positive values and the mean values of the five discriminant functions selected for the 18.3-20.4-km (60,000-67,000-ft) sub-layer as a function of the intensity of the turbulence	40
10	Examples of the vertical profiles of the stability and curvature terms that were determined when mountain waves were expected	56
11	Temperature, moisture, and wind distributions with height observed at Winnemucca on Dec. 2, 1965, at 1200 GMT	59
12	The XB-70 flight track and turbulence data of December 2, 1965 (Ehernberger, 1968)	61
13	Rawinsonde stations across the western United States	62

LIST OF FIGURES (Continued)

Figure		Page
14	General areal extent of XB-70 flights	63
15	Turbulent and non-turbulent regions for January 15, 1966	65
16	The major mountain-ridge crests of the western United States	66
17	Procedure for determining the vertical gradient of the curvature term	68
18	XB-70 flight track for March 15, 1966	69
19	XB-70 flight track for March 24, 1966	72
20	XB-70 flight track for April 1, 1966	73
21	The 18 x 18 grid employed for the determination of the fields of the synoptic parameters, and the 11 x 11 grid (denoted by the square) employed for the forecasting procedure	76
22	The weighting system employed in the smoothing process to determine the value at point A	77
23	Results of the three forecasting techniques	82

RELATIONSHIPS BETWEEN STRATOSPHERIC CLEAR AIR
TURBULENCE AND SYNOPTIC METEOROLOGICAL PARAMETERS
OVER THE WESTERN UNITED STATES BETWEEN 12-20 KM ALTITUDE

by

James R. Scoggins¹
Terry L. Clark²
Norman C. Possiel²

SUMMARY

This report presents results of a research project which had as its ultimate objective the development of a forecasting procedure for clear-air turbulence for supersonic aircraft flying over the western United States at altitudes of 12-20 km. Rawinsonde data from National Weather Service stations at 0000 and 1200 GMT, and aircraft turbulence data measured by VGH recorders on 46 flights of the XB-70 and 22 flights of the YF-12A aircraft were used in the analysis. Regions of turbulence and non-turbulence with horizontal lengths of about 200 km were defined along each flight track. This procedure resulted in 94 turbulent and 78 non-turbulent regions for the XB-70 flights, and 22 and 18, respectively, for the YF-12A flights.

Sixty-nine parameters classified as measured, derived, and time rate-of-change were obtained from the rawinsonde data for each turbulent and non-turbulent region defined along each flight track. These parameters were obtained from data at 100, 200, and 300 mb regardless of the flight altitude of the aircraft.

Three approaches were taken to relate the meteorological parameters to regions of turbulence and non-turbulence, *viz*, empirical probabilities, discriminant function analysis, and mountain-wave theory. In each of these approaches it was possible to relate three-fourths or more of the turbulent and non-turbulent regions to meteorological parameters and/or conditions.

Results from the three analysis techniques were combined to develop a forecasting procedure, based on the assumption that the parameters can be forecast, which appears to be valid for about 70-80 percent of the cases considered. This verification rate is no larger than those for the individual analysis techniques; however, it is believed that the confidence level of the combined method exceeds that of the individual methods. The forecasting techniques, which use all three analytical approaches, were computerized and may be used with relative ease to forecast CAT between 12-20 km over the mountainous region of the western United States.

¹ Director, Center for Applied Geosciences, and Professor of Meteorology

² Research Graduate Assistant now employed by Environmental Protection Agency

CHAPTER I. INTRODUCTION

Most measurements of turbulence made by aircraft have been at altitudes below 12 km and at subsonic speeds. Turbulence data were obtained between 1965 and 1967 from the supersonic XB-70 airplane during about 50 flights while cruising at altitudes generally between 12 and 20 km over the western United States. The XB-70 was a large airplane with a flexible structure which was sensitive to turbulence. Much of the data has been discussed by Kordes and Love (1967), and presented by Ehernberger (1968). In addition, data from about 15 flights of the YF-12A airplane also were available for use in this study.

Relatively little is known about the relationships between synoptic meteorological parameters and clear air turbulence (CAT) in the stratosphere, particularly as high as 15-20 km. Some relationships based on meteorological parameters measured by, or derived from, rawinsonde data are examined in this report. The analysis was carried out at the 100-, 200-, and 300-mb levels for all XB-70 flights. These levels encompassed the flight altitudes on most of the days, and on the other days the flight altitudes usually did not exceed the 100-mb level by more than 2 or 3 km.

It was assumed that synoptic meteorological conditions represented by the 100-, 200-, and 300-mb levels would indicate large-scale processes in which stratospheric perturbations were suitable for the formation of CAT occurrence. When CAT forms, it may be advected away from its source region (Moore and Krishnamurti, 1966) into a region where the large-scale conditions are not necessarily favorable for its production or continued existence. In addition, conditions may be more or less favorable for CAT between stations and may change significantly between observation times. Thus, one should not expect a perfect relationship between CAT and local values of atmospheric parameters. Rather, it seems more likely that a greater degree of success could be expected when average synoptic meteorological conditions over an area are associated with CAT observed within the area. In addition, it is known that the intensity of CAT may vary considerably over horizontal distances of a few km and vertical distances of less than 1 km.

The present research differs from much of the previous research in that areas of CAT of any intensity, as well as those without CAT, are associated with the distribution of average values of measured, derived, time rate-of-change of synoptic meteorological quantities, and combinations of these parameters. The approach taken in this research is to define turbulent and non-turbulent areas along each flight track, compute the average values of selected meteorological parameters for each area, then distinguish between CAT and non-CAT conditions by use of empirical probabilities, discriminant function analysis, and mountain-wave theory. Intuitively, it seems that it should be easier to distinguish between areas with CAT and those without CAT than between different degrees of intensity within an area. Also, if a critical range of values of a parameter exists, it should be possible to isolate it from the statistical distributions of the parameters.

The objective of this research was to develop a procedure for forecasting CAT in the stratosphere between 12 and 20 km for large, supersonic airplanes. The approach was to examine relationships between synoptic meteorological parameters and areas of CAT and non-CAT, then use these results to develop the forecasting procedure. This report contains the results and the forecasting procedure as well as major computer programs used in the research. The results suggest that CAT areas can be related to synoptic parameters in 70-80 percent of the cases considered.

CHAPTER II. BACKGROUND TO PRESENT RESEARCH

The large-scale processes associated with CAT may be related directly or indirectly to many parameters obtained from rawinsonde data. Some of these parameters are: vertical and horizontal wind shear, static stability, vertical motion, deformation, various stability indices, Richardson's number, vertical gradient of kinetic energy, and vorticity (Scorer, 1969; Badgley, 1969; Lumley and Panofsky, 1964; Colson and Panofsky, 1965; Moore and Krishnamurti, 1966; Endlich, 1964; Ball, 1970; Powell, 1968; Colquhoun and Bourke, 1967; Kronebach, 1964; and others). CAT is frequently encountered in small-scale sloping baroclinic layers of limited vertical and sometimes horizontal extent where conditions are favorable for small gradient Richardson numbers (Delay and Dutton, 1971; and Dutton, 1969), but forecasts of CAT usually are made from synoptic-scale data. The number of studies relating CAT to synoptic meteorological parameters is large. The results of only a few publications are considered here. Further information may be found in a summary report by Veazey (1970), and a compilation of papers edited by Pao and Goldberg (1969).

Ball (1970) found light-to-moderate CAT to be associated with irregularities in the temperature profile which included strong inversions as well as large lapse rates of temperature. A good relationship was found between the intensity of turbulence and various representations of static stability. Also, CAT was found to be associated with large horizontal gradients of temperature. There was a tendency for the intensity of CAT to increase with vertical vector wind shear, although the relationship was not as good as that found for static stability. Other researchers (see, for example, Ehernberger, 1968, and Mitchell and Prophet, 1969) also have observed CAT to be associated with irregularities in the temperature profile. The fact that CAT may be associated with temperature inversions is due to an increase in vertical vector wind shear (mechanical production) resulting from a sloping baroclinic layer (Dutton and Panofsky, 1970). Positive buoyancy is responsible for CAT when the lapse rate of temperature becomes large.

An analysis of project HICAT data (Waco, 1970) in the stratosphere between 13.7 - 21.4 km revealed that CAT was associated with low Richardson numbers resulting from large decreases in temperature with height or strong vertical vector wind shears. When the Richardson number was < 15 , the ratio of turbulent to non-turbulent cases was about 4 to 1. Another analysis of HICAT data (Powell, 1968) measured over Australia between 200 and 50 mb showed a better relationship between CAT and the stability index defined by $V\Delta\alpha/\Delta z$, where V is wind speed, α is wind direction, and z is height, than between CAT and the Richardson number.

A summary of results obtained from 4 five-day periods (Colquhoun, 1967) indicated that the stability index defined above, vorticity, vorticity advection, and an index of CAT derived by Colson and Panofsky (1965) were poor indicators of CAT. Better relationships were found between vertical vector wind shear and Richardson's number and CAT than between CAT and the parameters mentioned above. Kronebach (1964) found the Richardson number to be a better parameter for outlining areas of expected CAT than vertical or horizontal wind shear, or vertical or horizontal

gradients of kinetic energy. Richardson numbers less than 1 outlined about 40% of the reported occurrences of moderate or severe CAT. The wide range in results between CAT and Richardson number has been summarized by Veazey (1970).

CHAPTER III. STATISTICS OF METEOROLOGICAL VARIABLES VERSUS CLEAR AIR TURBULENCE (CAT) IN THE STRATOSPHERE

A. COMPUTATION OF SYNOPTIC METEOROLOGICAL PARAMETERS

Most of the altitudes for the XB-70 flights considered in this investigation were between the 200- and 100-mb levels. Synoptic charts were analyzed, in the usual manner, for the 300-, 200-, and 100-mb constant-pressure surfaces, and data were obtained from the analyzed charts by interpolation for each grid point shown in Fig. 1. The spacing between the grid points in this figure is approximately 158 km.

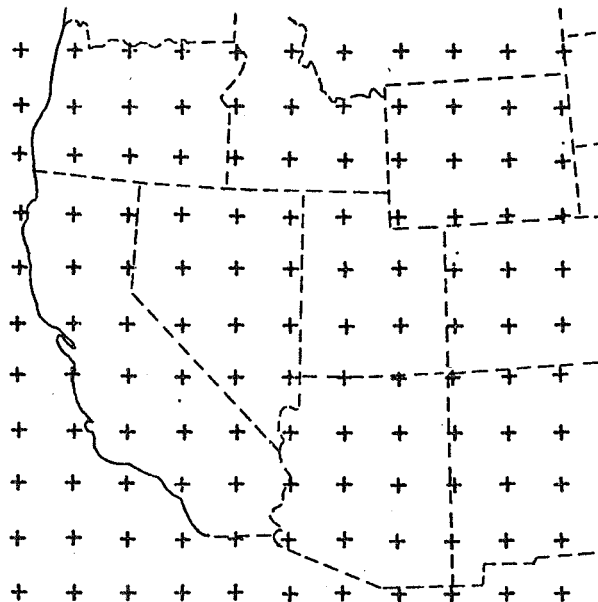


Fig. 1. Grid used in analyzing data from constant-pressure charts.

The following parameters were computed from 1200 GMT data for each grid point shown in Fig. 1 at each constant-pressure surface or as noted: Richardson number (200-100 mb), vector horizontal wind shear, lapse rate of temperature (200-100 mb), advection of relative vorticity, advection of temperature, temperature, CAT index (200-100 mb), zonal wind component, meridional wind component, scalar wind speed, relative vorticity, absolute vorticity, coriolis effect (βv), contour heights for 300 and 200 mb, vertical vector wind shear (200-100 mb), advection of absolute vorticity, horizontal gradient of temperature, and the time rate-of-change of each of these parameters over the 12-h period encompassing each flight. Finite-difference approximations were used to evaluate each of these parameters. All derivatives in the horizontal plane were evaluated over a distance of $2\Delta x$ where Δx is the spacing between grid points, while those in the vertical direction (Richardson number, lapse rate of

temperature, CAT Index, and vertical vector wind shear) were evaluated from data at the 100- and 200-mb levels (vertical distance ≈ 5 km). The 300-mb data were not used in the evaluation of vertical derivatives because the tropopause was generally between 300 and 200 mb so that the gradients between these levels were not representative of stratospheric conditions. In the horizontal plane, the computed values were associated with the midpoint of the interval or array of points used in the computation. A scalar analysis was performed for each parameter, and the flight track of the aircraft superimposed to make it possible to associate average values of synoptic meteorological parameters with turbulent and non-turbulent areas. The computational procedure for all parameters is given in the computer program in Appendix A.

Synoptic charts were prepared for the 70- and 50-mb surfaces but due to errors in the height data, which apparently resulted from errors in measured pressure at these altitudes, the charts could not be analyzed satisfactorily. The contour patterns did not agree with the measured wind which, in most cases, formed a consistent flow pattern. A similar problem was encountered at the 100-mb level in a large percentage of the cases which was the reason for omitting contour heights at this level.

B. SPECIFICATION OF TURBULENT AND NON-TURBULENT AREAS FOR EACH FLIGHT

Segments along each XB-70 flight track of 100-200 km in length in turbulent and non-turbulent air were selected with the centers of the segments separated by about the same or greater distances. Only those areas were selected which definitely fell into one category or the other. Single turbulence encounters of small lateral extent were not classified as turbulent, and neither were they included in the non-turbulent categories. An example of turbulent and non-turbulent areas for one flight is shown in Fig. 2. Using this method, there were 94 turbulent and 78 non-turbulent areas defined and used in this study.

The number of CAT and non-CAT areas selected was not based on the probability of individual occurrences of CAT nor on the percentage of time the airplane was in CAT. Even within a CAT area, turbulence was patchy and usually encountered several times. The degree of intensity of turbulence was not considered in the specification of areas.

C. FREQUENCY DISTRIBUTIONS OF SYNOPTIC METEOROLOGICAL PARAMETERS ASSOCIATED WITH TURBULENT AND NON-TURBULENT AREAS

For each turbulent and non-turbulent area the average values of the synoptic meteorological parameters listed previously were determined from the data obtained for the 300-, 200-, and 100-mb levels regardless of the flight altitude of the XB-70. Empirical frequency distributions of these variables were prepared for the turbulent and non-turbulent areas in terms of absolute frequencies, which represent the number of times turbulent or non-turbulent areas occurred for a given class interval of the variable, and the corresponding percentage frequencies, which represent the percentage of all turbulent or non-turbulent observations falling within the class interval. The frequency distributions for each parameter and a discussion of each are presented in Appendix B.

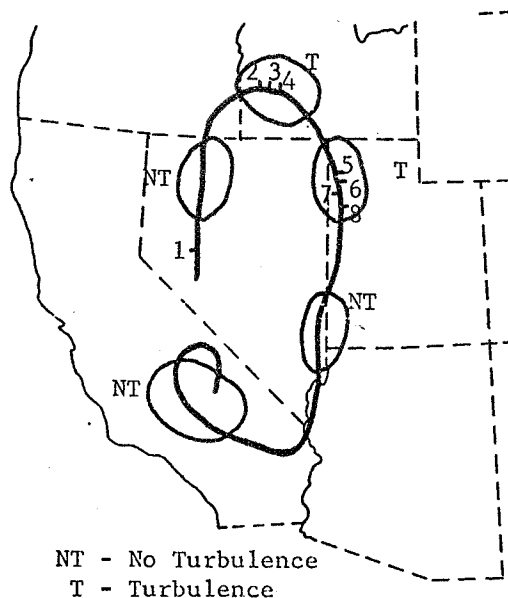


Fig. 2. An example of the classification of turbulent or non-turbulent areas for a flight made on November 2, 1965 (flight track taken from Ehernberger, 1968. Numbers on flight track indicate turbulence encounters.)

The frequency distributions associated with turbulent and non-turbulent areas were analysed for each variable to determine intervals of each variable by inspection over which the two frequency distributions differed. These distributions form the basis for establishing the association between turbulent and non-turbulent areas and meteorological parameters.

D. RANGE(S) OF SYNOPTIC METEOROLOGICAL PARAMETERS OBTAINED FROM EMPIRICAL FREQUENCY DISTRIBUTIONS ASSOCIATED WITH CAT AND NON-CAT AREAS

A summary of the results of the analysis of the empirical frequency distributions is shown in Tables 1 through 4. There are three columns in each table. The first is the parameter, the second states whether or not the turbulent or non-turbulent areas were related to the parameter, and the third gives the range(s) of the parameter and the ratio of the percentage of turbulent to non-turbulent areas associated with the range of values. T or NT is used to indicate more occurrences of areas of turbulence or non-turbulence, respectively. For example, in Table 1 the height of the 300-mb surface is related to the occurrence of turbulence and when the height ≥ 9.4 km there are more non-turbulent than turbulent cases in this range of heights. As another example, zonal wind speed is

Table 1. Limits of variables at 300 mb within which empirical frequency distributions differ for turbulent (T) and non-turbulent (NT) areas and the percentage of occurrence of turbulent and non-turbulent areas within the specified limits.

Parameter	Empirical frequency distributions for T and NT differ (yes or no)	Limits of parameters and the ratio T/NT (percent) within limits where the frequency distributions for T and NT differ	
<u>(a) Measured</u>			
Height	yes	$H \geq 9.4 \text{ km}$	NT(27/43)
Temperature	no		
Zonal wind speed	yes	$0 \leq u < 20 \text{ m s}^{-1}$ $u \geq 20 \text{ m s}^{-1}$	NT(44/73) T(43/22)
Meridional wind speed	no		
Scalar wind speed	yes	$V < 20 \text{ m s}^{-1}$ $V \geq 30 \text{ m s}^{-1}$	NT(32/58) T(39/13)
<u>(b) Derived</u>			
Relative vorticity	yes	$\zeta < -5 \times 10^{-5} \text{ s}^{-1}$ $-5 \times 10^{-5} \leq \zeta \leq 5 \times 10^{-5} \text{ s}^{-1}$	T(19/9) NT(61/78)
Absolute vorticity	yes	$\eta \leq 3 \times 10^{-5} \text{ s}^{-1}$	NT(12/5)
Advection of temperature	yes	$-\vec{v} \cdot \vec{\nabla} T < -10 \times 10^{-5} \text{ }^\circ\text{C s}^{-1}$	T(15/4)
Advection of relative vorticity	yes	$-\vec{v} \cdot \vec{\nabla} \zeta < -3 \times 10^{-9} \text{ s}^{-2}$	T(18/6)
Horizontal wind shear	yes	$ \partial \vec{v} / \partial n \geq 45 \times 10^{-6} \text{ s}^{-2}$	T(18/9)
<u>(c) Time rate-of-change</u>			
Height	no		
Temperature	yes	$\partial T / \partial t < 0 \text{ }^\circ\text{C s}^{-1}$ $20 < \partial T / \partial t \leq 40 \times 10^{-6} \text{ }^\circ\text{C s}^{-1}$	T(29/14) NT(16/39)
Zonal wind speed	no		
Meridional wind speed	no		
Scalar wind speed	yes	$\partial V / \partial t < -16 \times 10^{-5} \text{ m s}^{-2}$	T(26/12)
Relative vorticity	no		
Vorticity advection due to the coriolis force	no		
Advection of temperature	yes	$ \partial(-\vec{v} \cdot \vec{\nabla} T) / \partial t > 20 \times 10^{-10} \text{ }^\circ\text{C s}^{-2}$ $-10 \leq \partial(-\vec{v} \cdot \vec{\nabla} T) / \partial t \leq 10 \times 10^{-10} \text{ }^\circ\text{C s}^{-2}$	T(39/22) NT(40/57)
Advection of relative vorticity	no		
Horizontal wind shear	no		

Table 2. Limits of variables at 200 mb within which empirical frequency distributions differ for turbulent (T) and non-turbulent (NT) areas and the percentage of occurrences of turbulent and non-turbulent areas within the specified limits.

Parameter	Empirical frequency distributions for T and NT differ (yes or no)	Limits of parameters and the ratio T/NT (percent) within limits where the frequency distributions for T and NT differ
<u>(a) Measured</u>		
Height	yes	$H \geq 12.0$ km NT(31/47)
Temperature	no	
Zonal wind speed	yes	$0 \leq u < 20$ m s ⁻¹ $u \geq 20$ m s ⁻¹ NT(37/61) T(54/33)
Meridional wind speed	yes	$v < -10$ m s ⁻¹ T(34/21)
Scalar wind speed	yes	$v < 30$ m s ⁻¹ $v \geq 30$ m s ⁻¹ NT(58/87) T(42/14)
<u>(b) Derived</u>		
Relative vorticity	no	
Absolute vorticity	no	
Advection of temperature	no	
Advection of relative vorticity	no	
Horizontal wind shear	no	
<u>(c) Time rate-of-change</u>		
Height	yes	$\partial H/\partial t < -5 \times 10^{-4}$ m s ⁻¹ T(18/7)
Temperature	no	
Zonal wind speed	no	
Meridional wind speed	no	
Scalar wind speed	yes	$\partial v/\partial t < -16 \times 10^{-5}$ m s ⁻² $\partial v/\partial t > 15 \times 10^{-5}$ m s ⁻² T(17/10) NT(16/23)
Relative vorticity	no	
Vorticity due to the coriolis force	yes	$\beta v < -16 \times 10^{-11}$ s ⁻¹ $-16 \leq \beta v < 0 \times 10^{-11}$ s ⁻² T(43/29) NT(19/35)
Advection of temperature	yes	$\partial(-\vec{v} \cdot \vec{T})/\partial t > 30 \times 10^{-10}$ °C s ⁻² T(16/8)
Advection of relative vorticity	no	
Horizontal wind shear	no	

Table 3. Limits of variables at 100 mb within which empirical frequency distributions differ for turbulent (T) and non-turbulent (NT) areas and the percentage of occurrence of turbulent and non-turbulent areas within the specified limits.

Parameter	Empirical frequency distributions for T and NT differ (yes or no)	Limits of parameters and the ratio T/NT (percent) within limits where the frequency distributions for T and NT differ
<u>(a) Measured</u>		
Temperature	yes	$T < -65 \text{ }^\circ\text{C}$ $-65 \leq T < -55 \text{ }^\circ\text{C}$ NT(17/33) T(75/58)
Zonal wind speed	yes	$0 \leq u \leq 12 \text{ m s}^{-1}$ $u > 12 \text{ m s}^{-1}$ NT(39/54) T(56/40)
Meridional wind speed	yes	$v < -10 \text{ m s}^{-1}$ T(23/15)
Scalar wind speed	yes	$V \leq 9 \text{ m s}^{-1}$ $V \geq 21 \text{ m s}^{-1}$ NT(16/30) T(16/8)
<u>(b) Derived</u>		
Relative vorticity	yes	$\zeta < 0 \text{ s}^{-1}$ $\zeta > 10 \times 10^{-6} \text{ s}^{-1}$ NT(35/52) T(42/24)
Absolute vorticity	yes	$\eta > 12 \times 10^{-5} \text{ s}^{-1}$ T(22/9)
Advection of temperature	yes	$-\vec{v} \cdot \vec{\nabla} T < -4 \times 10^{-5} \text{ }^\circ\text{C s}^{-1}$ T(24/13)
Advection of relative vorticity	yes	$-\vec{v} \cdot \vec{\nabla} \zeta < -4 \times 10^{-10} \text{ s}^{-2}$ $-\vec{v} \cdot \vec{\nabla} \zeta > 4 \times 10^{-10} \text{ s}^{-2}$ T(22/13) NT(17/5)
Horizontal wind shear	yes	$\partial \vec{v} / \partial n > 15 \times 10^{-6} \text{ s}^{-1}$ T(29/16)
<u>(c) Time rate-of-change</u>		
Temperature	yes	$\partial T / \partial t > 40 \times 10^{-6} \text{ }^\circ\text{C s}^{-1}$ T(26/14)
Zonal wind speed	yes	$\partial u / \partial t < -16 \times 10^{-5} \text{ m s}^{-2}$ $0 \leq \partial u / \partial t < 11 \times 10^{-5} \text{ m s}^{-2}$ T(21/10) NT(28/47)
Meridional wind speed	yes	$\partial v / \partial t > 20 \times 10^{-5} \text{ m s}^{-2}$ T(19/10)
Scalar wind speed	no	⊘
Relative vorticity	yes	$\partial \zeta / \partial t \leq 30 \times 10^{-11} \text{ s}^{-2}$ $-10 \leq \partial \zeta / \partial t \leq 30 \times 10^{-11} \text{ s}^{-2}$ $\partial \zeta / \partial t > 30 \times 10^{-11} \text{ s}^{-2}$ T(33/20) NT(32/53) T(22/14)
Vorticity due to the coriolis force	no	
Advection of temperature	yes	$ \partial (-\vec{v} \cdot \vec{\nabla} T) / \partial t > 10 \times 10^{-10} \text{ }^\circ\text{C s}^{-2}$ T(40/27)
Advection of relative vorticity	no	
Horizontal wind shear	yes	$\partial \vec{v}_n / \partial t < -20 \times 10^{-11} \text{ s}^{-2}$ $-11 < \partial \vec{v}_n / \partial t < 0 \times 10^{-11} \text{ s}^{-2}$ T(32/13) NT(6/26)

Table 4. Limits of variables obtained from 100- and 200-mb data within which empirical frequency distributions differ for turbulent (T) and non-turbulent (NT) areas and the percentage of occurrence of turbulent and non-turbulent areas within the specified limits.

Parameter	Empirical frequency distributions for T and NT differ (yes or no)	Limits of parameters and the ratio T/NT (percent) within limits where the frequency distributions for T and NT differ
<u>(a) Derived</u>		
Vertical wind shear	yes	$\partial \bar{v} / \partial z < 30 \times 10^{-4} \text{ s}^{-1}$ $\partial \bar{v} / \partial z \geq 50 \times 10^{-4} \text{ s}^{-1}$
		NT(38/56) T(29/13)
Lapse rate of temperature	no	
CAT Index	no	
Richardson number	yes	Ri \leq 30 Ri $>$ 40
		T(49/33) NT(44/62)
<u>(b) Time rate-of-change</u>		
Vertical wind shear	yes	$\partial v_H / \partial t > 10 \times 10^{-8} \text{ s}^{-2}$
		T(16/4)
Lapse rate of temperature	yes	$ \partial \gamma / \partial t \geq 20 \times 10^{-9} \text{ }^\circ\text{C m}^{-1} \text{ s}^{-2}$ $-20 \leq \partial \gamma / \partial t \leq 0 \times 10^{-9} \text{ }^\circ\text{C m}^{-1} \text{ s}^{-2}$
		T(22/10) NT(29/49)
CAT Index	yes	$ \partial(\text{CAT Index}) / \partial t > 40 \times 10^{-3}$ $0 \leq \partial(\text{CAT Index}) / \partial t \leq 40 \times 10^{-3} \text{ s}^{-1}$
		T(38/20) NT(31/52)
Richardson number	no	

related to the occurrence of turbulence, and the frequency distributions show that in the range of speeds between 0 and 20 m s⁻¹, there are more non-turbulent than turbulent areas, and when the speed exceeds 20 m s⁻¹ there are more turbulent than non-turbulent areas. For all other speed ranges there was no significant difference in the percentage of occurrences of turbulent and non-turbulent areas.

Of the measured and derived parameters, there are only two which show a relationship with turbulence at all three levels. These are the zonal and scalar wind speeds. All other measured and derived parameters, except temperature and height (only two levels considered), are related to turbulence at two of the three levels.

There is only one parameter whose time rate-of-change is related to turbulence at all three levels, viz., the advection of temperature. The advection of relative vorticity is the only parameter whose time rate-of-change is not related to the occurrence of turbulence at any level.

Temperature and scalar wind speed are the only parameters related to turbulence at two of the three levels.

The parameters involving the 100- and 200-mb levels are shown in Table 4. Of the derived quantities, vertical wind shear and the Richardson number are related to turbulence, and of the time rate-of-change of the parameters only the Richardson number does not show any relationship with turbulence.

E. EMPIRICAL AND JOINT PROBABILITIES OF CAT FOR SELECTED RANGES AND LIMITS OF SYNOPTIC METEOROLOGICAL VARIABLES BASED ON FREQUENCY DISTRIBUTIONS

The frequency distributions for each parameter associated with turbulent and non-turbulent areas were examined and ranges or limits of the variables isolated within which the distributions differed. Outside the ranges or limits chosen, turbulent and smooth conditions associated with the variable occurred an equal percent, or there was no systematic difference between the two frequency distributions. In the ranges where the frequency distributions differed, the variable was associated with either turbulent or non-turbulent conditions depending upon which condition was observed more frequently. In some cases, the frequency distributions of variables or their time rate-of-change did not differ for turbulent and non-turbulent conditions, e.g., the lapse rate of temperature, temperature, and the CAT Index. These variables were not considered further in the analysis.

Many theories have been derived and many approaches taken to explain the occurrence of CAT. Different theories use different variables and different combinations of variables. In general, no one theory is adequate to explain the formation and existence of CAT in all cases. For this reason, many investigators have considered numerous parameters singly and in combination. The association between turbulence and the parameters specified above is considered for ranges or limits of each variable where the distributions differ as well as for combinations of the variables.

Empirical probabilities were computed when CAT occurred for any combination of three variables for specified ranges or limits of the variables. Many combinations were considered, and those for which a percentage of 75% or greater in the case of turbulence, and 25% or less in the case of no turbulence, are presented in Table 5. This table includes the case number, the parameters considered for each case, ranges and limits of the parameters, percent verification of each parameter (the number of CAT occurrences divided by the number of cases when the stated conditions were observed), and the percent verification of each combination of parameters. The column for the percent verification of each parameter gives the percent of turbulent cases when the variables were observed within the stated ranges or limits, while the number of turbulent cases divided by the number of total cases is shown in parentheses. Similar information is given in the column for percent verification for combinations of parameters for the stated combinations. Each case will now be briefly discussed.

Table 5. Empirical probabilities expressed in percent of CAT associated with selected variables and combinations of variables over ranges where frequency distributions differed for CAT and No-CAT encountered by the XB-70 airplane in the stratosphere.

Case	Parameters	Range of Parameters	Percent Verification of each Parameter	Percent Verification for Combinations of Parameters
<u>300 mb</u>				
1.	a. Height	$H \geq 9.4 \text{ km}$	42(25/59)	a, b and c - 23(7/30)
	b. Zonal wind speed	$0 \leq u < 20 \text{ m s}^{-1}$	42(41/98)	
	c. Relative vorticity	$-5 \times 10^{-5} \leq \zeta \leq 5 \times 10^{-5} \text{ s}^{-1}$	49(58/119)	
2.	a. Height	$H \geq 9.4 \text{ km}$	42(25/59)	a and c - 21(4/19)
	b. Scalar wind speed	$V < 20 \text{ m s}^{-1}$	40(30/75)	
	c. Local temperature change	$20 \times 10^{-6} < \frac{\partial T}{\partial t} \leq 40 \times 10^{-6} \text{ } ^\circ\text{C s}^{-1}$	33(15/45)	
3.	a. Zonal wind speed	$u \geq 20 \text{ m s}^{-1}$	71(41/58)	a and b - 80(24/30)
	b. Scalar wind speed	$V \geq 30 \text{ m s}^{-1}$	79(37/47)	
	c. Relative vorticity	$\zeta < -5 \times 10^{-5} \text{ s}^{-1}$	72(18/25)	
4.	a. Scalar wind speed	$V \geq 30 \text{ m s}^{-1}$	79(37/47)	a or b - 76(50/66)
	b. Relative vorticity	$\zeta < -5 \times 10^{-5} \text{ s}^{-1}$	72(18/25)	
	c. Advection of temperature	$-\vec{V} \cdot \vec{\nabla} T < -10^{-4} \text{ } ^\circ\text{C s}^{-1}$	82(14/17)	
5.	a. Scalar wind speed	$V \geq 30 \text{ m s}^{-1}$	79(37/47)	a or b - 76(50/66)
	b. Relative vorticity	$\zeta < -5 \times 10^{-5} \text{ s}^{-1}$	72(18/25)	
	c. Advection of relative vorticity	$-\vec{V} \cdot \vec{\nabla} \zeta < -3 \times 10^{-9} \text{ s}^{-2}$	77(17/22)	
6.	a. Scalar wind speed	$V \geq 30 \text{ m s}^{-1}$	79(37/47)	a or b - 76(50/66)
	b. Relative vorticity	$\zeta < -5 \times 10^{-5} \text{ s}^{-1}$	72(18/25)	
	c. Horizontal wind shear	$ \partial \vec{V} / \partial n \geq 45 \times 10^{-6} \text{ s}^{-1}$	62(23/37)	
7.	a. Advection of temperature	$-\vec{V} \cdot \vec{\nabla} T < -10^{-4} \text{ } ^\circ\text{C s}^{-1}$	82(14/17)	a or b - 77(23/30)
	b. Advection of relative vorticity	$-\vec{V} \cdot \vec{\nabla} \zeta < -3 \times 10^{-9} \text{ s}^{-2}$	77(17/22)	
	c. Horizontal wind shear	$ \partial \vec{V} / \partial n \geq 45 \times 10^{-6} \text{ s}^{-1}$	62(23/37)	
8.	a. Scalar wind speed	$V \geq 30 \text{ m s}^{-1}$	79(37/47)	a and c - 85(17/20)
	b. Local temperature change	$\partial T / \partial t < 0 \text{ } ^\circ\text{C s}^{-1}$	68(28/41)	
	c. Local scalar wind change	$\partial V / \partial t < -16 \times 10^{-5} \text{ s}^{-2}$	73(24/33)	

*The number outside parentheses is the percent of CAT cases occurring in the stated range of the variable, and those inside parentheses are the number of CAT cases divided by the total number of cases.

Table 5. (continued)

Case	Parameters	Range of Parameters	Percent Verification of each Parameter	Percent Verification for Combinations of Parameters
<u>300 mb (continued)</u>				
9.	a. Local temperature change	$\partial T/\partial t < 0 \text{ } ^\circ\text{C s}^{-1}$	68(28/41)	a and c - 78(14/18)
	b. Local scalar wind change	$\partial V/\partial t < -16 \times 10^{-5} \text{ s}^{-2}$	73(24/33)	
	c. Local temperature advection change	$ \partial(-\vec{v} \cdot \vec{v}_T)/\partial t > 20 \times 10^{-10} \text{ } ^\circ\text{C s}^{-2}$	69(37/54)	
<u>200 mb</u>				
10.	a. Zonal wind speed	$u \geq 20 \text{ m s}^{-1}$	66(51/77)	b and c - 79(15/19)
	b. Meridional wind speed	$v < -10 \text{ m s}^{-1}$	66(33/50)	
	c. Scalar wind speed	$V \geq 30 \text{ m s}^{-1}$	78(39/50)	
11.	a. Zonal wind speed	$u \geq 20 \text{ m s}^{-1}$	66(51/77)	
	b. Scalar wind speed	$V \geq 30 \text{ m s}^{-1}$	78(39/50)	
	c. Local height change	$\partial H/\partial t < -5 \times 10^{-4} \text{ m s}^{-1}$	74(17/23)	
12.	a. Scalar wind speed	$V \geq 30 \text{ m s}^{-1}$	78(39/50)	
	b. Local height change	$\partial H/\partial t < -5 \times 10^{-4} \text{ m s}^{-1}$	74(17/23)	
	c. Local scalar wind change	$\partial V/\partial t < -16 \times 10^{-5} \text{ s}^{-2}$	50(13/26)	
13.	a. Local height change	$\partial H/\partial t < -5 \times 10^{-4} \text{ m s}^{-1}$	74(17/23)	
	b. Local scalar wind change	$\partial V/\partial t < -16 \times 10^{-5} \text{ s}^{-2}$	50(13/26)	
	c. Coriolis effect	$\beta v < -16 \times 10^{-11} \text{ s}^{-2}$	63(40/63)	
<u>100 mb</u>				
14.	a. Absolute vorticity	$\eta > 12 \times 10^{-5} \text{ s}^{-1}$	75(21/28)	
	b. Horizontal wind shear	$\partial V/\partial n > 15 \times 10^{-6} \text{ s}^{-1}$	70(28/40)	
	c. Local horizontal wind shear change	$\partial \vec{v}_n/\partial t < -20 \times 10^{-11} \text{ s}^{-2}$	74(29/39)	
15.	a. Zonal wind speed	$u > 12 \text{ m s}^{-1}$	63(52/83)	b and c - 77(17/22)
	b. Local relative vorticity change	$ \partial \zeta/\partial t > 30 \times 10^{-11} \text{ s}^{-2}$	68(42/62)	
	c. Local horizontal wind shear change	$\partial \vec{v}_n/\partial t < -20 \times 10^{-11} \text{ s}^{-2}$	74(29/39)	

*The number outside parentheses is the percent of CAT cases occurring in the stated range of the variable, and those inside parentheses are the number of CAT cases divided by the total number of cases.

Table 5. (continued)

Case	Parameters	Range of Parameters	Percent Verification of each Parameter	Percent Verification for Combinations of Parameters
<u>100-200 mb</u>				
16.	a. Vertical wind shear	$\partial \vec{V} / \partial z < 30 \times 10^{-4} \text{ s}^{-1}$	45(36/80)	b and c - 23(7/30)
	b. Richardson number	$Ri > 40$	43(36/84)	
	c. Local lapse rate change	$-20 \times 10^{-9} \leq \frac{\partial \gamma}{\partial t} \leq 0$ $^{\circ}\text{C m}^{-1} \text{ s}^{-1}$	54(41/76)	
17.	a. Richardson number	$Ri > 40$	43(36/84)	a and b - 23(7/30)
	b. Local lapse rate change	$-20 \times 10^{-9} \leq \frac{\partial \gamma}{\partial t} \leq 0$ $^{\circ}\text{C m}^{-1} \text{ s}^{-1}$	54(41/76)	a, b and c - 21(6/28)
	c. Local CAT Index change	$0 \leq \partial I / \partial t \leq 40 \times 10^{-3} \text{ s}^{-1}$	43(31/72)	
18.	a. Vertical wind shear	$\partial \vec{V} / \partial z \geq 50 \times 10^{-4} \text{ s}^{-1}$	73(27/37)	a and b - 75(27/36)
	b. Richardson number	$Ri \leq 30$	65(46/71)	a or c - 75(40/53)
	c. Local vertical wind shear change	$\partial \vec{V}_H / \partial t > 10^{-7} \text{ s}^{-2}$	83(15/18)	
19.	a. Richardson number	$Ri \leq 30$	65(46/71)	b or c - 75(33/44)
	b. Local vertical wind shear change	$\partial \vec{V}_H / \partial t > 10^{-7} \text{ s}^{-2}$	83(15/18)	
	c. Local lapse rate change	$ \partial \gamma / \partial t \geq 20 \times 10^{-9}$ $^{\circ}\text{C m}^{-1} \text{ s}^{-1}$	74(14/19)	
20.	a. Local vertical wind shear change	$\partial \vec{V}_H / \partial t > 10^{-7} \text{ s}^{-2}$	83(15/18)	a or b - 75(33/44)
	b. Local lapse rate change	$ \partial \gamma / \partial t \geq 20 \times 10^{-9}$ $^{\circ}\text{C m}^{-1} \text{ s}^{-1}$	74(14/19)	a or c - 81(29/36)
	c. Local CAT Index change	$ \partial I / \partial t > 40 \times 10^{-3} \text{ s}^{-1}$	81(21/26)	b or c - 76(28/37)
				a, b or c - 76(34/45)
<u>Mixed Layers</u>				
21.	a. Scalar wind speed 300 mb	$V \geq 30 \text{ m s}^{-1}$	79(37/47)	a and b - 83(29/35)
	b. Scalar wind speed 200 mb	$V \geq 30 \text{ m s}^{-1}$	78(39/50)	a or c - 77(46/60)
	c. Scalar wind speed 100 mb	$V > 21 \text{ m s}^{-1}$	71(15/21)	

*The number outside parentheses is the percent of CAT cases occurring in the stated range of the variable, and those inside parentheses are the number of CAT cases divided by the total number of cases.

Table 5. (continued)

Case	Parameters	Range of Parameters	Percent Verification of each Parameter	Percent Verification for Combinations of Parameters
<u>Mixed Layers (continued)</u>				
22.	a. Scalar wind speed 300 mb	$V \geq 30 \text{ m s}^{-1}$	79(37/47)	a and b - 83(29/35)
	b. Scalar wind speed 200 mb	$V \geq 30 \text{ m s}^{-1}$	78(39/50)	a and c - 84(21/25)
	c. Vertical wind shear 200-100 mb	$\partial \vec{V} / \partial z \geq 50 \times 10^{-4} \text{ s}^{-1}$	73(27/37)	a, b and c - 83(19/23)
23.	a. Scalar wind speed 200 mb	$V \geq 30 \text{ m s}^{-1}$	78(39/50)	
	b. Advection of temperature 100 mb	$-\vec{V} \cdot \vec{\nabla} T < -4 \times 10^{-5} \text{ }^\circ\text{C s}^{-1}$	70(23/33)	
	c. Vertical wind shear 200-100 mb	$\partial \vec{V} / \partial z \geq 50 \times 10^{-4} \text{ s}^{-1}$	73(27/37)	
24.	a. Local scalar wind speed change 300 mb	$\partial V / \partial t < -16 \times 10^{-5} \text{ m s}^{-1}$	74(23/31)	a and b - 83(15/18)
	b. Scalar wind speed 200 mb	$V \geq 30 \text{ m s}^{-1}$	78(39/50)	
	c. Horizontal wind shear 100 mb	$\partial \vec{V} / \partial n > 15 \times 10^{-6} \text{ s}^{-1}$	70(28/40)	

*The number outside parentheses is the percent of CAT cases occurring in the stated range of the variable, and those inside parentheses are the number of CAT cases divided by the total number of cases.

Case 1: This case concerns the association between the variables and the absence of turbulence. Each of the variables considered separately does not differentiate well between CAT and no CAT; however, when all three variables occur within the stated ranges or limits simultaneously there is only a 23% chance that CAT will occur. While there is only approximately 15% of the total observations included in this category, there is a high probability that CAT will not occur when the stated conditions are observed.

Case 2: This case is similar to Case 1 with the exception that only two variables need to be considered in combination. The number of observations in this category is only about 10% of the total.

Case 3: This case differs from Cases 1 and 2 in that the probabilities indicate conditions favorable for CAT rather than its absence. Either of these variables considered alone may be used to explain a large percent of CAT occurrences within the specified ranges. The combinations of variables do not improve the percentages significantly, but the number of cases explained by the combination of variables b and c increases

considerably. This combination of variables explains 76% of the observations (approximately 1/3 the total number) falling within the stated ranges or limits.

Case 4: Each of these variables differentiates between turbulent and smooth areas of approximately 70 and 80% of the observations which fall within the specified ranges when considered singly, and approximately 75% of a much larger number of observations when the variables are considered jointly.

Case 5: This combination of variables adds little to the cases considered above.

Case 6: The percentages shown for this combination of variables are approximately equal to those already discussed except the number of observations increases considerably for combinations of the variables. The number of observations considered within the range of each variable is approximately 15-25% of the total; however, when the variables are considered jointly the percentage of the total increases to 30-40. This is a significant increase in the percentage of the number of observations accounted for, although the percentage verification does not increase.

Case 7: While the percent verification does not increase significantly in this case, the number of CAT areas accounted for approximately doubles when combinations of variables are considered.

Case 8: For the combination of variables a and c, the percentage verification increases over that for either of the variables considered alone. However, the number of observations decreases considerably when both variables are observed within the stated ranges. In this case, a slight improvement may be realized by considering two variables jointly, but the number of observations accounted for decreases.

Case 9: The percent verifications for variables a and c are 68 and 69, respectively, but when the variables are considered together the percent verification increases to 78% although the number of observations decreases by 50% to 18, which is approximately 10% of the total number. Thus, the percent verification increases but the number of observations falling within the stated limits decreases.

Case 10: This case is similar to Case 9 in that the percent verification increased when variables b and c were considered in combination, but the number of observations falling within the stated limits decreased considerably.

Cases 11, 12, and 13: In each of these cases at least one variable had percent verification of 75 or greater within the stated ranges, but any possible combination of the variables did not improve the percent verification.

Cases 14 and 15: These cases do not show any particularly significant results except that the combination of variables b and c in Case 15 increases the percent verification significantly, but is accompanied by

a decrease in the number of observations when these variables occur simultaneously within the stated ranges.

Cases 16 and 17: The variables in these cases for the ranges as specified are more favorable for smooth than turbulent conditions. The only significant improvement in the percent verification noted was a combination of the Richardson number and local changes in the lapse rate of temperature which led to a significant decrease in the percent verification of CAT but, at the same time, a decrease was observed in the number of observations falling within the stated limits.

Case 18: The combinations of variables for this case did not significantly improve the percent verification. However, when variables a or c were considered together, the number of observations increased significantly.

Case 19: The results of this case are similar to those for Case 18 in that the combination of variables b or c encompasses a much larger percentage of the observations, but the percent verification did not increase significantly.

Case 20: This case is interesting in that several combinations of the variables led to an increase in the number of observations encompassed, but the percent verification remained essentially unchanged.

Cases 21 through 24: The combinations of variables considered in these cases did not improve the percent verification significantly in most cases, and the number of observations accounted for by the combinations was generally lower than those for the individual variables.

With the exception of a very few cases, the data given in Table 5 show that single variables are associated with CAT in about the same way as multiple variables; however, more areas of turbulence are accounted for in many instances when variables are considered in combination. In the cases where the percent verification increased, the number of cases generally decreased. Thus, there is a trade-off between the percent verification, and the number of areas within which CAT would be expected for the stated conditions.

The best relationships between combinations of variables and non-CAT conditions are given by Cases 1 and 2 for the 300-mb level, and Cases 16 and 17 for parameters determined from 100- and 200-mb data. The number of occurrences for the stated combinations of variables in these four cases is not large; the combinations of the variables considered differentiate between turbulent and non-turbulent conditions for only approximately 15% of the observations. As shown in Table 5, the frequency distributions for turbulent and non-turbulent conditions show significant differences primarily when turbulence occurred rather than when turbulence did not occur.

The cases where variables or a combination of variables with a verification of at least 75%, and where a large number of cases were included, are 3, 6, and 7 for the 300-mb level, 10 for the 200-mb level, 14 and 15

for the 100-mb level, 18, 19, and 20 for variables based on data at the 100- and 200-mb levels, and 21 for mixed layers. In these cases, approximately one-fourth to one-third of the total number of observations are included. Cases 3, 10, and 21 show that scalar wind speed at the 100-, 200-, and 300-mb levels is related to turbulence in about the same way as other variables or combinations of variables. The Richardson number has been found by many investigators to be a good indicator of CAT in the troposphere, but for the data shown here for the stratosphere the Richardson number, even when used in combination with other variables, is not a key parameter which differentiates between CAT and non-CAT conditions.

The variables in the lower stratosphere and upper troposphere which appear to be most important in differentiating between turbulent and non-turbulent conditions are scalar wind speed, vorticity, horizontal vector wind shear, vertical vector wind shear, the advection of relative vorticity, absolute vorticity, and the time rate-of-change of vorticity, horizontal wind shear, vertical wind shear, lapse rate of temperature, and the CAT Index. Fortunately, most of these variables are available or may be determined easily from synoptic data. In addition, many of them can be predicted with reasonable accuracy.

F. VERIFICATION OF RESULTS AND A SUGGESTED PROCEDURE FOR FORECASTING CAT

An abundance of clear-air turbulence data in the stratosphere above 12.2 km (40,000 ft) does not exist. Some data were obtained, however, from about 20 flights of the YF-12A airplane flying in the same general area and altitudes as the XB-70. Meteorological parameters associated with CAT and non-CAT areas for these flights were computed in the same manner as those for the XB-70 data, but because of the small sample size (about 20 areas each of CAT and non-CAT) it was not possible to establish frequency distributions as was done for the XB-70 data. Instead, the results obtained from the XB-70 were checked as follows using YF-12A data. The number of parameters which exceeded the limits presented in Table 5 associated with CAT and non-CAT areas was counted at each pressure level and for the 100-200-mb layer. It was found that when CAT occurred there were more limits exceeded than when CAT did not occur. The average number which was exceeded when CAT occurred for all layers was about 10 as compared to about 6 for the non-CAT areas. In addition, it was found that the number of parameters whose limits were exceeded near the flight altitudes was generally greater in CAT areas as compared with those in non-CAT areas. For example, when the flight level was between 100 and 200 mb the number of parameters whose limit was exceeded at 200 mb was about 8-to-10 as compared with 2-to-6 when CAT did not occur. There were cases when these results were not obtained, but in these cases CAT was observed nearby (generally within 300 km).

A suggested procedure for using the XB-70 results to forecast CAT is as follows. Evaluate the parameters in Table 5, count the number of parameters exceeding the stated limits, and prepare charts showing the areal distribution of these numbers. Some indication of the altitude where the CAT would be expected can be estimated by comparing the relative number of limits exceeded at the 300-, 200-, and 100-mb levels.

Examples of this procedure for two XB-70 flights are shown in Figs. 3 and 4. These figures contain isopleths drawn for the number of limits

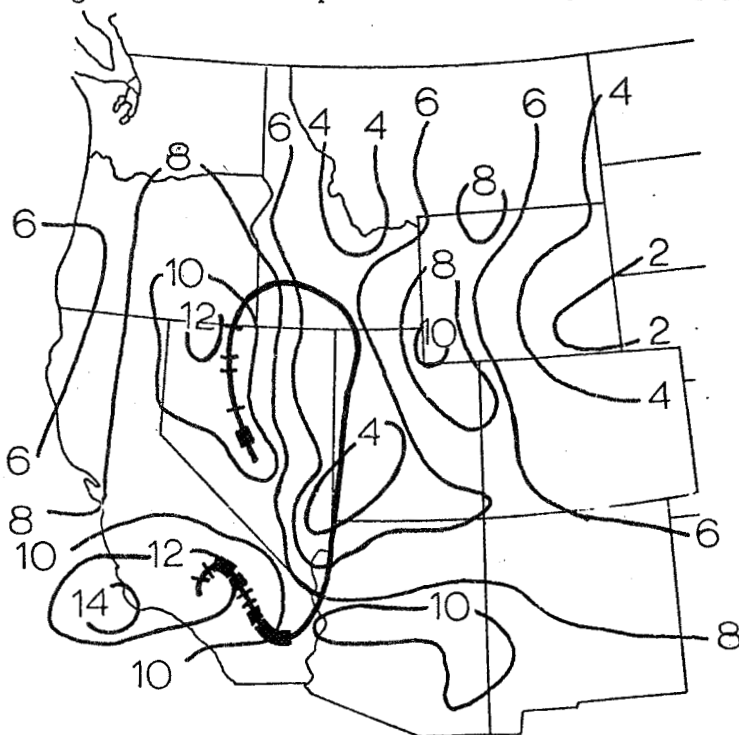


Fig. 3. Analysis of the number of parameters exceeding specified limits for October 16, 1965. The flight track of the XB-70 shows where turbulence was encountered.

exceeded for variables presented in Table 5, and the flight tracks of the airplane showing where turbulence was encountered. The parameters were evaluated from rawinsonde data encompassing the flight time. In both figures, most turbulence was encountered in regions where the number of limits exceeded is about 8 or more, and smooth flight conditions in regions of 6 or less. With the exception of the extensive turbulence encounter over Idaho in Fig. 4, the turbulent regions were encountered in or near regions where the maximum number of limits were exceeded. For both flights there was generally a greater percentage of exceedances near the flight altitude than below it, but additional research is needed before conclusions can be reached regarding the expected altitude of turbulence. Results from this technique are considered further in the composite forecasting method presented in Chapter VI.

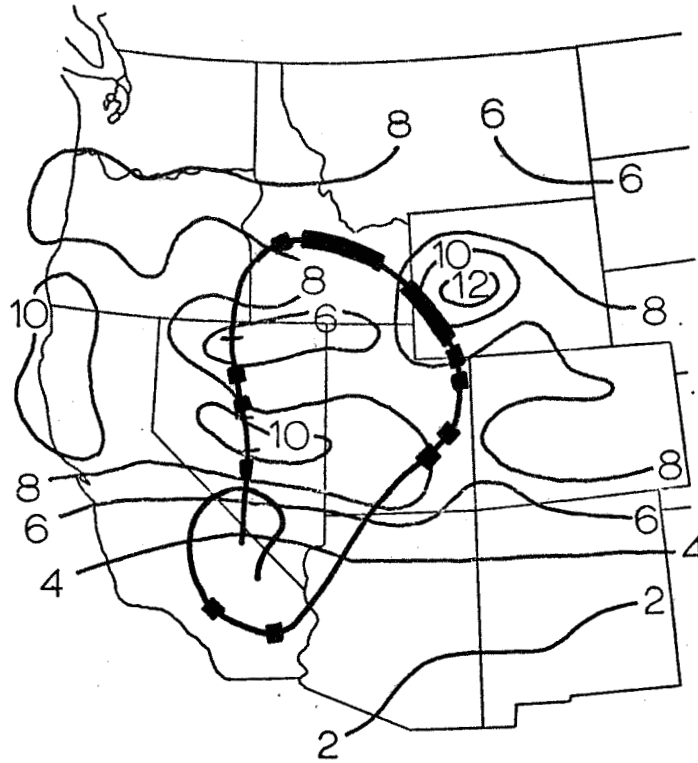


Fig. 4. Analysis of the number of parameters exceeding specified limits for January 3, 1966. The flight track of the XB-70 shows where turbulence was encountered.

CHAPTER IV. FORECASTING CLEAR-AIR TURBULENCE WITHIN SUB-LAYERS
OF THE STRATOSPHERE BY DISCRIMINANT FUNCTION ANALYSIS

by

Terry Lee Clark
Center for Applied Geosciences
Texas A&M University, College Station, Texas

A. ABSTRACT

A procedure incorporating discriminant functions, derived from a form of linear regression, which would forecast the occurrences of clear-air turbulence within 2.1-km (7000-ft) sub-layers of the lower stratosphere (12.2-20.4 km or 40,000-67,000 ft) over the western United States was devised. The values of 69 synoptic-scale parameters corresponding to turbulent and non-turbulent regions over the western United States were obtained from the United States rawinsonde network. The turbulent and non-turbulent regions were determined from turbulence data obtained from 46 stratospheric flights of the XB-70 aircraft during the period March 1965 to November 1967, and 23 stratospheric flights of the YF-12A aircraft during the period March 1970 to January 1972.

The regions associated with the XB-70 data sample were grouped into one or more of five categories determined by the altitude of the aircraft at the time the turbulence or non-turbulence was reported. Discriminant function analysis was then employed to construct functions which could discriminate the turbulent from the non-turbulent regions. The best functions obtained for the sub-layers of the XB-70 data sample were tested by using independent information from the YF-12A data sample. Five functions, which best discriminated the regions in a sub-layer for both samples, were selected for the procedure of forecasting turbulent regions. This procedure, for the most part, identified correctly over 85 per cent of the turbulent and non-turbulent regions in each of the five sub-layers.

Three different approaches were employed to investigate the possibility of forecasting the intensity of turbulence. One attempted to find a pair of synoptic-scale parameters of which simultaneous values would indicate the intensity of the turbulence predicted by the discriminant functions. Another examined the possibility of the values of the discriminant functions indicating the intensity of the predicted turbulence. The last approach attempted to construct discriminant functions which would indicate objectively the intensity of the predicted turbulence. This approach, which proved to be the most successful, produced a discriminant function which identified correctly 62.5 and 68.5 per cent of the moderate to severe turbulence and light turbulence reports, respectively. Discriminant function analysis proved useful in determining a procedure to forecast the intensity of clear-air turbulence.

B. INTRODUCTION

1. Statement of the problem

Clear-air turbulence (CAT), or turbulence formed by mechanisms other than those associated with convection and normally encountered in cloud-free areas, is a mesoscale atmospheric phenomenon which has been related to various mesoscale atmospheric parameters, such as vertical and horizontal wind shears, gradient Richardson number, and horizontal temperature gradient. This mesoscale phenomenon always has been a problem to aviation, since it can lead to discomfort for pilots and passengers and in extreme conditions produce vertical accelerations strong enough to damage the structure of the aircraft.

Since the advent of military and commercial stratospheric aircraft flights, an adequate procedure to forecast the spatial and temporal occurrences of stratospheric CAT is needed to warn aviators of the hazard. However, a successful forecasting procedure is difficult to develop without a firm foundation for the theory of CAT, and this has not been established. One of the reasons that an adequate foundation has not been established is that meaningful CAT data, especially stratospheric, are difficult to obtain systematically. Moderate or severe CAT over the United States in winter, the peak season for CAT, is encountered less than 5 per cent and light CAT is encountered between 10 and 15 per cent of over-all aircraft flight time (Endlich and Mancuso, 1967). Moreover, it is difficult to obtain representative data on the mesoscale atmospheric parameters associated with CAT. Also, it is unclear which of the many measurable mesoscale parameters should be incorporated into the forecasting procedure.

A forecasting procedure utilizing only the mesoscale parameters thought to be associated with CAT would be impractical for several reasons. For one, mesoscale parameters measured from aircraft would apply only to the localized regions in which they were measured. An exorbitant number of hours, measurements, recordings, and calculations would be necessary, therefore, to obtain the proper information to predict occurrences of CAT. Also, unlike synoptic-scale parameters, the values of mesoscale parameters change quickly with time and can be forecasted accurately for periods of less than 3 to 5 h (Robinson, 1967). This would require more than several mesoscale sampling missions each day.

2. Objectives

The objective of this research is to determine, from a statistical approach, algebraic functions involving selected synoptic-scale parameters which would indicate areas and altitudes where stratospheric CAT would occur. Although CAT is thought to be caused primarily by mesoscale parameters, synoptic-scale parameters are used, since their values are much easier to obtain on a regular basis and can be forecasted for much longer periods of time than mesoscale parameters. Moreover, it has been shown by Scoggins

et al. (1972) from statistical and synoptic approaches that there is an interrelationship between mesoscale and synoptic-scale atmospheric phenomena.

Discriminant function analysis, first developed by Fisher (1936), was chosen as the statistical approach, since it proved to be reasonably successful in previous studies (Panofsky and Brier, 1958; Miller, 1962; Cox, 1973). The functions were determined from aircraft CAT data sampled by an XB-70 aircraft during the period March 1965 to November 1967 and were tested by independent CAT data sampled by a YF-12A aircraft during the period March 1970 to January 1972.

The research included investigations of several procedures of indicating the intensities of CAT. Three different procedures were examined. The first attempted to determine the intensity of the CAT by examining the simultaneous values of pairs of synoptic-scale parameters; another examined the numerical values of individual discriminant functions; and the third employed predictive functions derived from discriminant function analysis.

C. BACKGROUND TO RESEARCH

1. Previous studies

In the last two decades, many articles have been written concerning the mechanisms and prediction of CAT. As should be expected, some of the results and conclusions reached by the various authors do not concur completely since a firm foundation of the theory of CAT has not been established.

One conclusion which many researchers support is that CAT is caused primarily by unstable shear-gravity or gravity-inertia waves breaking into small eddies and transferring kinetic energy downscale (Kuettner, 1952; Clodman, Morgan and Ball, (1961); Holmboe, 1963; Endlich and Mancuso, 1964; Thompson, 1973). This process is illustrated in Fig. 5. It is theorized that shear-gravity waves will become unstable when the condition

$$(\rho - \rho') \lambda < \frac{\rho \rho' (u' - u)^2}{\rho + \rho'} \frac{2\pi}{g}$$

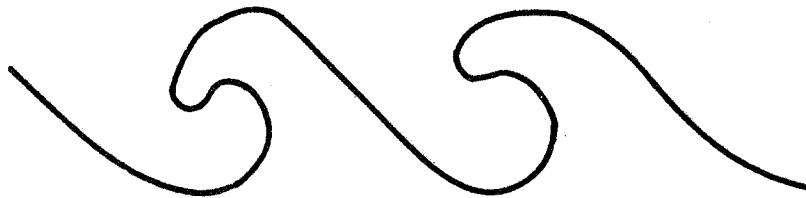
is satisfied (Haltiner and Martin, 1957). (The lambda represents the wave length and the primed and unprimed quantities represent the conditions in the layer above and below, respectively, a surface of discontinuity.) In support of this theory, Hicks and Angell (1968) have shown that CAT occurred in relatively stable layers where considerable wind shear was present (conditions favoring breaking waves) after the presence of waves were discovered by radar in the same areas.



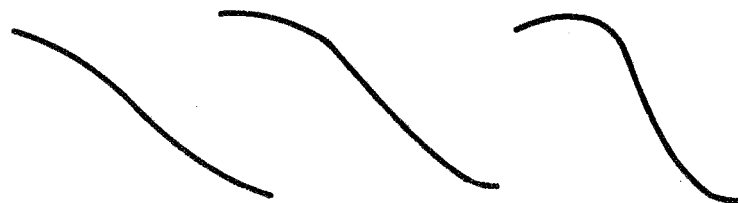
Stable gravity waves



Gravity waves becoming unstable



Breaking gravity waves and eddies



Braided phenomenon indicating turbulence

Fig. 5. Illustration of the stages of breaking gravity waves resulting in the formation of clear-air turbulence. The stages were detected by radar and reported by Hicks and Angell (1968).

According to another widely accepted theory, the motion becomes turbulent when the value of the Richardson number, which is the ratio of the buoyant force to the shearing stress, i.e.,

$$Ri = \frac{g}{\bar{\theta}} \frac{\partial \bar{\theta} / \partial z}{|\partial \bar{\mathbf{v}} / \partial z|^2} \quad (1)$$

becomes smaller than some critical value. In this equation, g is gravity, θ is potential temperature, $\bar{\mathbf{v}}$ is the average vector wind, z is altitude, and a bar denotes an average. However, the critical number is uncertain, since the manner in which to calculate the Richardson number has many variations. Veazey (1970) indicated that from 31 studies utilizing measured data, the critical Richardson number varied from 0.5 to 5.0, while Lumley and Panofsky (1964) believe the correct value is 0.25.

Many studies have been undertaken based on using these two theories and others to relate atmospheric parameters to the formation of CAT. Endlich (1964) remarked that the sufficient conditions which lead to the formation of CAT have not been formalized, but certain mesoscale features appear adequate. They are a large vertical variation of wind speed and direction, the presence of an inversion, a sharp curvature of trajectory, and the presence of appreciable vertical motion. Ehernberger (1968) reaffirmed that wind velocity, vertical wind shear, and temperature parameters obtained from rawinsonde measurements were related to stratospheric CAT. In addition, Colson (1969) found a good relationship between relative vorticity and CAT, while Waco (1970) discovered that the vertical gradient of potential temperature within 0.3 km (1000 ft) of the turbulent layer correlated well with high-altitude CAT.

With these and other theories and correlations as the bases for their studies, many researchers have attempted to construct successful procedures to forecast CAT. The first procedures reflected the inaccessibility of computers and therefore were simplified. Harrison (1959), for instance, examined data reported by commercial aircraft to determine the probability of an aircraft encountering CAT. He based his procedure upon the horizontal wind shear and the relative position of the jet stream.

As computers became accessible, standard meteorological data became easier to analyze and utilize. As a result, procedures to forecast CAT became more numerous and complex. Over the last few years, statistical analysis has been used widely as a research tool in developing forecasting procedures. Waco (1970) used the Chi-squared and Kolmogorov-Smirnov tests to determine the best atmospheric parameters which could be used in a forecasting procedure. Mancuso, Endlich, and Davies (1966), who found a 0.45 correlation coefficient between turbulence and the product of vertical wind shear and deformation, developed a technique to determine the climatology of turbulence. Cox (1973) used discriminant function analysis to determine functions, with synoptic-scale parameters as variables, which would discriminate occurrences and non-occurrences of stratospheric CAT.

2. Theory

The method of discriminant function analysis, a form of regression analysis, is hardly a new one, since Fisher (1936) developed it almost four decades ago. Since then, several studies have been undertaken by using the analysis to attempt to predict such non-numerical predictands as occurrences of precipitation (Panofsky and Brier, 1958), ceiling heights (Miller, 1962), and occurrences of CAT (Cox, 1973).

Discriminant function analysis formulates equations, composed of any number of terms involving parameters related to an event, which are capable of producing information identifying the occurrences and non-occurrences of that event. The greater the number of terms in the discriminant function, the greater the probability of obtaining an expression which perfectly discriminates Event 1 (the occurrence) from Event 2 (the non-occurrence) in a given data sample. However, it should be emphasized that the greater the number of terms in the discriminant function, the greater the probability of limiting the success of the discriminant function to the dependent sample only. In this research, the maximum number of terms considered was three.

Linear and non-linear discriminant function analyses are beneficial as research tools, since the ability of selected combinations of variables and the resulting functions to discriminate Event 1 from Event 2 in a sample can be determined easily. Additionally, once the most successful combination of variables has been determined, the resulting discriminant function can be used as a forecasting implement. After the values of the pertinent atmospheric parameters have been substituted into the discriminant function, the value of the function would indicate to which event the case would belong. If the functional value exceeded zero, the case would be classified as an occurrence of Event 1. If the functional value was less than zero, the case would be classified as an occurrence of Event 2.

a) Linear discriminant function analysis. The general form of the linear discriminant function is

$$L = c_0 + c_1 X_1 + c_2 X_2 + c_3 X_3 + \dots c_k X_k, \quad (2)$$

where $X_1, X_2, X_3, \dots X_k$ are numerical predictors and represent synoptic-scale atmospheric parameters in this research. The coefficients $c_1, c_2, c_3, \dots c_k$ are chosen in a manner to maximize the quantity

$$T^2 = \left(\frac{\bar{L}_1 - \bar{L}_2}{S_L} \right)^2,$$

where \bar{L}_1 and \bar{L}_2 are the average functional values for the respective Events, or Groups, and S_L is the standard deviation of L computed by pooling the sums of squares computed within each group.

The values of these coefficients were determined from the following set of equations:

$$c_1 \overline{x_1^2} + c_2 \overline{x_1 x_2} + c_3 \overline{x_1 x_3} + \dots + c_k \overline{x_1 x_k} = \frac{N_1 N_2 d_1}{(N_1 + N_2)^2}, \quad (3)$$

$$c_1 \overline{x_2 x_1} + c_2 \overline{x_2^2} + c_3 \overline{x_2 x_3} + \dots + c_k \overline{x_2 x_k} = \frac{N_1 N_2 d_2}{(N_1 + N_2)^2}, \quad (4)$$

$$c_1 \overline{x_3 x_1} + c_2 \overline{x_3 x_2} + c_3 \overline{x_3^2} + \dots + c_k \overline{x_3 x_k} = \frac{N_1 N_2 d_3}{(N_1 + N_2)^2}, \quad (5)$$

$$\begin{array}{ccccccc} \vdots & \vdots & \vdots & \vdots & \vdots & & \\ c_1 \overline{x_k x_1} + c_2 \overline{x_k x_2} + c_3 \overline{x_k x_3} + \dots + c_k \overline{x_k^2} & = & \frac{N_1 N_2 d_k}{(N_1 + N_2)^2}, & & & & (6) \end{array}$$

where $x_i = X_i - \bar{X}_{1+2}$ is the deviation of the value of the parameter, X_i , from the pooled mean of Groups 1 and 2; $d_i = \bar{X}_i - \bar{X}_i'$ is the difference between the mean of the parameter X_i of Group 1 and the mean of the parameter X_i of Group 2; and N_1 and N_2 are the total number of cases in the turbulent and non-turbulent Groups, respectively.

A part of the right-hand side of Eqs. (3) through (6), $N_1 N_2 / (N_1 + N_2)^2$, was used here in order to eliminate the need for a corrective term for the mean. If $N_2 / (N_1 + N_2)$ represents a predictand for all cases of Group 1 and $-(N_1 / (N_1 + N_2))$ represents a predictand for all cases of Group 2, the average value of the predictand is zero, since

$$N_1 \left(\frac{N_2}{N_1 + N_2} \right) + N_2 \left(\frac{-N_1}{N_1 + N_2} \right) = 0.$$

Therefore, the sum of the squares of the predictands is given by:

$$N_1 \left(\frac{N_2}{N_1 + N_2} \right)^2 + N_2 \left(\frac{-N_1}{N_1 + N_2} \right)^2 = \frac{N_1 N_2}{N_1 + N_2}.$$

After the k equations and k unknowns are solved by determinantal methods, the coefficients are substituted into the following equation so that c_0 , the corrective coefficient, can be determined:

$$c_0 = -c_1 x_1^* - c_2 x_2^* - c_3 x_3^* - \dots - c_k x_k^* , \quad (7)$$

where $x_i^* = (\overline{X_i} + \overline{X_i'})/2$ is the mean of the sum of the means of the parameter X_i of Groups 1 and 2. After the corrective coefficient has been calculated, the discriminant function of Eq. (2) is in a working form (Panofsky and Brier, 1958). When $L = 0$, in the case of a two-variable function, the resulting line in the $X_1 X_2$ plane represents the linear discriminant function which best discriminates Events 1 and 2. Figure 6 illustrates figuratively the discrimination performed by an ideal, linear, discriminant function involving atmospheric parameters X_1 and X_2 .

b) Non-linear discriminant function analysis. One disadvantage of the technique of using linear discriminant functions arises when the function discriminating Events 1 and 2 can discriminate best by becoming non-linear. The coefficients are determined from a set of equations similar to those which are used for the linear discriminant function analysis but containing powers of one or more of the variables. These equations assume the following form:

$$c_1 \overline{x_1^2} + c_2 \overline{x_1 x_2^2} + c_3 \overline{x_1 x_3^2} + \dots + c_k \overline{x_1 x_k^2} = \frac{N_1 N_2 d_1}{(N_1 + N_2)^2} , \quad (8)$$

$$c_1 \overline{x_2^2 x_1} + c_2 \overline{x_2^4} + c_3 \overline{x_2^2 x_3} + \dots + c_k \overline{x_2^2 x_k} = \frac{N_1 N_2 d_2}{(N_1 + N_2)^2} , \quad (9)$$

$$c_1 \overline{x_3 x_1} + c_2 \overline{x_3 x_2^2} + c_3 \overline{x_3^2} + \dots + c_k \overline{x_3 x_k} = \frac{N_1 N_2 d_3}{(N_1 + N_2)^2} , \quad (10)$$

$$\vdots \quad \quad \quad \vdots \quad \quad \quad \vdots \quad \quad \quad \vdots \quad \quad \quad \vdots$$

$$c_1 \overline{x_k x_1} + c_2 \overline{x_k x_2^2} + c_3 \overline{x_k x_3^2} + \dots + c_k \overline{x_k^2} = \frac{N_1 N_2 d_k}{(N_1 + N_2)^2} . \quad (11)$$

Figure 7 illustrates figuratively the improvement in the discrimination when the non-linear function is used. The broken line from point A to B represents the best linear discriminant function. This line did not discriminate perfectly occurrences of Events 1 and 2, since

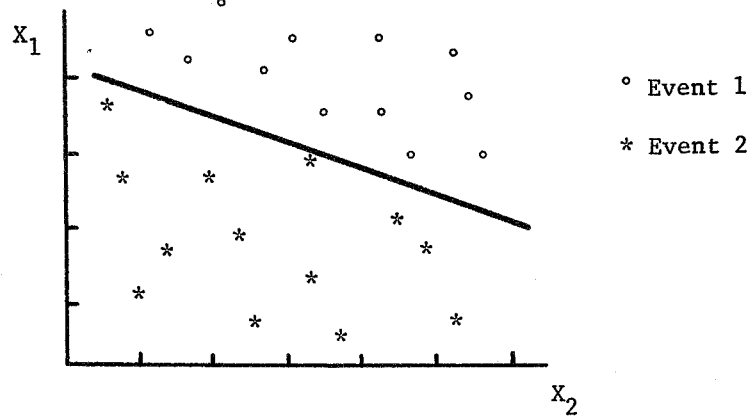


Fig. 6. Illustration of the discrimination of two events by an ideal, linear discriminant function.

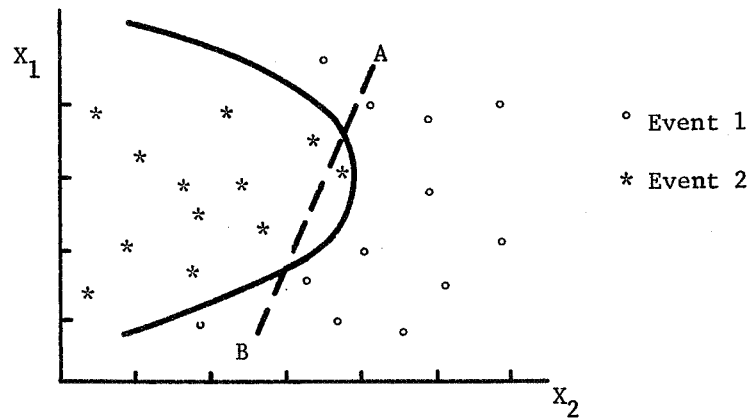


Fig. 7. Illustration of the discrimination of two events by an ideal, non-linear discriminant function. The dashed line, AB, represents the best linear discriminant function.

it incorrectly identified two occurrences of Event 1 and one occurrence of Event 2. Theoretically, utilizing non-linear discriminant function analysis, in some cases, should improve the ability to discriminate occurrences and non-occurrences of CAT (Groups 1 and 2, respectively), since only a few of the terms in turbulence theory are non-linear. An example is the square of the vertical wind shear in the denominator of the Richardson number, Eq. (1).

D. DATA

1. Aircraft

The turbulence data employed in this research were provided by the NASA Flight Research Center, Edwards, California, and were obtained by two instrumented supersonic aircraft while in flight in the 12.2-20.4-km (40,000-67,000-ft) layer of the atmosphere over the western United States. The XB-70 aircraft, which has been flown at speeds up to Mach 3.0 and altitudes over 21.3 km (70,000 ft), obtained turbulence data from 46 flights during the period of March 1965 to November 1967 (Fulton, 1968). These data were used in this research as the dependent sample. Data from 23 flights of the YF-12A aircraft, obtained during the period of March 1970 to January 1972, were used in this research as the independent sample.

The aircraft flights were not distributed evenly over the months of the calendar. However, the monthly percentages of the flights generally corresponded to the monthly percentages of all occurrences of turbulence reported by the Air Weather Service (Starch, 1968). This fact enhances the value of the aircraft sample.

Each aircraft was instrumented with a NASA VGH (velocity-vertical acceleration-height) recorder which provided continually air speed, normal accelerations at the center of gravity of the aircraft, and aircraft altitude. The peak-to-peak normal accelerations, measured in g-units, were assumed to be direct indications of the intensity of the encountered turbulence. It was assumed that both aircraft would respond identically to turbulence. These normal accelerations were encountered by the two aircraft along planned routes, which differed with each mission. However, since the primary purpose of the missions was to test the aircraft, in a few cases alternative routes were scheduled if moderate or severe turbulence was thought to occur along the selected route (Wilson et al., 1971).

The flight routes of the XB-70 aircraft and the encounters of turbulence were superimposed upon geographical maps of the western United States (Ehernberger, 1968). For every encounter of CAT, the time of encounter, peak-to-peak normal accelerations at the center of gravity of the aircraft, distance flown through

the turbulence, and pressure altitude were listed for each flight. The map of the data obtained from the XB-70 aircraft on November 2, 1965, is shown in Fig. 2. Similarly, maps were produced utilizing the information provided by the YF-12A aircraft.

Segments of the flight route, ~ 200 km in length, were classified as "turbulent" if more than one occurrence of turbulence was encountered along that portion. Some other segments of similar length were classified as "non-turbulent" if no turbulence was encountered by the aircraft along that portion. Turbulent and non-turbulent regions encompassing individual segments were established. Efforts were undertaken to maximize both the number of classified segments of a flight route and the distance separating each classified segment. It was necessary to separate the classified segments of the flight routes as far as possible in order to minimize the interdependence of the values of the synoptic parameters characteristic of one segment with those of another. As a result of this procedure, the 46 XB-70 aircraft flights yielded 94 turbulent and 78 non-turbulent segments, while the 23 YF-12A flights yielded 18 turbulent and 22 non-turbulent segments.

2. Meteorological

Since most of the data obtained from the aircraft missions were collected during midday, the preceding 1200 GMT and succeeding 0000 GMT rawinsonde data for the corresponding XB-70 and YF-12A flight days were utilized to analyze 300-, 200-, and 100-mb constant-pressure maps. Although large portions of the flight routes were well above the 100-mb surface, rawinsonde data above that level were not utilized since the accuracy of wind measurements above the 100-mb level deteriorates. In addition, Scoggins and Incrocci (1973) concluded that occurrences of stratospheric CAT were correlated with upper tropospheric and lower stratospheric (9.1-16.2 km or 30,000-53,000 ft) conditions.

Values of 69 atmospheric parameters characterizing each turbulent and non-turbulent region were determined from the many constant pressure charts by averaging the values of the parameters observed in the region containing the segment. It was assumed that the mean values of the parameters were representative of the values observed in the regions. The 69 atmospheric parameters are listed in Chapter III, and in Appendices A and B.

Synoptic-scale parameters which involved partial derivatives were computed by utilizing a square grid of 158-km spacing (illustrated by Fig. 1), and those which involved time changes were computed from the 1200 GMT to 0000 GMT time period. Values of all the parameters, except those involving rates of change, were determined from the 1200 GMT information since it was desired to characterize the state of the atmosphere before the turbulence was encountered. All the values which pertained to the XB-70 sample were stored on magnetic tape and those which pertained to the YF-12A sample were punched onto computer cards.

E. ANALYSIS OF DATA

1. Stratification

Since one objective of this research was to determine altitudes where CAT would occur, it was necessary to categorize the data into groups representing atmospheric sub-layers. The synoptic data pertaining to the regions in a sub-layer could, therefore, be utilized to determine discriminant functions which would predict the occurrence of turbulence in that particular sub-layer. The sub-layer, especially for the sample of dependent (XB-70) data, needed to be large enough to insure adequate sub-sample sizes, and to possess a sufficient number of turbulent and non-turbulent regions from which statistical results could be drawn.

Sub-samples were obtained by establishing 2.1-km (7000-ft) thick sub-layers from the 12.2- to 20.4-km (40,000- to 67,000-ft) layer sampled by the two aircraft. The thickness of the sub-layers was chosen on the basis of the distribution of data in the vertical and the desire to minimize the number of sub-layers. It is unknown whether the results would have been improved if a different thickness was chosen. By overlapping each sub-layer with adjacent sub-layers by 0.61 km (2000 ft), some of the regions and the appropriate synoptic data were used for more than one sub-layer. The number of regions in each sub-layer was increased to enhance the statistical significance of the data. The 112 turbulent and 100 non-turbulent regions from the XB-70 and YF-12A samples were separated into one or more of the following sub-layers:

12.2 - 14.3	(40,000 - 47,000),
13.7 - 15.9	(45,000 - 52,000),
15.2 - 17.4	(50,000 - 57,000),
16.8 - 18.9	(55,000 - 62,000), and
18.3 - 20.4 km	(60,000 - 67,000 ft).

2. Determination of variables used

The determination of synoptic-scale atmospheric parameters used in the analyses of turbulence is difficult since our understanding of CAT mechanisms is limited drastically. To compound the problem, the process of determining appropriate variable combinations for use in the discriminant function analysis also is difficult. The variables in one combination should be uncorrelated and each variable should, ideally, demonstrate some bimodality with respect to turbulent and non-turbulent regions in order for the analysis to yield accurate results. However, most parameters are at least slightly correlated physically, temporally, or spatially, and few parameters from a large sample are found to demonstrate a satisfactory degree of bimodality.

A variable-combination selective process was used by Miller (1962). Out of 75 atmospheric parameters available to predict ceiling heights, Miller's process defined only five which contained enough discriminatory information. In addition, Miller noted that there was no reason to believe that the selected

predictors were the best set obtainable from all the available predictors. Such an approach was neither feasible in this study, because of constraints imposed by budgetary considerations, nor sufficiently promising to warrant consideration.

Ideally, linear discriminant functions constructed from all possible two- and three-variable combinations should be calculated from the dependent data sample and tested from the independent data sample in order to determine the most significant combinations of variables. However, this is far from being practical, since the process would involve 54,740 linear discriminant functions and many hours of computer time that were not available for this work.

The first variable combinations used in this research were adopted from Cox (1973), who utilized the resulting functions to attempt to forecast the occurrence of turbulence in the stratosphere without stratification of the data. These combinations were selected as the result of a statistical study. Correlation matrices comprised of correlation coefficients between all 69 variable combinations were selected on the basis of two requirements. The first was that the absolute value of the correlation coefficient for the combined turbulent and non-turbulent regions be less than 0.30, while the second was that the absolute difference between the absolute values of the correlation coefficients for the turbulent and non-turbulent regions be greater than or equal to 0.30. Other two-variable and all three-variable combinations were chosen on the basis of their physical relationships to CAT.

3. Determination of linear discriminant functions

Based upon the theory of discriminant function analysis discussed previously, a computer program was designed to calculate the values of the coefficients once the combination of variables had been selected. The 112 combinations selected by Cox were used to construct 112 discriminant functions for each of the five sublayers. After the functions were constructed from XB-70 data, the computer was used to calculate the values of the functions by using simultaneous values of the proper variables from the dependent data sample. Theoretically, if the functional value exceeded zero, turbulence would be expected to occur; turbulence would not be expected to occur if the functional value was less than zero; and no conclusions would have resulted if the functional value equalled zero.

The initial indication of success of a discriminant function was based upon how well it identified both the turbulent and non-turbulent regions of the XB-70 sample in the appropriate sublayer. The computer program calculated the percentage of the total number of turbulent and non-turbulent regions identified correctly. Any function was considered to have potential as a turbulent predictive equation if both of the turbulent and non-turbulent verification percentages exceeded 60 per cent.

The two-variable combinations, for which the discriminant functions showed an initial indication of success, were used with a third variable to form three-variable combinations. For example, if the discriminant function comprised of the two-variable combination, A and B, discriminated rather well, functions comprised of combinations A-B-C, A-B-D, A-B-E, and so on were determined. The addition of the third variable usually yielded the same degree of success or improved the success of the two-variable combination. The three-variable functions which yielded results better than their two-variable counterparts were retained and the others were discarded.

The three-variable combinations, for which the discriminant functions indicated an initial success, were used again in an altered form. One variable at a time was changed in an attempt to improve the results. This process resulted in a fewer number of improvements than the one previously discussed. Attempts to improve the three-variable functions in a sub-layer ceased when at least five of them yielded results which identified correctly 70 per cent or more of the turbulent and non-turbulent cases.

4. Determination of non-linear discriminant functions

After the best linear discriminant functions were chosen for the five sub-layers, non-linear discriminant function analysis was employed. The computer program employed to construct linear discriminant functions was altered to construct non-linear functions composed of squared variables from the dependent data sample. Each of the three-variable combinations of the selected linear discriminant functions was used in this program three times, but each time a different variable in the combination was squared. The program again was altered so that discriminant functions comprised of more than one squared variable could be constructed.

As a result of this analysis, the discriminating line became a discriminating curve. A large majority of these discriminating curves yielded results that were worse than the discriminating lines. However, those non-linear functions which brought improvement were retained and their linear counterparts discarded.

5. Determination of predictive procedure for turbulence

The functions selected for the predictive procedure for each sub-layer, excluding the 16.8 to 18.9-km (55,000 to 62,000-ft) sub-layer, were determined by the following procedure. Those linear and non-linear functions which correctly discriminated at least 70 per cent of the turbulent and non-turbulent regions of the XB-70 sample for the sub-layers for which they were constructed were applied to the appropriate sub-layer of the YF-12A data. For each sub-layer, five of these discriminant functions, which produced the best results for the YF-12A sample, were selected. Those functions constructed

from the XB-70 sample that produced satisfactory results when applied to the YF-12A sample were considered to have a greater probability of discriminating turbulent regions when applied as a forecasting tool than those that did not. This assumes that the samples are representative.

A different procedure to determine the predictive functions used in the forecasting procedure was employed for the 16.8 to 18.9-km (55,000 to 62,000-ft) sub-layer, since very few of the many discriminant functions constructed from the XB-70 sample for this sub-layer produced acceptable results when applied to the YF-12A sample. Discriminant functions to be used in this sub-layer were determined from a combined sample of the XB-70 and YF-12A data. The percentage of the turbulent and non-turbulent regions identified correctly by each function for both of the XB-70 and YF-12A data samples was calculated. The five functions selected for this sub-layer were required to produce satisfactory results for each of the two samples. However, no independent data were available to test the formulated functions as in the cases of the other sub-layers.

6. Procedure for predicting the intensity of turbulence

An accurate predictive procedure to forecast the areas and heights of CAT in the stratosphere is desired. Therefore, an attempt to establish an objective forecasting procedure was a primary objective of this research. However, once that procedure has been determined and proven to be successful, the question as to the intensity of the predicted turbulence remains unanswered. It is to the pilot's advantage to know the intensity of the turbulence. If turbulence was expected to occur along the desired route, the pilot could alter his planned route, or reduce the speed of the aircraft when approaching and flying through the predicted turbulent area. Under certain conditions, the influence of turbulence on the aircraft can be decreased by reducing the speed of the aircraft, since the force exerting normal acceleration upon the aircraft is proportional to the product of the density of the atmosphere at that level and the speed of the aircraft (Burnham, 1969).

Three different procedures were investigated, one observational and two statistical in nature. The first approach examined the simultaneous values of several selected pairs of parameters for several intensities of turbulence. The turbulent regions of a sub-layer were categorized into three groups according to the intensities of the turbulence reports. The "light turbulence" group consisted of regions where turbulence caused normal accelerations at the center of gravity of the aircraft of less than 0.30 g-units; the "moderate turbulence" group included those which caused accelerations equal to or greater than 0.30 and less than 0.50 g-units; while the "severe turbulence" group included those which caused accelerations equal to or greater than 0.50 g-units.

The values of selected pairs of parameters and the intensities of the turbulence encountered within each sub-layer were plotted on graphs. An example for the 16.8 to 18.9-km (55,000 to 62,000-ft) sub-

layer with the 300-mb zonal wind speed and the 200-mb temperature as the pair of synoptic-scale parameters is illustrated in Fig. 8. The lines separating turbulence of different intensities were drawn subjectively. From this figure, it can be seen that the turbulent regions are grouped in a general fashion according to the intensity of the turbulence. However, since there was no objective procedure to choose which two variable combinations would be appropriate to indicate the intensity of the turbulence, another approach was pursued.

This approach utilized the values of the individual discriminant functions and the average value of the five chosen for each sub-layer. It was hoped that the values of the functions would indicate the intensity of the turbulence. The advantage of such a relationship is that the necessary information would already be available, since the functional values must be calculated to determine whether turbulence would occur.

The computed values of the five selected discriminant functions, which exceeded zero, as well as the arithmetic mean, for each sub-layer were plotted on a logarithmic scale and as a function of the intensity of the turbulence reported in that sub-layer. Only the functional values for the turbulent regions correctly identified by the discriminant function were plotted. The plots for the values of the functions for the 18.3 to 20.4-km (60,000 to 67,000-ft) sub-layer are illustrated in Fig. 9. The small circles in this illustration represent the mean of the functional values for the intensity group and the solid lines represent the range within one standard deviation of the mean.

The plots showed that some of the discriminant functions tended to have increasing values for increasing intensities of turbulence. However, the overlap of the functional values in the groups of intensities was too great to distinguish the intensity of the expected turbulence. Therefore, it was concluded that the results from this approach were unacceptable as a procedure for forecasting the intensity of turbulence. This confirmed the results obtained by Cox (1973).

The final approach made direct use of discriminant function analysis. This procedure required that the regions of the XB-70 and YF-12A aircraft data samples be separated into two groups unlike those used in the first discriminant function analysis. The regions where moderate or severe turbulence was reported were separated from those where light or no turbulence occurred.

From the combined XB-70 and YF-12A data samples, linear and non-linear discriminant functions were constructed and evaluated. The function which proved to discriminate best the intensities of the turbulence involved a three-variable combination -- the squares of two zonal wind-speed terms, and a vertical shear term. The resulting non-linear discriminant function is

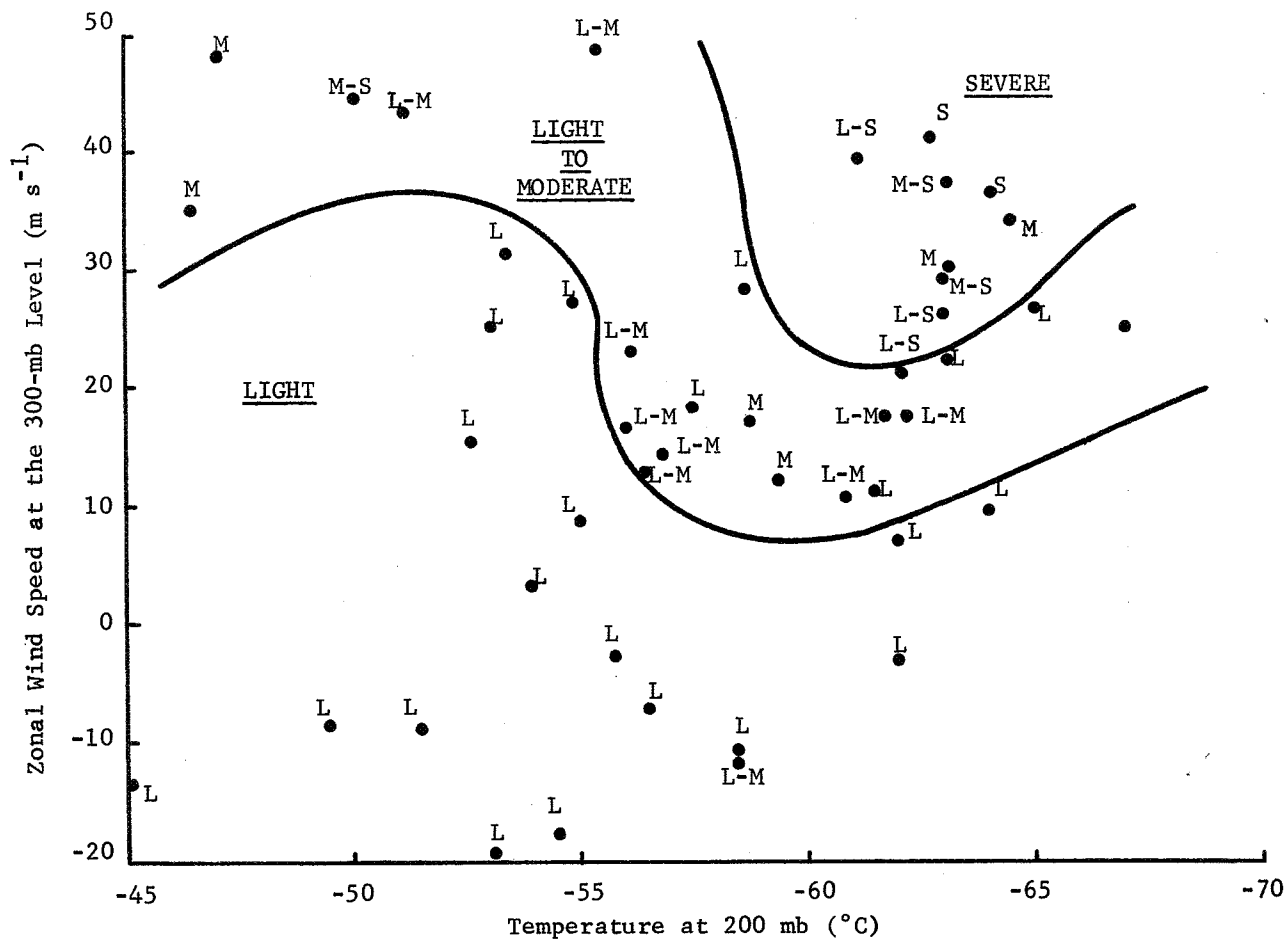


Fig. 8. Subjective discrimination of the intensities of the turbulence encountered by the XB-70 and YF-12A aircraft within the 16.8 - 18.9-km (55,000 - 62,000-ft) sub-layer.

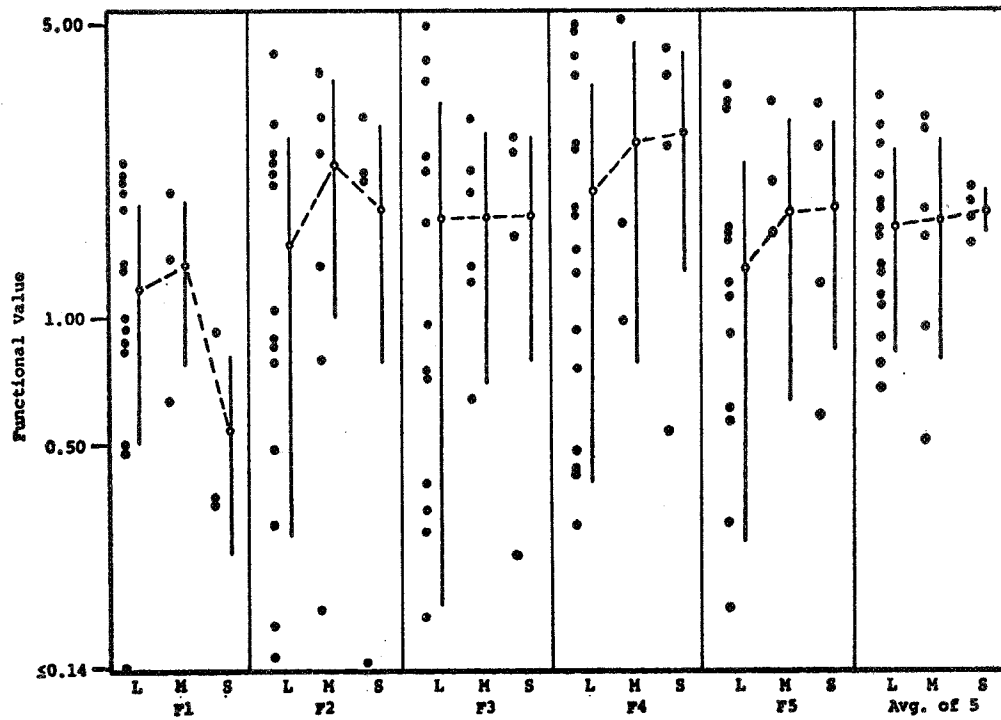


Fig. 9. Logarithmic plots of the positive values and the mean values of the five discriminant functions selected for the 18.3 - 20.4-km (60,000 - 67,000-ft) sub-layer as a function of the intensity of the turbulence. The open circles represent the mean value of the indicated function for the indicated intensity of turbulence. The solid lines represent the range within one standard deviation of the mean. The dashed lines connect the means of each function for each intensity category.

$$\begin{aligned}
L_T = & -0.266 + 8.424(10^{-5})(u_3)^2 \\
& + 28.84(\partial \vec{V}_h / \partial z)_{2-1} \\
& + 5.353(10^{-4})(u_1)^2 .
\end{aligned} \tag{12}$$

The set of parameters used in this equation has been associated with the occurrence of CAT in the lower stratosphere (Ehernberger, 1968; Cox, 1973).

If CAT was predicted in a given sub-layer and if $L_T > 0$, moderate to severe CAT would be expected; if $L_T < 0$, light CAT would be expected; and if $L_T = 0$, no predictive conclusions would be obtained. From this approach, out of the 56 moderate to severe turbulent regions and the 130 light or non-turbulent regions, 62.5 and 68.5 per cent, respectively, were identified correctly. The results indicate that discriminant function analysis is useful for the establishment of a procedure to predict the intensity of turbulence.

It should be noted, however, that the turbulence data used in this research was not well-suited for determining a procedure which forecasts the intensity of CAT. The pilots of the aircraft did not search for occurrences of moderate to severe CAT in areas of encountered light CAT. There is no guarantee that intensities of CAT other than those encountered by the aircraft were non-existent. All the intensities in regions of CAT must be disclosed in order to obtain a data sample suitable for use in determining discriminant functions capable of forecasting the intensity of CAT.

F. RESULTS

The five functions selected for each of the five sub-layers are listed in Table 6. The definition of the symbols used in the functions are listed at the end of this table. The percentages of the turbulent (T) and non-turbulent (NT) regions identified correctly by the individual discriminant functions and the number of turbulent and non-turbulent regions in each sub-layer for the two samples are listed in Table 7. It is important to note that the vast majority of the discriminant functions formulated for the 12.2 to 14.3-km (40,000 to 47,000-ft) sub-layer incorrectly identified the only non-turbulent region for this sub-layer from the independent data sample; hence a zero verification percentage resulted. Conversely,

Table 6. The five discriminant functions selected for each sub-layer.

	x_1	x_2	x_3	c_0	c_1	c_2	c_3
<u>12.2-14.3-km (40,000-47,000-ft) Sub-Layer</u>							
F1	v_1	T_1	$\partial(-\vec{V} \cdot \vec{\nabla} \zeta)_3 / \partial t$	1.430	-2.077×10^{-2}	2.305×10^{-2}	1.835×10^{11}
F2	H_2	V_2^2	v_1	6.191	-5.896×10^{-4}	1.942×10^{-4}	-1.551×10^{-2}
F3	u_2	v_2	$\partial(-\vec{V} \cdot \vec{\nabla} T)_2 / \partial t$	-0.108	3.710×10^{-3}	-9.847×10^{-3}	-6.785×10^6
F4	H_2	u_1	βv_3	6.969	-5.959×10^{-4}	8.573×10^{-2}	-1.533×10^8
F5	H_3	u_1	$(\partial \Gamma_{2-1} / \partial t)^2$	8.656	-9.394×10^{-4}	8.746×10^{-3}	1.152×10^{14}
<u>13.7-15.4-km (45,000-52,000-ft) Sub-Layer</u>							
F1	H_3	V_1	η_1	1.656	-3.662×10^{-4}	2.902×10^{-2}	1.386×10^4
F2	H_2	V_2	v_2	7.307	-6.413×10^{-4}	1.498×10^{-2}	-2.941×10^{-3}
F3	H_2	$(\beta v_1)^2$	Ri_{2-1}	8.725	-7.153×10^{-4}	2.281×10^{18}	-3.558×10^{-3}
F4	V_2	T_1	$\partial(-\vec{V} \cdot \vec{\nabla} \zeta)_1 / \partial t$	1.840	1.230×10^{-2}	3.445×10^{-2}	4.439×10^{12}
F5	T_1	Ri_{2-1}	$\partial(\beta v_2) / \partial t$	2.242	3.373×10^{-2}	-2.671×10^{-3}	2.296×10^{13}

Table 6. (continued)

	x_1	x_2	x_3	c_0	c_1	c_2	c_3
<u>15.2-17.4-km (50,000-57,000-ft) Sub-Layer</u>							
F1	V_3	T_2	$(\partial \vec{V}_h / \partial z)_{2-1}$	-0.548	2.379×10^{-2}	-4.828×10^{-3}	-6.731×10^1
F2	V_3	$\partial \zeta_1 / \partial t$	$\partial (\partial \vec{V}_h / \partial z)_{2-1} / \partial t$	-0.318	1.395×10^{-2}	-1.547×10^8	8.229×10^5
F3	H_2	V_2	v_2	-1.461	9.413×10^{-5}	1.470×10^{-2}	-3.385×10^{-2}
F4	V_1	T_1	ζ_2	1.110	2.685×10^{-2}	2.323×10^{-2}	6.758×10^2
F5	V_1	T_1	$(\partial (-\vec{V} \cdot \vec{\nabla} \zeta)_1 / \partial t)^2$	1.395	2.498×10^{-2}	2.740×10^{-2}	6.029×10^{24}
<u>16.8-18.9-km (55,000-62,000-ft) Sub-Layer</u>							
F1	V_1	$(\partial \vec{V} / \partial n)_1$	ζ_2	-0.294	2.173×10^{-2}	4.041×10^3	1.198×10^2
F2	V_1	$(-\vec{V} \cdot \vec{\nabla} T)_3$	Γ_{2-1}	-0.227	1.969×10^{-2}	4.870×10^2	3.628×10^1
F3	V_1	Γ_{2-1}	ζ_2^2	-0.252	2.053×10^{-2}	4.217×10^1	4.660×10^6
F4	V_1	u_1	ζ_2	-0.316	3.575×10^{-2}	-1.563×10^{-2}	1.073×10^2
F5	$\partial T_1 / \partial t$	$\partial C_i / \partial t$	$(-\vec{V} \cdot \vec{\nabla} T)_1$	-6.297	2.721×10^3	-3.198	-2.829×10^3

Table 6. (continued)

	x_1	x_2	x_3	c_0	c_1	c_2	c_3
	<u>18.3-20.4-km (60,000-67,000-ft) Sub-Layer</u>						
F1	V_1	$(\partial \vec{V} / \partial n)_1$	ζ_2	-0.568	3.855×10^{-2}	4.598×10^3	9.611×10^2
F2	V_1	v_1	ζ_2	-0.565	3.915×10^{-2}	-4.348×10^{-3}	1.271×10^3
F3	H_3	$\partial T_1 / \partial t$	Γ_{2-1}	4.643	-5.067×10^{-4}	5.170×10^3	5.142×10^1
F4	H_2	$\partial Ci / \partial t$	$(-\vec{V} \cdot \vec{\nabla} T)_1$	6.171	-5.206×10^{-4}	-5.892	2.493×10^2
F5	V_1	$(\partial \vec{V}_h / \partial z)_{2-1}$		3.204	-1.113×10^{-2}	-5.609×10^1	

List of Symbols

V	Scalar wind speed	η	Absolute vorticity
u	Zonal wind speed	T	Temperature
v	Meridional wind speed	Γ	Temperature lapse rate
$\partial \vec{V}_h / \partial z$	Vertical vector wind shear	H	Pressure height
$\partial \vec{V} / \partial n$	Horizontal vector wind shear	β	Coriolis parameter
ζ	Relative vorticity	Ri	Richardson number
Ci	CAT Index developed by Colson and Panofsky (1965)		

Subscripts 1, 2, and 3 denote the 100-, 200-, and 300-mb levels, respectively.

Table 7. Verification percentages*of the turbulent (T) and non-turbulent (NT) regions for the functions presented in Table 6. The number of turbulent and non-turbulent regions for each sub-layer is indicated.

	F1		F2		F3		F4		F5		Number of Regions	
	T	NT	T	NT	T	NT	T	NT	T	NT	T	NT
<u>12.2-14.3 km (40-47 x 10³ ft)</u>												
XB-70	83.3	90.0	81.8	90.0	83.3	80.0	81.8	70.0	78.8	70.0	33	10
YF-12A	66.7	00.0	75.0	00.0	85.7	00.0	75.0	00.0	66.7	00.0	14	1
<u>13.7-15.9 km (45-52 x 10³ ft)</u>												
XB-70	84.8	92.3	72.7	92.3	78.8	84.6	72.7	76.9	75.8	69.2	33	13
YF-12A	53.8	00.0	93.3	100.0	92.3	100.0	69.2	100.0	61.5	100.0	15	1
<u>15.2-17.4 km (50-57 x 10³ ft)</u>												
XB-70	76.1	88.2	78.3	82.4	69.6	88.2	80.4	70.6	78.3	70.6	46	17
YF-12A	92.9	60.0	78.6	40.0	86.7	33.3	71.4	40.0	71.4	60.0	15	6
<u>16.8-18.9 km (55-62 x 10³ ft)</u>												
XB-70	60.0	83.3	65.7	80.0	65.7	80.0	57.1	86.7	68.6	60.0	35	30
YF-12A	80.0	41.7	70.0	50.0	70.0	58.3	80.0	58.3	60.0	75.0	11	13
<u>18.3-20.4 km (60-67 x 10³ ft)</u>												
XB-70	72.7	75.0	72.7	70.0	69.7	70.0	69.7	67.5	60.6	62.5	33	40
YF-12A	66.7	55.6	66.7	55.6	66.7	77.8	33.3	66.7	66.7	77.8	3	9

*Because of missing meteorological data some percentages are based on a number of regions less than shown in the table; however, in no case was the number reduced by more than 3.

the majority of the discriminant functions formulated for the 13.7 to 15.9-km (45,000 to 52,000-ft) sub-layer correctly identified the only non-turbulent region for this sub-layer from the independent data; hence a 100 per cent verification for four of the five chosen discriminant functions resulted.

The results of the individual discriminant functions determined in this research were much better than those obtained for the functions formulated by Cox (1973). Cox made no effort to stratify the synoptic and turbulence data before formulating discriminant functions. Instead, the complete dependent data sample was used to formulate discriminant functions, which attempted to identify turbulent regions in unspecified layers of the lower half of the stratosphere. He then stratified the turbulent and non-turbulent regions into three 3-km (10,000-ft) sub-layers in order to examine the verification percentages of the four discriminant functions selected. The combinations of the variables used in the functions, the ability of the functions to discriminate the regions, and the number of turbulent and non-turbulent regions in each of the two samples are listed in Table 8. Cox found that the functions discriminated best for the regions of the 13.8 to 16.8-km (45,000 to 55,000-ft) sub-layer and noted that nine of the ten variables used in these functions represented atmospheric conditions within this layer.

In every sub-layer, more than ten different variables have been shown to be related to stratospheric clear-air turbulence. It would be advantageous to consider more than three variables when determining whether turbulence should occur within a sub-layer. Therefore, it was believed that the predictive capabilities of the discriminant functions considered collectively would be improved by incorporating the best five discriminant functions of each sub-layer.

The forecasting procedure employing this concept was based upon the simultaneous values of the five functions of a sub-layer. If four or five of the values of the discriminant functions for a region in a sub-layer exceeded zero, clear-air turbulence would be expected to occur in that region of the sub-layer. If one or two of the values of the discriminant functions for a region in a sub-layer were less than zero, no turbulence would be expected to occur in that region of the sub-layer. When only three of the values were either greater or less than zero, no predictive information was obtained.

The percentage of turbulent and non-turbulent regions for the XB-70 (dependent) and YF-12A (independent) data samples in each sub-layer, correctly identified by the forecasting procedure, are shown in Table 9. Also shown for each sub-layer is the number of

Table 8. Summary of results obtained by Cox (1973).

Function	Number of regions		
	T	NT	
$F1 = F1(V_3^\dagger, V_1, (\partial\vec{V}/\partial n)_2)$			
$F2 = F2(u_3, u_1, (\partial\vec{V}_h/\partial z)_{2-1})$	XB-70	93	56
$F3 = F3(u_2, (\partial\vec{V}/\partial n)_1, T_1)$	YF-12A	16	21
$F4 = F4(V_1, \zeta_2)$			

Verification percentages of Functions

	F1		F2		F3		F4	
	T	NT	T	NT	T	NT	T	NT
<u>Total XB-70 sample</u>	61.7	71.8	62.8	62.8	62.8	61.5	64.9	57.7
<u>≤ 13.8 km (45,000 ft)</u>								
XB-70	53.0	*	60.0	*	60.0	*	53.0	*
YF-12A	*	*	*	*	*	*	*	*
<u>13.8-16.8 km (45,000-55,000 ft)</u>								
XB-70	75.0	95.0	71.0	90.0	71.0	85.0	71.0	80.0
YF-12A	77.0	38.0	77.0	75.0	62.0	38.0	77.0	38.0
<u>> 16.8 km (55,000 ft)</u>								
XB-70	58.0	67.0	60.0	50.0	60.0	47.0	66.0	55.0
YF-12A	*	8.0	*	17.0	*	17.0	*	42.0

*Insufficient Data

†Subscripts 1, 2, 3 denote the 100-, 200-, and 300-mb levels, respectively.

regions where no predictive conclusions (NPC) were obtained by the forecasting procedure. The results for both data samples were generally in good agreement, with the verification percentage exceeding eighty in most instances. Statistical variations in the relatively small sample sizes (10 to 60) in each sub-layer could easily account for the differences noted.

Table 9. Verification percentages (VP) of the turbulent and non-turbulent regions* in the sub-layers of the XB-70 (dependent) and YF-12A (independent) samples for the turbulence forecasting procedure. Also listed is the number of regions where no predictive conclusions were obtained (NPC).

Sub-Layer (km)	Turbulence						Non-Turbulence					
	XB-70			YF-12A			XB-70			YF-12A		
	VP(%)	N	NPC	VP(%)	N	NPC	VP(%)	N	NPC	VP(%)	N	NPC
12.2 - 14.3	93.3	33	3	81.8	14	1	90.0	10	0	00.0	1	0
13.7 - 15.9	87.5	33	1	100.0	15	1	92.3	13	0	100.0	1	0
15.2 - 17.4	86.4	46	2	90.9	15	3	88.2	17	0	80.0	6	1
16.8 - 18.9	74.1	35	8	88.9	11	1	93.3	30	0	60.0	13	2
18.3 - 20.4	86.2	33	4	100.0	3	1	90.9	40	7	87.5	9	1

*Based on turbulence and non-turbulence encounters in each sub-layer. If, in a region defined as turbulent or non-turbulent, the aircraft was changing altitude the discriminate functions for each sub-layer penetrated by the aircraft were evaluated. This resulted in more encounters than regions.

G. SUMMARY

The development of discriminant functions, with synoptic-scale parameters as variables, capable of predicting the areas and altitudes of stratospheric clear-air turbulence was the primary goal of this research. Also, predictive methods indicating the intensity of the predicted turbulence were investigated. The data employed in this study consisted of two samples of turbulence data obtained by the XB-70 and YF-12A aircraft, and 69 synoptic-scale parameters determined from rawinsonde data; discriminant function analysis was the primary analytical tool.

The samples of turbulence data were obtained from stratospheric flights (12.2 to 20.4 km or 40,000 to 67,000 ft) during the period March 1965 to January 1972. With each report of turbulence, the following information was provided: 1) geographical location; 2) time of the encounter; 3) peak-to-peak normal accelerations at the center of gravity of the aircraft; 4) distance flown in turbulence; and 5) pressure altitude. Since the encounters of turbulence were scattered along the flight routes, segments of the flight routes approximately 200 km in length were classified as turbulent or non-turbulent. As a result, 94 turbulent and 78 non-turbulent segments were defined from the XB-70 sample and 18 turbulent and 22 non-turbulent segments were defined from the YF-12A sample.

The values of 69 synoptic-scale parameters, assumed to represent atmospheric conditions along the turbulent and non-turbulent segments, were determined from data obtained from the United States rawinsonde network. The parameters involving partial derivatives were computed from a square grid having a spacing of ~ 158 km, and those involving time changes were computed over a 12-h time period encompassing each flight. All others were determined from 1200 GMT information. These values and the segments they represent were grouped into classes representing 2.1-km (7000-ft) sub-layers of the stratosphere.

Two- and three-variable combinations of synoptic-scale parameters then were selected by a statistical process and by intuition. Discriminant function analysis was employed to formulate discriminant functions for the five sub-layers of the dependent, XB-70 aircraft, data sample. For each sub-layer, five functions that best discriminated the turbulent from the non-turbulent regions within that sub-layer were retained and the others were discarded. The occurrence of turbulence would be predicted in the sub-layer when four or more of the five appropriate functions had values greater than zero. If two or less had values greater than zero, turbulence would not be predicted. No predictive information would be available if three of the functions had values greater than or less than zero. This procedure, for the most part, correctly identified over 85 per cent of the turbulent and non-turbulent regions in each of the five sub-layers.

After the forecasting procedure was finalized, three different approaches were investigated to predict the intensity of the turbulence. The first attempted to find pairs of synoptic-scale parameters whose simultaneous values would indicate the intensity of the expected turbulence. One pair of parameters (the 300-mb zonal wind speed and the 200-mb temperature) was rather successful in grouping the intensities of the turbulence reported by both aircraft.

Another approach was examined since there was no objective manner to select the pairs of atmospheric parameters in the first approach. This approach examined the possibility of the functional values being correlated to the intensities of the turbulence. Although the mean of some of the values increased with increasing intensities, the functional values were not distributed well enough for this approach to be useful.

The last approach employed discriminant function analysis to formulate a function which would indicate the intensity of the turbulence. A function involving the squares of the 100- and 300-mb zonal wind speeds, and the vertical wind shear proved to be rather successful. Out of the 56 moderate or severe turbulent segments and the 130 light or non-turbulent segments, 62.5 and 68.5 per cent, respectively, were identified correctly. The results indicate that discriminant function analysis can be used as a technique to develop a procedure to forecast the intensity of turbulence.

H. CONCLUSIONS

The results of this research indicate that there is, indeed, a relationship between selected combinations of synoptic-scale parameters of the upper troposphere and lower stratosphere and stratospheric CAT. They suggest further the possibility that synoptic-scale parameters influence the mesoscale features which are responsible for the occurrences of CAT. The discriminant functions formulated from selected combinations of some of these parameters were successful in discriminating between the turbulent and non-turbulent regions in sub-layers of the stratosphere. The percentages of the regions identified correctly were considerably improved over those resulting from the functions formulated from non-stratified data by Cox (1973). This indicates that turbulent and non-turbulent segments of the XB-70 and YF-12A samples were identified more accurately by discriminant functions formulated from stratified data samples than those from the entire sample. The functions formulated in this research could prove to be valuable for an objective forecasting procedure for stratospheric CAT.

There seems to be a possibility that the intensity of turbulence can be predicted by discriminant function analysis. A discriminant function which indicated the intensity of the expected turbulence was constructed and indicated correctly over 60 per cent of the moderate-or-severe turbulent and light turbulent regions. Further research should improve the verification percentage.

The success of discriminant functions as predictors of CAT derived in this research will depend partly upon the degree of representativeness of the data samples used. It also will depend upon the effect of the unequal number of turbulent and non-turbulent regions in some of the sub-layers of the data samples. It also will depend on the quality of the data used for verification and on the representativeness of off-track data to conditions along the track.

The variable combinations selected were chosen on the basis of their theoretical relationships to turbulence and as a result of a variable correlation analysis and intuition. Ideally, the variables in a combination should not be correlated with each other and should demonstrate some bimodality with respect to the occurrences and non-occurrences of turbulence regions. However, since the ideal criterion for the variable combination would have severely limited the number of combinations, an altered form was used. There is no certainty, however, that the variable combinations of the most successful discriminant functions formulated in this research are the best possible.

There are a few disadvantages in the nature of the turbulence data reported by the two aircraft that could have influenced the results. For one, most of the flights were in the Spring and very few in the Summer. Moreover, turbulence very likely could have existed in other altitudes of the regions where the aircraft reported no turbulence. Similarly, moderate or severe turbulence could have existed in other altitudes of the regions where the aircraft reported only light turbulence. The primary purpose of the aircraft missions was to test the handling and structure of the aircraft, and not to search for regions of turbulence (Wilson *et al.*, 1971). Finally, it should be emphasized that the reported intensity of the turbulence was a function of the product of aircraft speed and air density at the flight altitude. Due to the high speed of the aircraft, stable gravity waves could have caused the aircraft to encounter normal accelerations in regions where no turbulence existed.

CHAPTER V. THE CURVATURE OF THE WIND PROFILE AS A FACTOR IN THE
FORMATION OF CLEAR AIR TURBULENCE

by

Norman Charles Possiel, Jr.
Center for Applied Geosciences
Texas A&M University, College Station, Texas

A. ABSTRACT

This study concerns the importance of the curvature of the wind profile to the amplitude of mountain waves. Mechanisms favorable for clear-air turbulence (CAT) are discussed in relation to such wave motions.

Relationships between CAT encountered in the stratosphere by an-XB-70 aircraft over mountain-wave areas and the curvature of the wind profile in the troposphere are studied. Expected mountain-wave areas are defined from topographical and tropospheric wind criteria. Areal fields of the vertical gradient of curvature are determined and related to the distribution of mountain-wave areas and turbulent and non-turbulent regions encountered by the XB-70. The results indicate that turbulent regions in the stratosphere are most likely over mountain-wave areas where the vertical gradient of curvature is positive, and that turbulent-free regions can be expected outside of mountain-wave areas where the vertical gradient of curvature is negative. These relationships were tested by using two independent XB-70 flights.

B. INTRODUCTION

The development of supersonic military and commercial aircraft has led to an increase in concern about the occurrence of turbulence in the stratosphere. The United States and the Soviet Union are using supersonic aircraft in their military programs, and the Anglo-French Concorde is in commercial service. Test flights by the XB-70 supersonic aircraft over the western United States during 1967 and 1968 have provided a measure of the extent and intensity of stratospheric turbulence encounters (Ehernberger, 1968). These data are amenable to analysis aimed at revealing the nature of the turbulence.

With respect to the topography of the western United States, it has been suggested that mountain waves may play a fundamental role in the generation of stratospheric turbulence (Ehernberger, 1968; Foltz, 1967; Burnham, 1968). Mountain waves are quasi-stationary gravity waves with typical wavelengths of 1 to 25 km which form when the wind crosses a mountain ridge with speeds in excess of some critical value and the Scorer parameter decreases rapidly with height.

The rate of the vertical decrease of the Scorer parameter depends upon static stability and the curvature of the wind profile. While it is assumed generally that stability is the dominant factor, Scoggins and Incrocci (1973) have shown that curvature is of equal importance. When mountain waves form, the local structure of the atmosphere is modified; this may lead to conditions favorable for the formation of CAT (Foltz, 1967).

Results of the Sierra Wave Project (Holmboe and Klieforth, 1957) indicate that stratospheric turbulence is more intense and frequent over mountainous regions than over flat terrain. Indeed, turbulence encountered on 14 flights by the RAE PR9 Canberra aircraft in the stratosphere while flying through mountain waves over the western United States was reported to be as severe and extensive as that experienced near large thunderstorms (Burnham, 1968). Clear-air turbulence, such as experienced by aircraft in the stratosphere, is believed to be caused by the breakdown of organized wave motions into turbulent flow, or by the encounter of the aircraft with a succession of waves while traveling at supersonic speeds. Turbulence encountered in the vicinity of thunderstorms, however, is due to horizontal variations in the vertical-motion field caused by buoyancy and wind shears associated with the local structure of the storm. This study will be concerned with clear-air turbulence caused by mechanical production since it is this type which is associated with mountain waves.

1. Statement of the problem

The prediction of the specific location of turbulence is a difficult problem because there is a large difference in scale between clear-air turbulence (CAT) and the standard rawinsonde observations (Reiter and Foltz, 1967), which provide the only routine data at upper-tropospheric and lower-stratospheric altitudes. Even so, such data must be considered judiciously, because the soundings may not be taken within many miles of the track of the aircraft. Clear-air turbulence is a mesoscale phenomenon with typical horizontal dimensions less than 150 km (Reiter, 1969). Rawinsonde observations, however, are made on a synoptic scale where stations are on the order of 400 km apart. Thus, any direct measurement of CAT by rawinsonde data is mainly fortuitous (Dutton and Panofsky, 1970). However, Scoggins et al. (1972), in a detailed study of several dynamic, kinematic, and thermodynamic atmospheric variables, suggested that it is possible to relate mesoscale phenomena to synoptic-scale conditions which, in turn, may often be determined adequately from rawinsonde data.

2. Objectives

Scoggins and Incrocci (1973) examined the relationships between mountain wave conditions and turbulence encountered by the XB-70 in the stratosphere. They achieved some success in associating days with turbulence with characteristics of the vertical profile of the Scorer parameter, k^2 , determined from rawinsonde data. In particular, they

found that the curvature term, which is a measure of the curvature of the wind with height, becomes important in the determination of the magnitude of l^2 when mountain waves were expected or observed. Therefore, the objectives of this research are to:

- a) Examine, from a theoretical point of view, the influence of curvature on the formation and amplitude of mountain waves;
- b) Examine and "clarify" the theoretical relationship between mountain waves and the generation of turbulence; and,
- c) Establish the relationship between curvature and turbulence encountered by the XB-70 in the stratosphere over mountainous terrain.

C. BACKGROUND TO PRESENT RESEARCH

1. Theoretical influence of curvature upon mountain waves

Corby and Wallington (1956), from Scorer's (1949) lee-wave theory, derived an equation that expresses the maximum value of the amplitude of mountain waves, A_m :

$$A_m = \frac{L^2 \sin^2 \varphi}{(l_s^2 + L^2 \cos^2 \varphi)^{\frac{1}{2}} (n\pi - \varphi + \tan \varphi)}, \quad [m^{-1}] \quad (13)$$

where

$$L^2 = (l_i^2 - l_s^2),$$

i denotes a lower layer,

s denotes an upper layer,

$$l^2 \text{ is the Scorer parameter} = \left(g \frac{\beta}{U^2} - \frac{U''}{U} \right) \quad [m^{-2}],$$

$\frac{g\beta}{U^2}$ is the stability term,

$\frac{U''}{U}$ is the curvature term (hereafter referred to as curvature),

U is horizontal wind speed $[m \text{ s}^{-1}]$,

U'' indicates the second derivative of horizontal wind speed with respect to height, z ,

$$g \approx 9.8 \text{ m s}^{-2}$$

$\beta = \frac{1}{\bar{\theta}} \frac{\partial \bar{\theta}}{\partial z}$, where $\bar{\theta}$ is mean potential temperature in a layer $[K]$,

φ is a phase angle between 0 and $\pi/2$, and

n is an integer with values of 1, 2, 3....

From Eq. (13), Corby and Wallington state that lee waves having large amplitude will exist when L^2 is large. By examination of conditions which lead to large values of L^2 , the influence of curvature is revealed.

The variable, L^2 , attains its largest value when:

- a) l_s^2 approaches zero, and
- b) l_i^2 has a large positive value.

It is evident that l_s^2 will approach zero if the stability term is small and the curvature term is large and positive. Similarly, l_i^2 will have a large positive value if the stability term is large and the curvature term is large and negative.

In consideration of air mass characteristics, L^2 will thus attain its largest magnitude where the stability decreases and the curvature increases with altitude in the troposphere. This relationship is illustrated by several examples of vertical profiles of the stability term and the curvature term that were determined when mountain waves were expected (Fig. 10). Similar conditions were observed during the Sierra Wave Project (Holmboe and Klieforth, 1957) upstream of the ridge crest. Therefore, the curvature term is important in determining the magnitude of L^2 and from Eq. (13) the mountain-wave amplitude. Moreover, since the curvature term generally varies more with altitude than the stability term, as shown in Fig. 10, the former may exert the greater influence.

2. Large-amplitude mountain waves in the stratosphere

Although Scorer's (1949) lee-wave theory characterizes wave motions in the troposphere, he later (Scorer, 1954) suggested that high level "nacreous" clouds may be induced by mountain-wave motions. Gotaas (1961) concluded, after considerable case studies and documentation, that these clouds must indeed be generated by mountain waves.

Corby and Sawyer (1958) and Hines (1960) state that a broad spectrum of waves can be generated by air flowing over irregular terrain. Some of these waves have large amplitude in the upper troposphere and lower stratosphere, and can be propagated horizontally in airstreams which contain favorable wind and stability conditions near the tropopause (Corby and Sawyer, 1958). Hines (1960) states that waves initiated by tropospheric wind disturbances can be propagated upward through the stratosphere to considerable heights. In addition, Sawyer (1960), in a numerical application of the basic wave equations, found that large-amplitude mountain waves can exist near the tropopause.

Eliassen and Palm (1961) state that mountain waves having a wavelength of at least 30 km are capable of being propagated from the mountain top into the stratosphere. Palm and Foldvik (1960), in their study of mountain-wave characteristics, found that a mountain ridge 700-m high can cause a 400-m displacement of the airstream at an altitude of 20 to 30 km. Further evidence of high-altitude

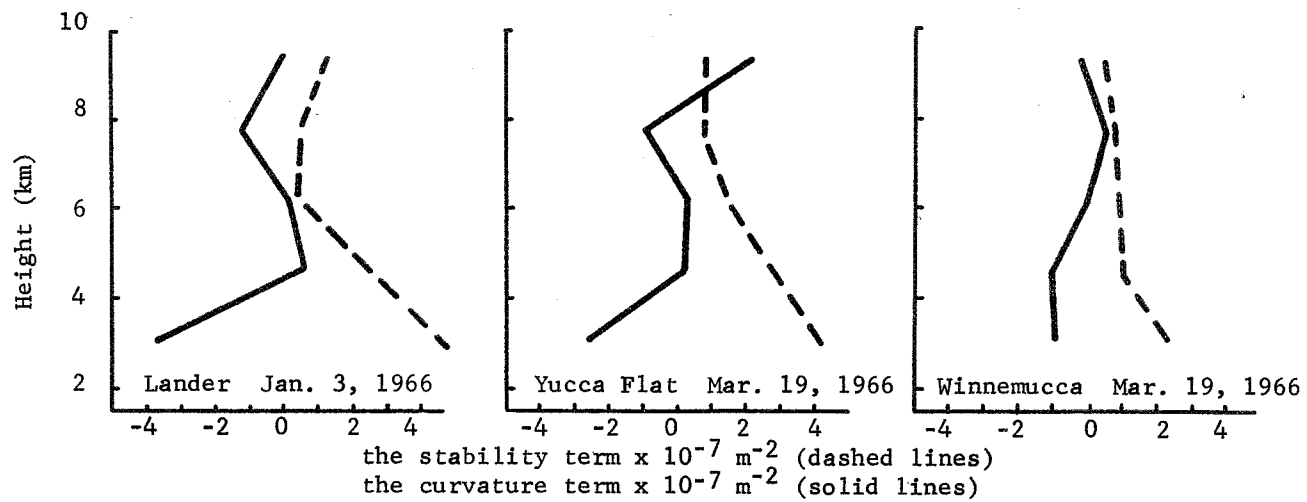


Fig. 10. Examples of the vertical profiles of the stability and curvature terms that were determined when mountain waves were expected.

mountain waves was found during the Sierra Wave Project when sail plane flights reached a height of 10 km during strong wave conditions (Holmboe and Klieforth, 1957).

3. Influence of wave motions upon energy transfer and the generation of turbulence

It has been suggested that energy of the tropospheric airstream may be propagated vertically by the spectrum of mountain-induced waves (Hines, 1960). Although the exact mechanism behind the transfer of energy is not known, wave energy is propagated with the speed of the group velocity of the wave pattern (Haltiner and Martin, 1957). Hines and Reddy (1967) state that this wave energy may be intensified by the wind and temperature structure at high levels, although no indication was given of any particular wind or temperature distributions which would favor intensification. However, for energy to be propagated to high levels of the atmosphere the wind direction must remain essentially constant from the surface to the level where the energy is absorbed (Eliassen and Palm, 1961).

Eliassen and Palm (1961) assert that wave energy propagated to high levels may be converted to turbulent energy. Reiter and Foltz (1967) offer the theory that the energy of standing lee waves may "cascade" downscale and "feed" small-scale motions which, in turn, may be experienced by aircraft as CAT. They also state that aircraft measurements have indicated that CAT found in thermally stable regions can be associated with the breakdown of organized waves into turbulent eddies.

Dutton and Panofsky (1970) state that large perturbations such as mountain waves may initiate atmospheric turbulence. From the theoretical discussion in this study, it was shown that large-amplitude mountain waves may be generated by an increase in curvature with height (increasing wind shear). In addition, an examination of the airflow through a lee-wave train indicates that sinking air between crests and troughs causes the formation of thermal inversions. The following discussion of CAT mechanisms shows how these same wind and stability conditions are favorable for the generation of turbulence.

One CAT mechanism is a large wind shear across a narrow thermal inversion (Lumley and Panofsky, 1964). The Richardson number, Ri , believed to be an important indicator of turbulent flow is defined by:

$$Ri = \frac{g}{\bar{\theta}} \frac{\partial \bar{\theta} / \partial z}{|(\partial \bar{v} / \partial z)|^2}, \quad (14)$$

where \bar{V} is the average vector horizontal wind, and the other variables are as previously defined. Lumley and Panofsky (1964) state that when Ri decreases below some critical value, Ri_c , the generation of turbulence by wind shear exceeds its dissipation by buoyancy. The existence of turbulence, therefore, depends essentially upon the square of the wind shear since its dissipation by buoyancy is dependent upon the first power of the gradient of potential temperature (Dutton and Panofsky, 1970). For example, as air descends from the crest to the trough of a wave, an internal thermal discontinuity is formed; Dutton and Panofsky suggest that in the formation of this discontinuity both isotachs and isentropes will be compressed. At some stage in this process the Richardson number will decrease below the critical value and turbulence will begin.

The breakdown of unstable shear-gravity waves into turbulence is another mechanism for the generation of CAT. Shear-gravity waves may form as perturbations on an internal surface of thermal discontinuity embedded in wind shear (Haltiner and Martin, 1957). These conditions are similar to those expected in large-amplitude mountain waves. If the wind shear is strong enough across the discontinuity, the wave will become unstable and break down into turbulence (Dutton and Panofsky, 1970). From wave theory, when the last term (involving the radical) in the equation

$$c = \frac{\rho U + \rho^* U^*}{\rho + \rho^*} \pm \sqrt{\frac{g\lambda(\rho - \rho^*)}{2\pi(\rho + \rho^*)} - \frac{\rho\rho^*(U - U^*)^2}{(\rho + \rho^*)^2}}, \quad (15)$$

where:

* denotes the upper layer,

ρ is density $[\text{gm cm}^{-3}]$,

U is horizontal wind speed $[\text{m s}^{-1}]$,

$g \approx 9.8 \text{ m s}^{-2}$, and

λ is the wave length $[\text{m}]$,

becomes imaginary, shear-gravity waves will be unstable.

Equation (15) was applied to rawinsonde data for 1200 GMT, December 2, 1965, from Winnemucca, Nevada. The observed temperature, moisture, and wind speed profiles (Fig. 11) indicate that mountain waves were possible over the station at that time. A value for the radical term was calculated across the discontinuities at both the 625- and the 330-mb levels. The results indicate that shear-gravity waves were likely to be stable at the 625-mb level but unstable at the 330-mb level. This does not necessarily mean that CAT would be occurring but it does imply that conditions were favorable for turbulence. It

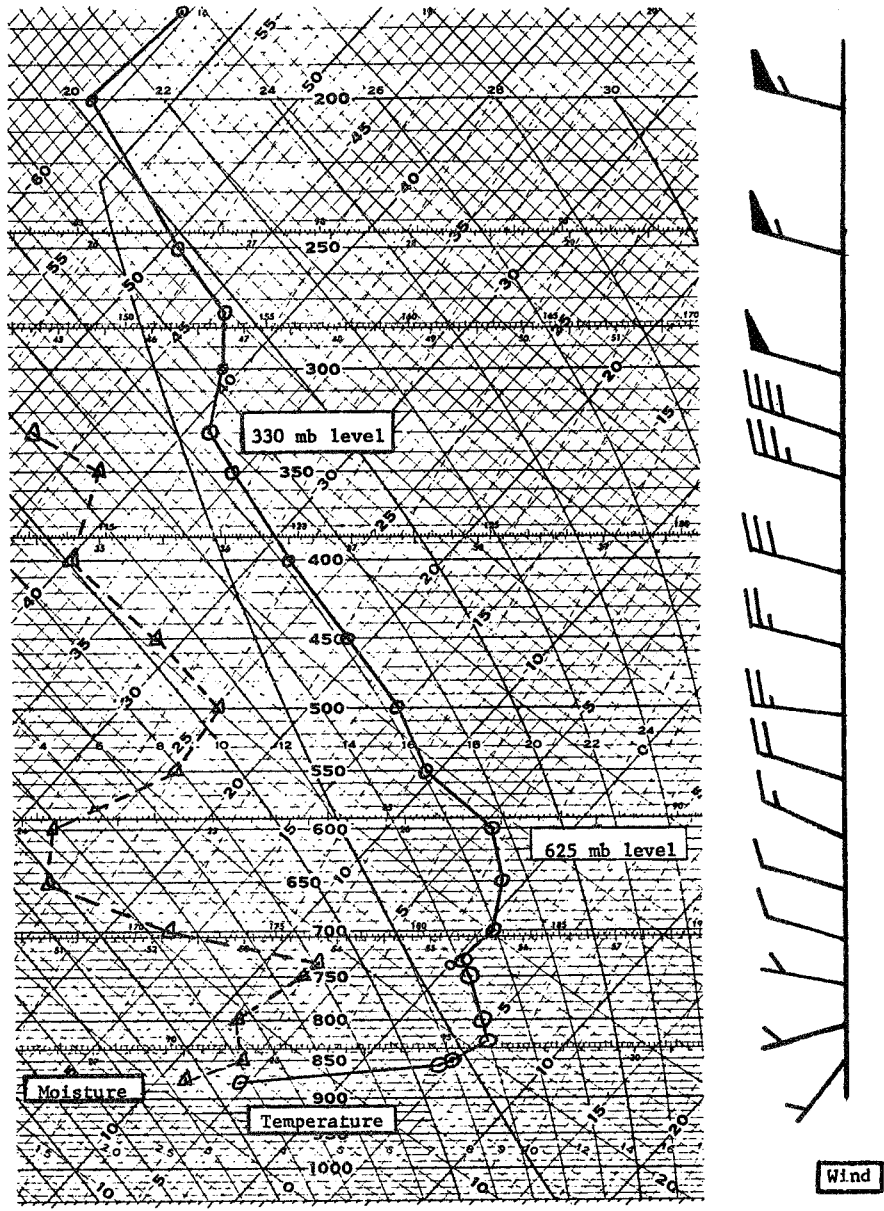


Fig. 11. Temperature, moisture, and wind distributions with height observed at Winnemucca on Dec. 2, 1965, at 1200 GMT.

is important to note that the XB-70 encountered turbulence on that day at 1735 GMT at an altitude of 13.8 km (45,000 ft) above Winnemucca (turbulence encounter #4 in Fig. 12).

The preceding discussion indicates that although the small-scale and rapid dissipation of turbulence prohibits a direct observation of turbulent flow, the statement that atmospheric wind and stability conditions associated with mountain waves are theoretically favorable for the generation of CAT is entirely plausible. Thus, since curvature is related to large-amplitude waves, and these waves are associated with conditions favorable for CAT, curvature may be an important parameter in the formation of CAT.

D. DESCRIPTION OF DATA

1. Meteorological data

Atmospheric data from rawinsonde ascents were available on microfilm for both 0000 GMT and 1200 GMT from the National Weather Service. Data from 27 rawinsonde stations across the western United States were analyzed both to determine expected mountain-wave areas and to perform calculations necessary for this study. The locations of the 27 stations are shown in Fig. 13.

2. Aircraft data

Data were available from 46 XB-70 test flights over the western United States from March 1965 to November 1967. The general extent of the area traversed by the aircraft is shown in Fig. 14. During most of these flights the aircraft cruised above 12.2 km (40,000 ft) and at supersonic speeds. Turbulence experienced by the aircraft was measured by a recorder which provided a time trace of the pressure, altitude and vertical accelerations at the center of gravity of the aircraft. The data used in this study consisted of the maximum normal acceleration, a_{nmax} , for each encounter, together with the pressure-height and the distance flown in turbulence. An example of the form in which the aircraft data were obtained is presented in Fig. 12.

Since it was the objective of this research to study the interrelationships between mountain-wave areas, CAT and non-CAT regions, and the distribution of the vertical gradient of curvature, flight tracks covering a large area with portions over mountain-wave regions were considered to be germane to the study. Thus, the track length was measured by using a planimeter, and expected mountain-wave areas were determined from the meteorological data. Seventeen flights were available where the XB-70 traveled at least 2×10^3 km and flew at least 100 km over each expected mountain-wave region during each flight. In addition, strong mountain waves were found on eight of the days, as determined by the characteristics of vertical ascent rates of rawinsonde balloons (Scoggins and Incrocci, 1973). Of the 17 flights, 15 were chosen for analysis, and two were used as independent test cases.

Encounter number	Greenwich time	$\Delta a_{n,max}$ g units	Distance in turbulence, n. mi. (km)	h_p , ft (m)
1	1750Z	0.20	0.9 (1.7)	45.7×10^3 (13.9 $\times 10^3$)
2	1752Z	.15	.9 (1.7)	45.5 (13.9)
3	1755Z	.25	1.2 (2.2)	45.0 (13.7)
4	1755Z	.40	6.1 (11.3)	45.2 (13.8)
5	1756Z	.20	3.2 (5.9)	45.6 (13.9)
6	1803Z	.25	2.3 (4.3)	46.6 (14.2)
7	1803Z	.15	2.3 (4.3)	46.2 (14.1)
8	1804Z	.25	1.2 (2.2)	46.3 (14.1)
9	1807Z	.40	4.7 (8.7)	50.2 (15.3)
10	1809Z	.25	2.5 (4.6)	49.8 (15.2)
11	1809Z	.25	2.9 (5.4)	49.4 (15.1)
12	1813Z	.20	5.7 (10.6)	48.7 (14.8)
13	1815Z	.40	2.6 (4.8)	46.8 (14.3)
14	1817Z	.30	5.2 (9.6)	52.1 (15.9)
15	1817Z	.45	1.0 (1.9)	49.5 (15.1)
16	1818Z	.30	7.2 (13.3)	49.0 (14.9)
17	1819Z	.15	2.3 (4.3)	49.5 (15.1)
18	1822Z	.30	4.1 (7.6)	50.0 (15.2)
19	1828Z	.20	1.1 (2.0)	59.6 (18.2)
20	1833Z	.20	5.5 (10.2)	57.8 (17.6)

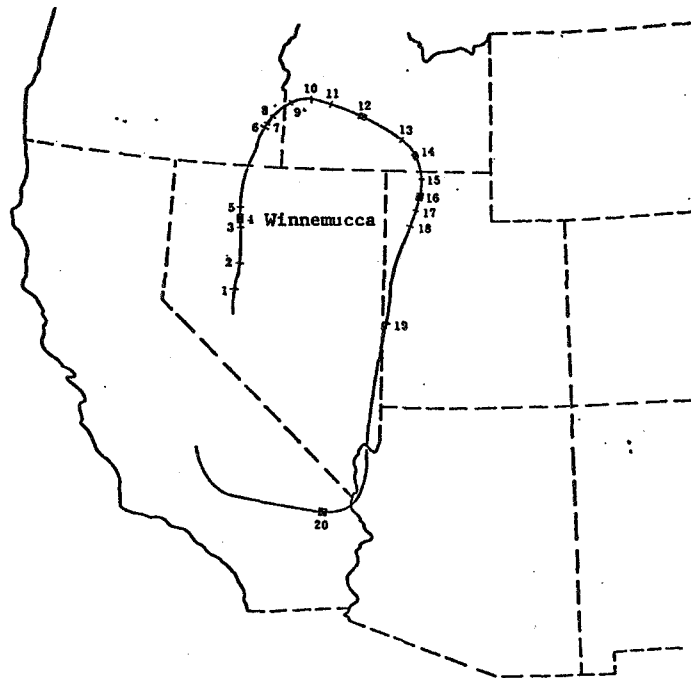


Fig. 12. The XB-70 flight track and turbulence data of December 2, 1965 (Ehernberger, 1968).

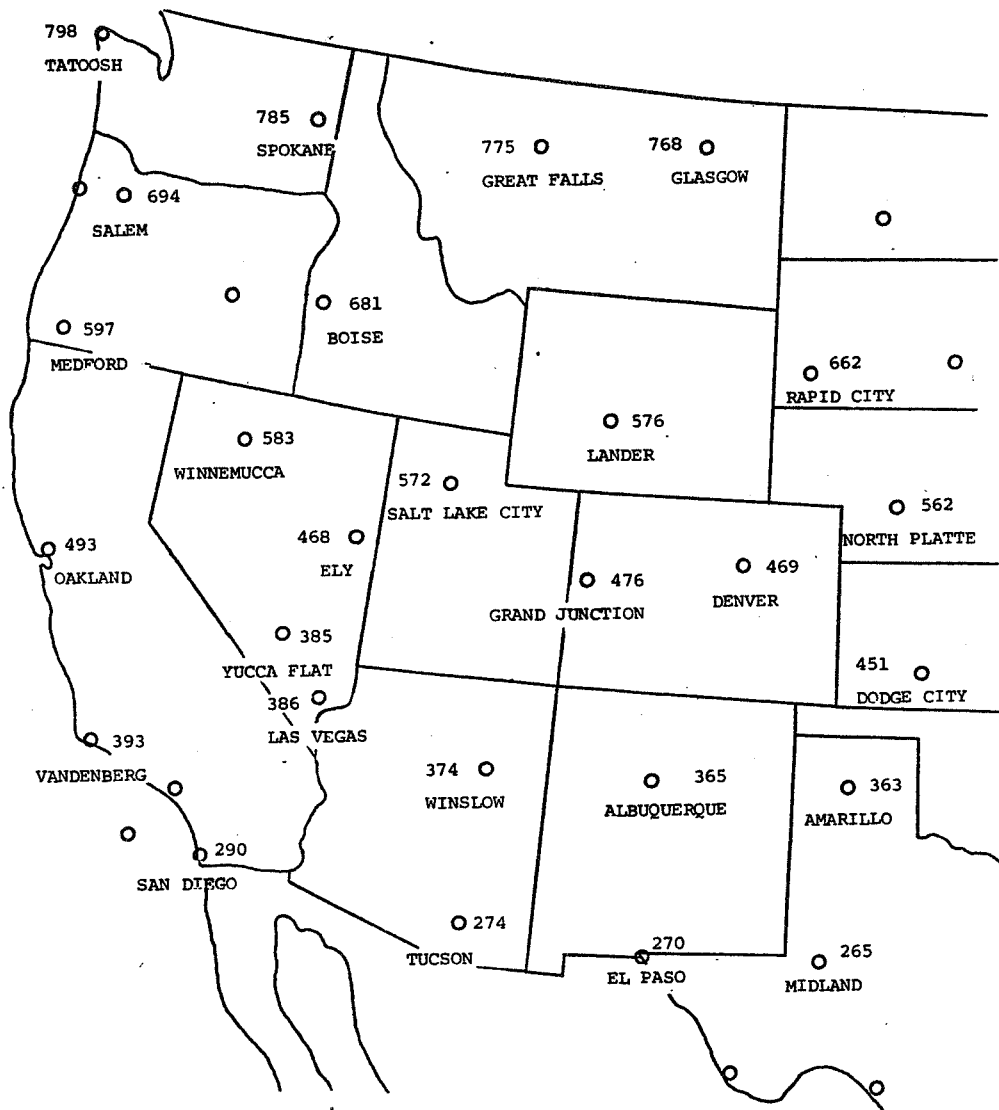


Fig. 13. Rawinsonde stations across the western United States.

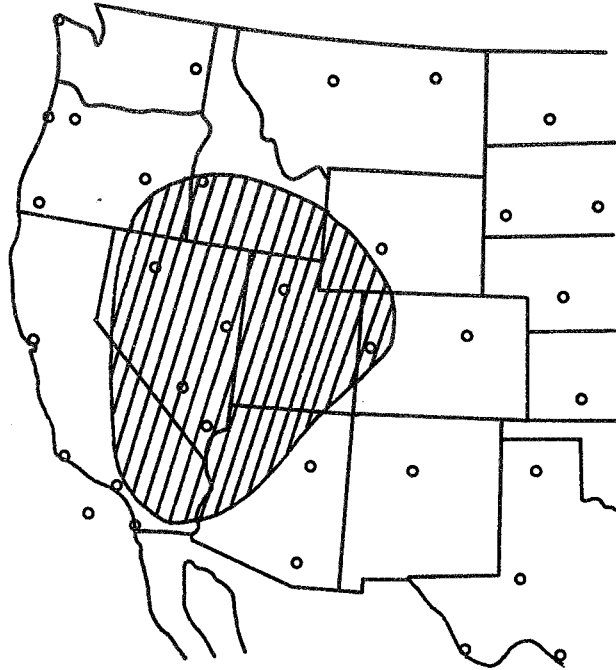


Fig. 14. General areal extent of XB-70 flights.

E. ANALYSIS OF DATA

1. Grouping of the turbulence encounters

Turbulent and non-turbulent regions were defined along sections of each flight track according to the following criteria:

- a) all turbulent and non-turbulent regions must be at least 200 km long;
- b) all regions must be separated by at least 100 km;
- c) all turbulent regions must contain at least two turbulence encounters, or one encounter at least 200 km long;
- d) all non-turbulent regions must not contain any turbulence encounters; and,
- e) all non-turbulent regions must be at least 100 km from any isolated turbulence encounters.

The region-length requirement was designed to compensate for the difference in horizontal dimensions between CAT regions and the spacing of meteorological data so that the turbulent and smooth sections of the flight tracks could be related to synoptic-scale conditions. In addition, the distance between successive regions was maximized in an effort to minimize the interdependent influences between the regions. Moreover, non-turbulent regions were defined along sections free of turbulence, and turbulent regions were defined where a substantial amount of turbulence was encountered to insure

that any relationships between the two types of regions and specific meteorological conditions were representative. That is, the effects of any spurious encounters and any isolated encounters, which would not be reflected in rawinsonde data, were removed. Portions of any flight track not contained in either a turbulent or a non-turbulent region were not analyzed.

As an example, Fig. 15 shows the location of turbulent and non-turbulent regions for January 15, 1966. From the above set of criteria, 47 turbulent regions and 43 non-turbulent regions were defined for the 15 flight days.

2. The areal distribution of expected mountain waves

The terrain of the western United States is very conducive to the formation of mountain waves (Harrison and Sowa, 1966). The numerous sections of parallel ridges, such as those located over Nevada, Utah, and Idaho, together with the major ranges (the Rockies, Cascades, and Sierra Nevadas) serve to intensify and complicate wave patterns. The locations of the crests of these ridges are shown in Fig. 16.

To study the effects of mountain waves it is necessary to understand the atmospheric conditions which lead to their formation. Gazzola (1964) suggests general criteria for the vertical variation of wind speed and direction necessary to initiate waves of large amplitude. The criteria are:

- a) a minimum wind speed of 7 to 15 m s^{-1} normal to and at the crest of the ridge;
 - b) wind direction which does not vary considerably with height;
- and
- c) an increase in wind speed with height to the upper troposphere (10 to 12 km).

In addition, Scoggins and Incrocci (1973) suggest a minimum wind speed of 10 m s^{-1} at the mountain ridge and an increase in speed with height. The following criteria were used in this study to define areas where conditions were favorable for the formation of mountain waves. These criteria are:

- a) 700-mb wind speed of at least 8 m s^{-1} normal to the mountain ridge;
- b) wind direction variation of not more than 40 deg between 700 mb and 350 mb; and
- c) 350-mb wind speed of at least 10 m s^{-1} normal to the mountain ridge.

Harrison and Sowa (1966) state that moderate waves have been found to carry CAT a distance of 280 km (150 nm) downwind from the mountain crest. This distance is not a direct function of the height of the mountain since CAT has been found to accompany only lee waves of wavelength about 25 km or less, this being within the range normally generated by mountain ridges (Foltz, 1967). Based upon

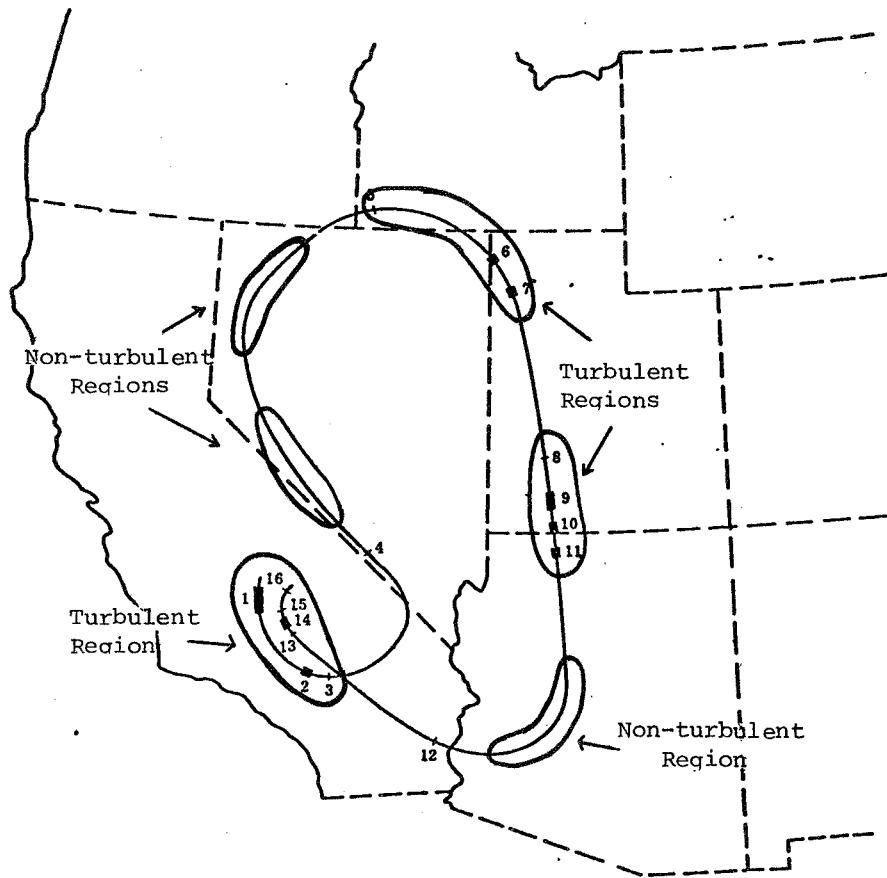


Fig. 15. Turbulent and non-turbulent regions for January 15, 1966.

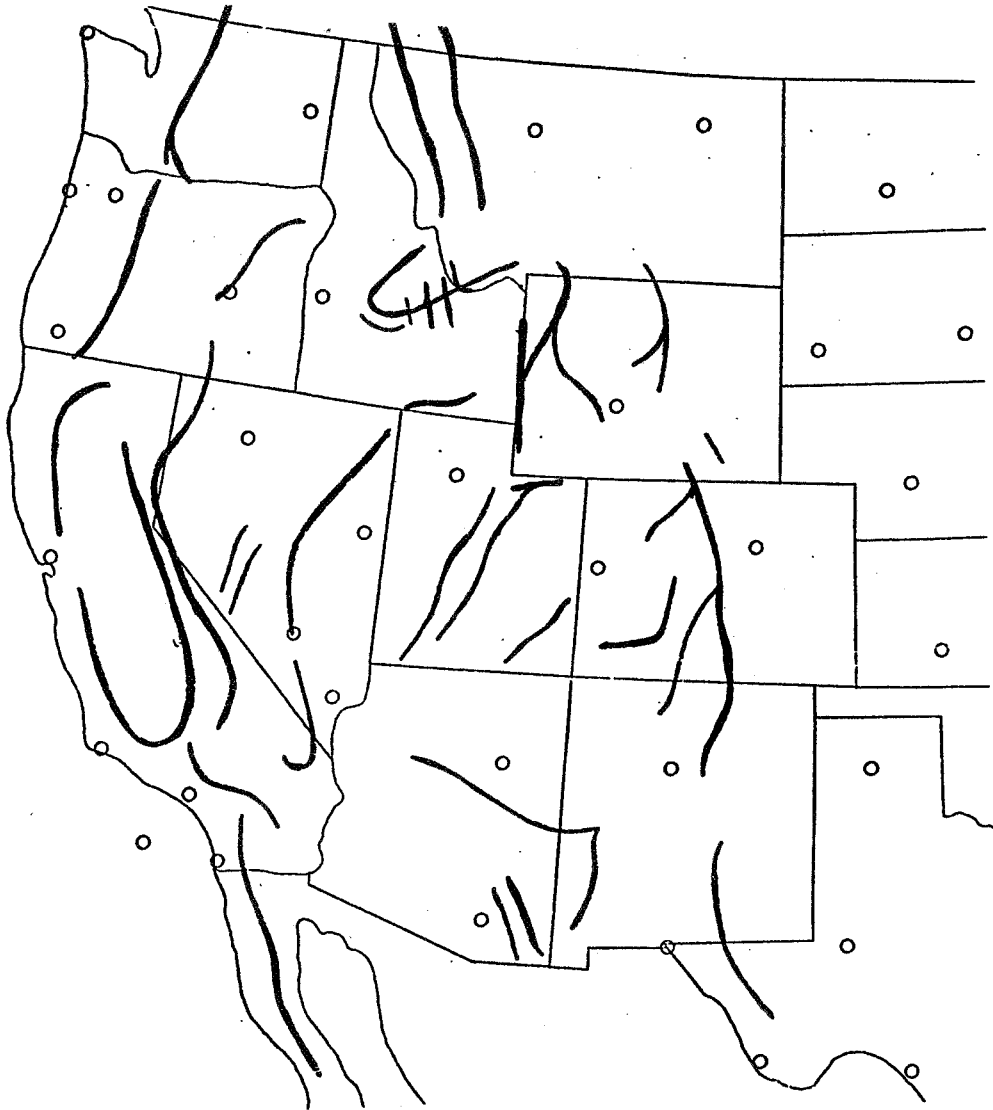


Fig. 16. The major mountain-ridge crests of the western United States.

this, the horizontal range of expected mountain-wave areas in this study was defined to extend from the mountain crest to 250 km (135 nm) downwind. Thus, expected mountain-wave areas were determined for each flight day in consideration of the meteorological criteria, ridge locations, and downwind distance.

3. Evaluation of the vertical gradient of curvature

As shown by Scoggins and Incrocci (1973), the curvature term can be as important as the stability term to the magnitude of the Scorer parameter during mountain-wave conditions. Theoretically, an increase of curvature with height ($\Delta(U''/U) > 0$) is conducive to the formation of large-amplitude mountain waves since during these conditions, curvature (U''/U) acts to cause l^2 to decrease with altitude. Thus, CAT would be expected to occur where mountain-wave areas and positive values of $\Delta(U''/U)$ coincide.

Fields of the areal extent of the vertical gradient of (U''/U) were defined for each of the 15 flight days to determine relationships between this term, conditions favorable for mountain waves, and CAT encountered by the XB-70 in the stratosphere. Values of (U''/U) were determined at 3.0 and 7.6 km (10,000 and 25,000 ft). These two levels were chosen because they correspond closely with mountain crests and the altitude where the curvature term generally reaches a maximum value (Scoggins and Incrocci, 1973).

Figure 17 shows the procedure that was used to determine (U''/U) and the vertical gradient of curvature, $\Delta(U''/U)$, for each flight day. In step 1, values of scalar wind speed were determined at 1.5-km (5000-ft) intervals from 1.5 to 9.1 km (5000 to 30,000 ft) for each rawinsonde station. The vertical wind shears were computed by finite differencing between successive levels as shown in step 2. In step 3, the curvature, U'' , was computed for levels 2 and 5 as shown. The values of the curvature term, (U''/U), were computed as shown in step 4 by dividing each value of curvature by the wind speed at that level. A scalar analysis was then performed on the values of (U''/U) from the 27 stations for both levels. In step 5, the areal fields of $\Delta(U''/U)$ were determined by graphically subtracting the (U''/U) field at level 2 (3 km or 10,000 ft) from that at level 5 (7.6 km or 25,000 ft). By superimposing the expected mountain-wave areas on the turbulent and non-turbulent regions and the $\Delta(U''/U)$ fields, their interrelationships were established.

An example of the analysis is discussed for one typical flight. On March 15, 1966, the XB-70 traveled 3700 km, 49 per cent of which was flown over expected mountain-wave areas (Fig. 18). Two turbulent and five non-turbulent regions were defined along portions of the track. All the turbulent regions occurred in the mountain-wave areas from western California across western Nevada into southeast Oregon where $\Delta(U''/U) > 0$. In addition, four of the non-turbulent regions occurred where $\Delta(U''/U) < 0$ outside of any mountain-wave areas. Moreover, the remaining non-turbulent region occurred while the aircraft was flying over an extensive mountain-wave area,

Procedure:	Step 1	Step 2	Step 3	Step 4	Step 5
Variable:	Wind Speed	Wind Shear	Curvature	Curvature Term	Gradient of Curvature Term

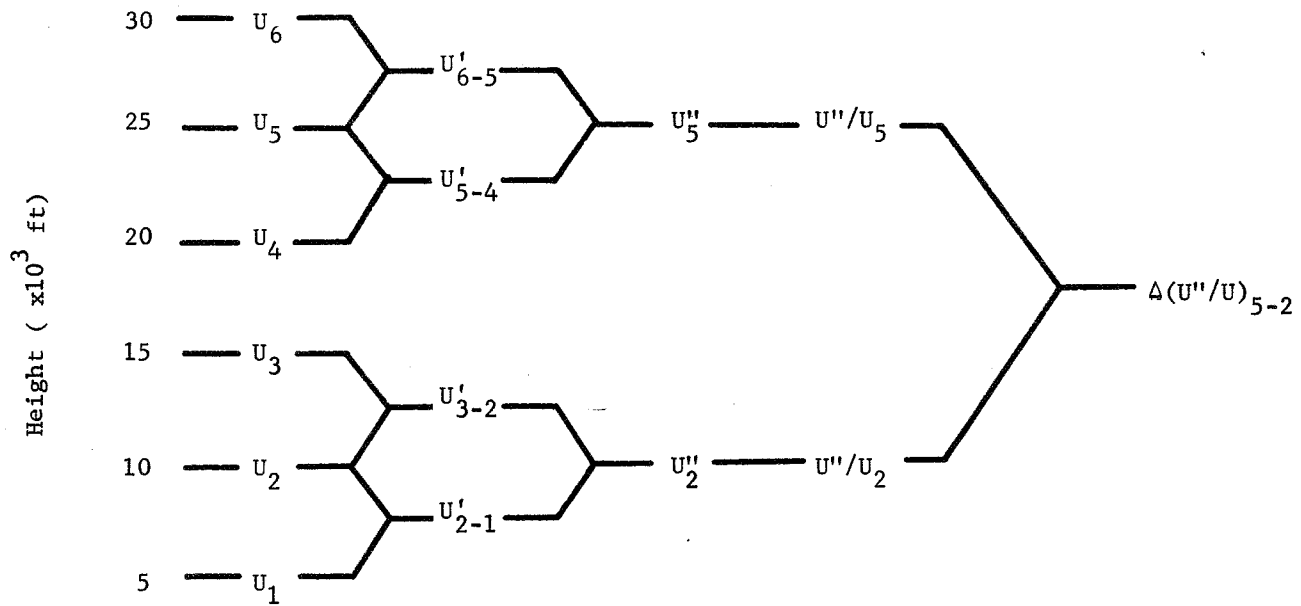


Fig. 17. Procedure for determining the vertical gradient of the curvature term.

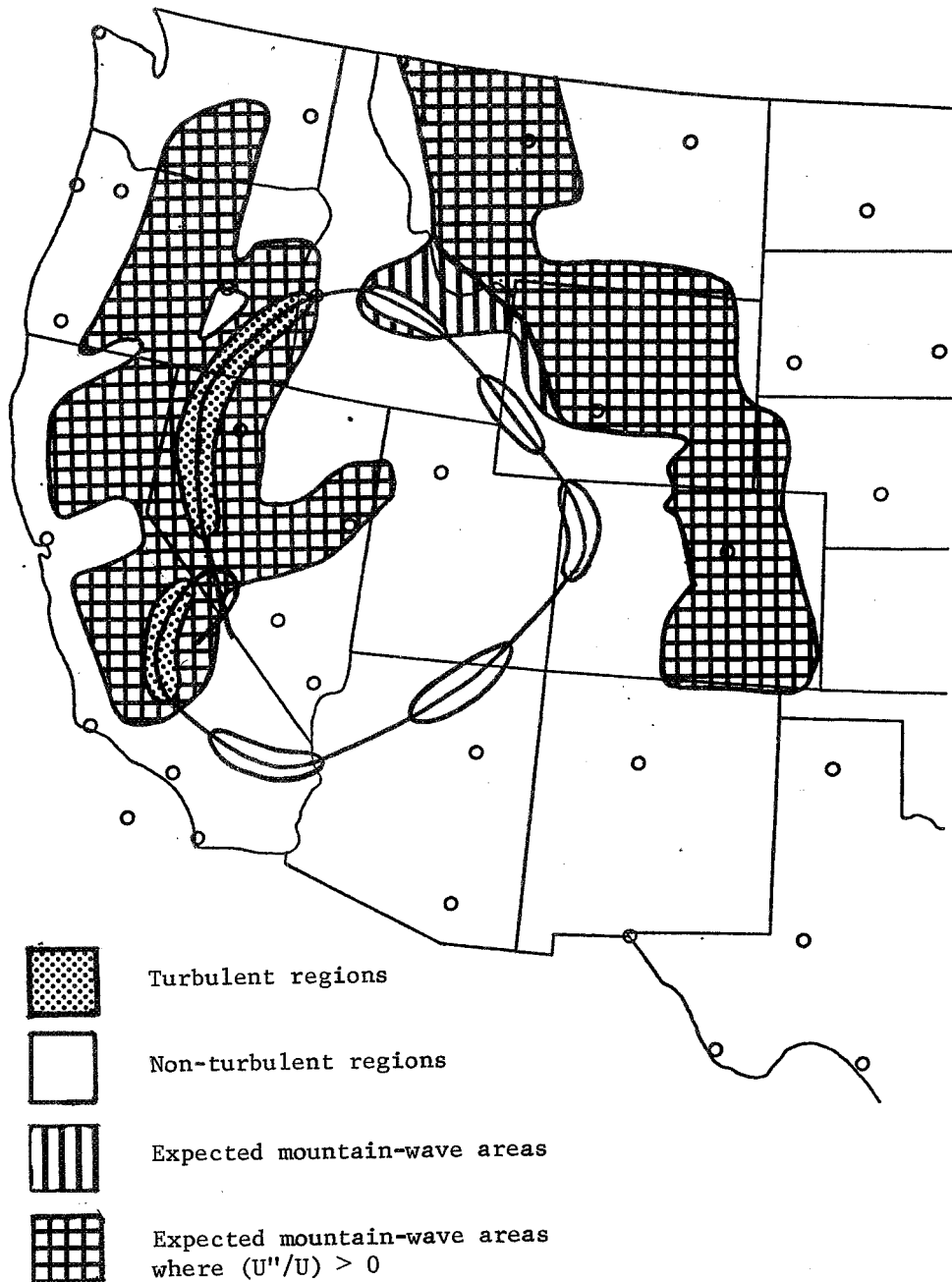


Fig. 18. XB-70 flight track for March 15, 1966.

but where $\Delta(U''/U) < 0$. Thus, areas of positive and negative values of the vertical gradient of curvature together with the location of areas expected to contain mountain waves appear to define sections of the flight track where turbulent and non-turbulent regions are likely to occur. These results are typical of the other flights analyzed.

F. RESULTS

The results of the study are presented in Table 10 from which it was determined that 42 of the 47 turbulent regions occurred over mountain-wave areas and that 37 of these were located where the curvature term increased with height, i.e., where $\Delta(U''/U) > 0$. In addition, the five turbulent regions which occurred outside of mountain-wave areas were located such that three occurred where $\Delta(U''/U) > 0$ and two where $\Delta(U''/U) < 0$. It also was determined that 31 of the 32 non-turbulent regions defined outside mountain-wave areas occurred where the curvature decreased with height, i.e., $\Delta(U''/U) < 0$. There were 11 non-turbulent regions defined within mountain-wave areas, and all 11 occurred where $\Delta(U''/U) < 0$. The results indicate that CAT generally occurs in expected mountain-wave areas where $\Delta(U''/U) > 0$, with smooth conditions outside mountain-wave areas where $\Delta(U''/U) < 0$.

The results were tested by using two independent flights. Meteorological data were examined for these days by using the same criteria as previously defined to determine where mountain waves were expected, and (U''/U) was computed as before. The flight tracks were superimposed over the expected mountain-wave areas and the fields of $\Delta(U''/U) < 0$.

On March 24, 1966, (Fig. 19), three turbulent and three non-turbulent regions were defined. The two turbulent regions located within the expected mountain-wave area occurred where $\Delta(U''/U) > 0$, whereas the one turbulent region located outside of the expected mountain-wave area occurred where $\Delta(U''/U) < 0$. In addition, the three non-turbulent regions were located outside of the expected mountain-wave area where $\Delta(U''/U) < 0$. All three turbulent regions defined on April 1, 1966, (Fig. 20), were located in expected mountain-wave areas where $\Delta(U''/U) > 0$. Moreover, the two non-turbulent regions occurred outside expected mountain-wave areas where $\Delta(U''/U) < 0$.

In summary, these two cases show that the turbulent regions inside mountain-wave areas were located where $\Delta(U''/U) > 0$, and that all the non-turbulent regions both inside and outside mountain-wave areas were located where $\Delta(U''/U) < 0$. Thus, these two independent test cases support the results given in Table 10, i.e., CAT in the stratosphere generally occurs where mountain waves are expected and the curvature increases with height, while smooth conditions generally are observed outside these areas and

Table 10. The sign of $\Delta(U''/U)$ for the turbulent and non-turbulent regions occurring within and outside of expected mountain-wave areas.

Flight Date	Turbulent				Non-Turbulent			
	Inside Mountain-Wave Areas		Outside Mountain-Wave Areas		Inside Mountain-Wave Areas		Outside Mountain-Wave Areas	
	$\Delta(\frac{U''}{U}) > 0$	$\Delta(\frac{U''}{U}) < 0$	$\Delta(\frac{U''}{U}) > 0$	$\Delta(\frac{U''}{U}) < 0$	$\Delta(\frac{U''}{U}) > 0$	$\Delta(\frac{U''}{U}) < 0$	$\Delta(\frac{U''}{U}) > 0$	$\Delta(\frac{U''}{U}) < 0$
April 20, 1965	4	1						
June 16, 1965	5							1
July 01, 1965				1		4		2
Oct. 14, 1965	2					1	1	2
Oct. 16, 1965	1		1					2
Nov. 02, 1965	1		1					4
Dec. 02, 1965	3							2
Jan. 03, 1966	4		1					1
Jan. 12, 1966	2			1				3
Feb. 09, 1966	2							4
Mar. 10, 1966	3	1				1		1
Mar. 15, 1966	2					1		4
Mar. 17, 1966	2	2				4		
Mar. 19, 1966	3							4
April 26, 1966	3	1						1
Totals	<u>37</u>	<u>5</u>	<u>3</u>	<u>2</u>	<u>0</u>	<u>11</u>	<u>1</u>	<u>31</u>
	<u>42</u>		<u>5</u>		<u>11</u>		<u>32</u>	
	47				43			

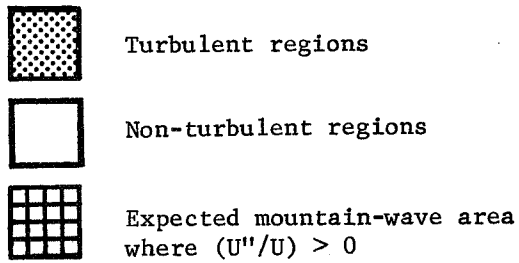
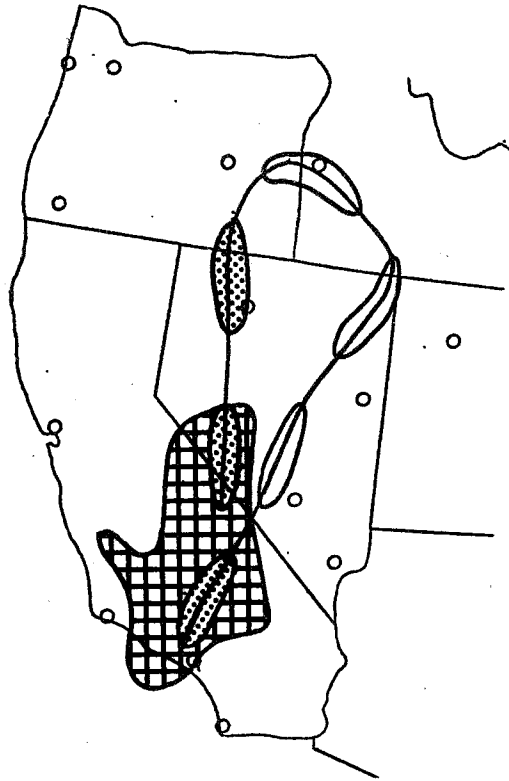


Fig. 19. XB-70 flight track for March 24, 1966.

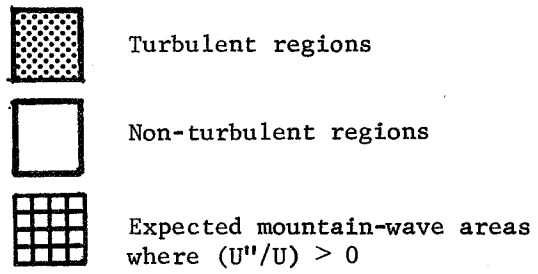
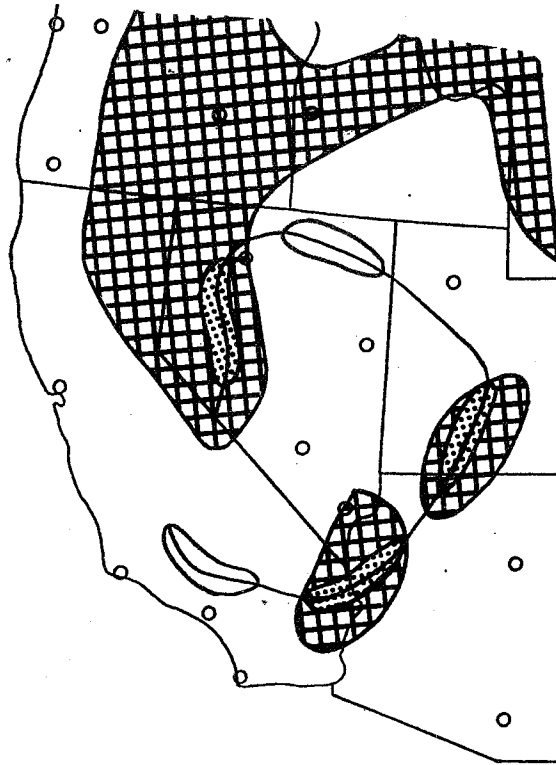


Fig. 20. XB-70 flight track for April 1, 1966.

where curvature has a negative change with height.

To substantiate further the validity of the results, the 17 flights were separated by a random process into two sub-samples consisting of 8 and 9 flights, respectively. Each sub-sample was analyzed in the same manner as the complete sample of 17. It was found that the results for each sub-sample varied by 10 per cent or less within each category, and by less than 10 per cent when compared to the totals presented in Table 10. This indicates that the results of Table 10 are not biased by sample size, but are an accurate representation of what might be expected from any number of flights.

G. SUMMARY AND CONCLUSIONS

The purpose of this research was to relate stratospheric turbulence encountered by the XB-70 airplane over the mountainous regions of the western United States to expected mountain-wave areas and changes in the curvature of the wind profile with height. A theoretical investigation indicates that a positive change of curvature with height in the troposphere contributes to large-amplitude lee waves. Such large-amplitude waves may be important in the transfer of energy upward into the stratosphere and may create conditions favorable for the generation of CAT in that region of the atmosphere.

The theoretical results then were applied to actual atmospheric conditions during XB-70 flights in the stratosphere. The distribution of the vertical gradient of curvature $\Delta(U''/U)$ was determined for the western United States for 15 flight days. Ninety independent turbulent and non-turbulent regions were defined from the XB-70 data, and expected mountain-wave areas were determined from topographical criteria and tropospheric wind conditions from each flight day. The turbulent and non-turbulent regions together with the mountain-wave distributions were examined in relation to the field of $\Delta(U''/U)$ for each day.

It was determined that 37 out of 42 turbulent regions over expected mountain-wave areas were located where $\Delta(U''/U) > 0$, and that 31 out of 32 non-turbulent regions outside of expected mountain-wave areas occurred where $\Delta(U''/U) < 0$. In addition, $\Delta(U''/U)$ was negative for all non-turbulent regions within expected mountain-wave areas. Two independent cases were analyzed and both were found to support these results. Moreover, essentially the same results were obtained from an analysis of two random sub-samples of the data.

In conclusion, the results of this study show that the curvature of the wind profile is an important tropospheric variable in the determination of stratospheric CAT regions. In addition, CAT regions are likely to occur where the curvature increases with height in the troposphere in areas where mountain waves are expected, and that turbulent-free regions are most likely to occur outside mountain-wave areas where the curvature decreases with altitude.

CHAPTER VI. COMPOSITE CAT FORECASTING PROCEDURE

A. INTRODUCTION

The ultimate purpose of this research was to develop an objective CAT forecasting procedure for the western part of the United States. The procedure incorporates the three techniques discussed previously. The first technique, statistical analysis, is based upon critical values of 25 synoptic parameters. The number of parameters in a region which exceeds the critical values was considered to be proportional to the probability of the occurrence of CAT in that region. The discriminant function method was based upon the values of five different functions, with synoptic parameters as variables, for each of five overlapping sub-layers between 12.2 and 20.4 km (40,000 and 67,000 ft). The number of positive functional values in a sub-layer was considered to be proportional to the probability of the occurrence of CAT in that sub-layer. The last technique was based upon Scorer's curvature-of-the-wind-profile term in the 3.0-7.6-km (10,000-25,000-ft) layer. It was assumed that regions where the gradient of the curvature was positive were regions where large-amplitude mountain waves and stratospheric CAT would occur.

In order to be practical, the CAT forecasting procedure must require minimal manual effort, expense, and time. In addition, the meteorological data required for the analysis must be readily available. Therefore, a computer program was written to carry out the procedure. This computer program: (1) computed, from standard rawinsonde data, the numerous fields of synoptic parameters (for 1200 and succeeding 0000 GMT) required for the procedure; (2) applied the three CAT forecasting techniques to the grid points; and (3) printed a grid map with the results of the three techniques. Once the rawinsonde data have been obtained and read into the computer, the forecast can be completed within a short time. The computer program is presented in Appendix C.

B. APPROACH

1. Method of analysis

a) Data input. To minimize the time required to arrive at a forecast, the amount of data input was minimized. Synoptic parameters were determined from 1200 and succeeding 0000 GMT atmospheric data obtained from 26 stations of the western United States rawinsonde network. The geographical locations of the rawinsonde stations are shown in Fig. 13. Although some of the stations are not located in the forecast region, the measurements obtained from them should improve the meteorological parameters computed for the forecast region.

The atmospheric data employed by the CAT forecasting procedure consist of the geopotential heights and temperatures at the 300-, 200-, and 100-mb levels and the wind velocity at the 100-mb level (hereafter referred to as primary parameters), and wind speeds at 1.5-km (5,000-ft) intervals in the 1.5 to 9.1-km (5,000 to 30,000-ft) layer.

(b) Determination of synoptic fields. The fields consisted of values of parameters representing points separated approximately 158 km on an 18 x 18 grid over the western half of the United States. The 18 x 18 grid and that portion of the grid located in the forecast region are illustrated in Fig. 21.

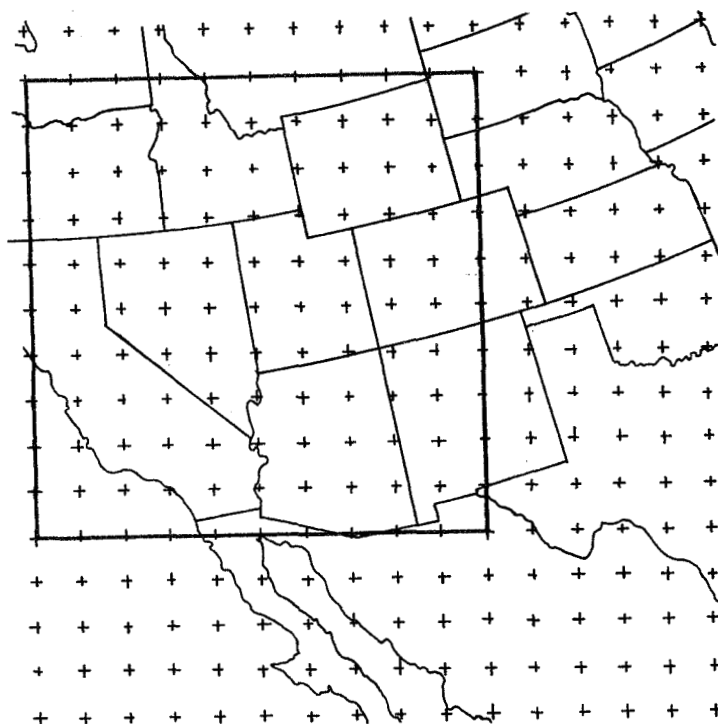


Fig. 21. The 18 x 18 grid employed for the determination of the fields of the synoptic parameters, and the 11 x 11 grid (denoted by the square) employed for the forecasting procedure. (The two outer rows of grid points have been omitted.)

The determination of the synoptic fields began by converting the geographical coordinates (latitude and longitude) of the rawinsonde stations into grid coordinates (row and column). The values of the primary parameters extracted from the rawinsonde data were assigned to the respective positions on the grid. A double-linear interpolation process was then employed to assign values of the parameters to all the points on the grid. Six iterations were performed for the curvature-term technique, while only four were needed for the remaining two techniques. The value of a parameter at a point was determined by those values obtained from the rawinsonde stations included in the scan radius. A scan radius of 3.0 was used to determine the wind fields at and below 9.1 km (30,000 ft), while a scan radius of 4.0 proved to be more suitable for the fields of the remaining parameters. A smoothing process using a system of weights illustrated in Fig.22 was employed to improve the representativeness of the fields. The other details are shown in the computer program in Appendix C.

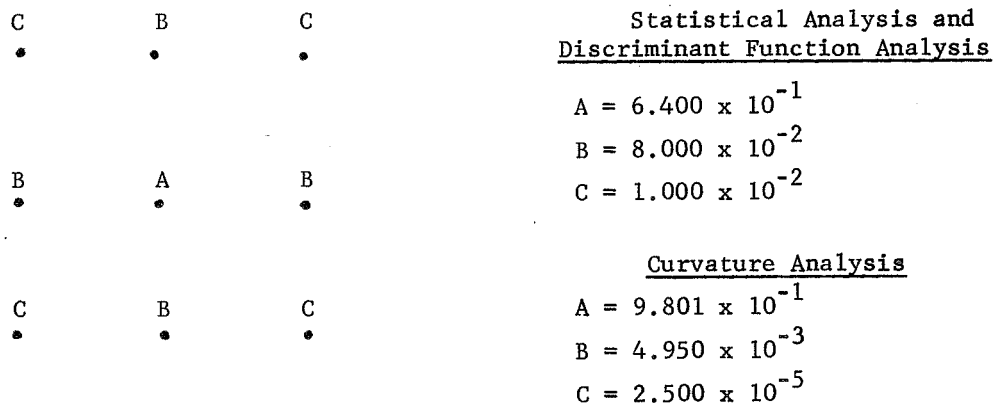


Fig. 22. The weighting system employed in the smoothing process to determine the value at point A.

Only one field was required for the technique involving the curvature-of-the-wind term from Scorer's parameter. This term was computed at 26 points on the grid corresponding to the location of the rawinsonde stations using information extracted from the rawinsonde data obtained from these stations. The details of this calculation are discussed in the preceding chapter. The field was then determined for each grid point by interpolating and smoothing the 26 values.

After the fields required for the curvature technique were completed, the fields for the remaining two techniques were determined. First, the 1200 and succeeding 0000 GMT fields of the primary parameters were determined for the 300-, 200-, and 100-mb geopotential surfaces. The values on these primary fields were used directly in the statistical and discriminant function techniques and/or used to determine the fields of other parameters.

The geostrophic wind fields for the 300- and 200-mb geopotential surfaces were determined from the corresponding geopotential height fields. Therefore, the winds at these two levels were not required as data input. The winds at these levels are in geostrophic balance most of the time so the fields of the zonal and meridional winds were calculated from the geostrophic wind equation:

$$u \text{ or } v = \frac{g}{f} \frac{\Delta H}{2 \Delta n} \quad (17)$$

where n is along either x or y , f is the coriolis parameter, g is gravity, and H is geopotential height. The scalar wind speeds at 200 and 300 mb were determined by the square root of the sum of the squares of the two wind components at each grid point:

$$V_{ij} = \left[(u_{ij})^2 + (v_{ij})^2 \right]^{\frac{1}{2}} \quad (18)$$

The fields of the zonal and meridional wind components at the 100-mb level were determined by first computing the values of the components for each rawinsonde station. These components were calculated from the velocity vector at the 100-mb level, which was part of the input data. Unlike the other wind fields, the 100-mb wind fields were determined by interpolating and smoothing the wind data plotted at the rawinsonde stations.

The fields of all variables required in the forecasting procedure were computed for each grid point from values of the primary parameters as previously described. Table 11 summarizes all the fields required.

Table 11: List of parameters required in forecasting procedure.

$H_{3,2,1}$	$(\partial \vec{V}_h / \partial z)_{2-1}$	$\partial \Gamma_{2-1} / \partial t$
$T_{3,2,1}$	$(\partial \vec{V} / \partial n)_{3,1}$	$\partial (-\vec{V} \cdot \vec{\nabla} T)_{3,2} / \partial t$
$(-\vec{V} \cdot \vec{\nabla} T)_{3,2,1}$	$\beta v_{3,2,1}$	$\partial Ci / \partial t$
Γ_{2-1}	$V_{1.5,3.0,4.6,6.1,7.6,9.6}$	$\partial v_{3,2} / \partial t$
Ri	$\zeta_{3,2,1}$	$\partial (\partial v / \partial n)_1 / \partial t$
Ci	η_1	$\partial (\partial \vec{V}_h / \partial z)_{2-1} / \partial t$
$v_{3,2,1}$	$(-\vec{V} \cdot \vec{\nabla} \zeta)_3$	$\partial (\beta v_2) / \partial t$
$u_{3,2,1}$	$\partial H_2 / \partial t$	$\partial \zeta_1 / \partial t$
$v_{3,2,1}$	$\partial T_{3,1} / \partial t$	$\partial (-\vec{V} \cdot \vec{\nabla} \zeta)_{3,1} / \partial t$

Explanation of Symbols

V	Scalar wind speed	η	Absolute vorticity
u	Zonal wind speed	T	Temperature
$\partial \vec{V}_h / \partial z$	Vertical vector wind shear	Γ	Temperature lapse rate
v	Meridional wind speed	H	Pressure height
$\partial \vec{V} / \partial n$	Horizontal vector wind shear	β	Coriolis parameter
ζ	Relative vorticity	Ri	Richardson number
Ci	CAT Index developed by Colson and Panofsky (1965)		

Subscripts 1, 2, and 3 denote the 100-, 200-, and 300-mb levels respectively, and subscripts 1.5, 3.0, 4.6, 6.1, 7.6, and 9.6 denote the height in km.

c) Application of the techniques. In the curvature technique, it was postulated that large-amplitude mountain waves would form in areas where positive values of the curvature term occurred. Since theory predicts that large-amplitude mountain waves are associated with positive values of the curvature term, and since CAT may be associated with these waves, CAT was predicted when the value of the term exceeded zero.

The statistical analysis technique was applied to every grid point on the pertinent fields. At each grid point, the values were compared to the critical values of the 25 chosen parameters. Both the critical values and the significant parameters were chosen by statistical methods (see Chapter III). At every grid point, the number of parameters having values in the critical, or turbulent, range (either greater than or less than the critical value, depending upon the parameter) was determined. It was reasoned that the greater the number of parameters having values in the critical range, the greater the likelihood of the existence of CAT. It was found that areas of CAT generally corresponded to regions where 8 or more of the significant parameters had values in the critical range, while areas of non-CAT generally corresponded to regions where 6 or less of the significant parameters had values in the critical range.

The discriminant function analysis technique was applied to each grid point on the pertinent fields of synoptic parameters. The values of the 25 discriminant functions (five for each of the 2.1-km (7,000-ft) sub-layers discussed in detail in Chapter IV) were computed at each grid point where the computer program determined the number of discriminant functions, in each of the five sub-layers, having values greater than zero. It was assumed that the greater the number of positive functional values in a sub-layer of a region, the greater the likelihood of CAT in that sub-layer.

The purpose of the forecasting procedure resulting from all three techniques was to indicate geographical areas where a supersonic aircraft flying in the lower stratosphere was likely to encounter CAT. Therefore, the discriminant function analysis technique was used in a manner to give a forecast for the entire layer. The computer program determined the number of sub-layers having more than three out of the five discriminant functions with positive values. It was reasoned that the greater this number, the greater the likelihood that an aircraft flying through the stratosphere would encounter CAT.

The group of discriminant functions in the 16.8-18.9-km (55,000-62,000-ft) sub-layer tended to underforecast CAT. To improve results, this sub-layer was considered to have more than three functions with positive values if the sub-layer below (15.2-17.4-km or 50,000-57,000 ft) and the sub-layer above (18.3-20.4-km or 60,000-67,000 ft) both had more than three functions with positive values. This did not alter the forecast for this layer often, but brought the results more in agreement with adjacent layers.

2. Development of the composite CAT forecasting procedure

The three forecasting techniques were applied to the meteorological fields on days of selected aircraft flights. Only those days where flight tracks extended over a large portion of the western United States were considered. These days were more suited for the purpose since the ranges of values of the synoptic parameters were greatest along the longer tracks. Moreover, these days provided more encounters of CAT for given synoptic conditions. The forecast procedure developed, therefore, considers this greater range of values as well as greater geographical domain. A flow chart of the computer program is given in Appendix C.

Thirty-six days on which extensive aircraft flight tracks were available were selected. Of these, 6 flights occurred in the winter months; 16 in the spring months; 3 in the summer months; and 11 in the autumn months. Most of the flight tracks extended over California, Nevada, Idaho, Utah, and Arizona.

The necessary fields of parameters for these flight days were determined, and results of all three techniques at each grid point were produced for each flight day. An example of the grid map is illustrated in Fig. 23. The numerical results correspond to the technique identified in the legend in the lower portion of the figure.

The maps with the numerical results were compared to the geographical maps containing the areas and heights where the aircraft encountered CAT. As explained earlier, the results of the techniques are assumed to be related to the occurrence of CAT in the stratosphere. The comparison of the maps provided a method which determined, for each technique, those values of the numerical results associated with the occurrence and non-occurrence of CAT.

It was found that CAT areas were generally associated with a value of the curvature greater than or equal to $-1.0 \times 10^{-7} \text{m}^{-2}$, and non-CAT areas with smaller values. Areas where 7 or more of the significant parameters, selected by statistical analysis, had critical values were generally associated with CAT, and 5 or less with non-CAT conditions. The areas of the map where only 6 parameters had critical values were considered to be grey areas or areas where there were equal probabilities of the aircraft encountering CAT or no CAT. The areas of the map where 3 of 5 discriminant functions in 3 or more layers exceeded zero generally corresponded to CAT, and the remaining areas to non-CAT. The critical values for each technique are summarized in Table 12.

For most of the days employed, each technique identified the CAT and non-CAT areas reasonably well. However, at some grid points, the forecasts resulting from the techniques did not agree. Therefore, a procedure for combining the techniques to give the best results was required.

The procedure for combining the three techniques was based upon a consensus of the results of the three techniques at each grid point. Generally, a CAT forecast resulted when 2 or 3 techniques said "yes," and a no-CAT forecast resulted when 2 or 3 said "no." However, if the statistical forecast technique identified a grid point to be in a grey zone, the forecast resulting from the procedure was considered the same as that given by the technique involving the analysis of the curvature term. This procedure was followed because the curvature technique appeared to provide slightly better results than those for the other two techniques. This caused the forecasting procedure to weight the curvature technique slightly more than the others. Examples of CAT forecasts resulting from various combinations of the three techniques are given in Table 13.

-19.	-16.	-12.	11.	27.	33.	35.	29.	-2.	-34.	-41.
5 9	5 9	4 9	312	512	512	411	411	412	311	3 9
-8.	-6.	-6.	-6.	2.	23.	34.	37.	6.	-30.	-34.
5 9	5 8	3 8	2 5	312	511	510	412	412	410	3 9
-0.	1.	-0.	-4.	-7.	-8.	15.	31.	23.	-8.	-19.
5 8	3 6	2 5	2 4	2 5	2 9	210	311	510	5 9	5 6
7.	9.	11.	9.	-2.	-22.	-19.	4.	10.	-2.	-11.
5 7	2 8	2 8	3 7	3 8	2 7	2 9	2 9	2 9	3 7	3 6
12.	15.	23.	22.	10.	-18.	-33.	-20.	-9.	-7.	-12.
410	311	312	2 8	1 9	2 8	2 6	2 6	2 5	2 5	2 5
10.	14.	24.	25.	18.	1.	-23.	-24.	-12.	-3.	-5.
411	511	512	5 9	3 9	2 9	2 8	2 6	2 5	2 5	2 5
5.	6.	13.	21.	22.	18.	-5.	-25.	-9.	15.	20.
4 7	4 7	410	5 9	5 8	5 7	3 6	2 5	2 5	3 5	3 5
3.	-0.	2.	17.	25.	23.	0.	-19.	-2.	22.	23.
4 6	4 5	4 5	4 6	5 7	5 7	2 6	3 4	3 4	3 4	4 4
-4.	-9.	-4.	16.	29.	30.	25.	33.	41.	31.	9.
4 7	4 7	4 5	4 5	4 4	4 4	4 4	4 4	4 5	4 5	4 5
-12.	-11.	0.	27.	41.	54.	99.	99.	99.	54.	-4.
4 7	4 6	4 6	4 6	4 5	4 4	4 4	4 4	4 4	4 4	4 4
-15.	-7.	16.	41.	50.	73.	99.	99.	99.	70.	-5.
5 7	4 6	4 6	4 6	4 4	4 4	4 4	4 5	4 5	4 5	4 4

X#1 .
X#2 X#3

X#1: Vert. Grad. of Curvature Term ($x \cdot 10^{-8} m^{-2}$)
X#2: Discriminant Function Analysis
X#3: Statistical Analysis Method

Fig. 23. Results of the three forecasting techniques.

Table 12. Critical values that distinguish between CAT and non-CAT for each technique.

Technique	Values for CAT	Values for non-CAT
Statistical Analysis	≥ 7	≤ 5
Discriminant Function Analysis	≥ 3	≤ 2
Curvature Analysis	$\geq -1.0 \times 10^{-7} \text{m}^{-2}$	$< -1.0 \times 10^{-7} \text{m}^{-2}$

Table 13. Examples of forecasts from various combinations of the three techniques.

<u>VALUES</u>			Forecast
Statistical Analysis	Discriminant Function Analysis	Curvature Analysis	
≤ 5	≥ 3	$\geq -1.0 \times 10^{-7} \text{m}^{-2}$	CAT
6	≥ 3	≥ -1.0	CAT
6	< 3	≥ -1.0	CAT
≥ 7	≥ 3	≥ -1.0	CAT
≥ 7	< 3	≥ -1.0	CAT
≥ 7	≥ 3	< -1.0	CAT
≤ 5	< 3	≥ -1.0	non-CAT
≤ 5	< 3	< -1.0	non-CAT
≤ 5	≥ 3	< -1.0	non-CAT
6	< 3	< -1.0	non-CAT
6	≥ 3	< -1.0	non-CAT
≥ 7	< 3	< -1.0	non-CAT

In certain instances, the forecasting procedure weighted the results of one technique more than the others. Certain extreme numerical values were defined for each technique. These extremes are listed in Table 14. If the numerical result of one technique reached an extreme value, the forecast was based on that technique only. If the numerical results for two or more techniques reached extreme values, and the suggestions from those techniques did not agree, the forecast neglected the extreme values and was determined in the manner discussed above.

C. VERIFICATION PROCEDURE

Two turbulence data samples were employed to test the forecasting procedure. The first sample was composed of CAT and non-CAT data from 23 XB-70 flight days, and the second sample was composed of 10 XB-70 flight days and 3 YF-12A flight days. The verification rates of the two samples were later compared. These samples were selected for use in verification because the aircraft tracks were extensive. The extensive flights enabled large areas of CAT and non-CAT occurring on the same day to be identified. The data for all the days were included in the development of the combined forecasting method.

Table 14. Extreme values of the numerical results from the three techniques.

Technique	Extreme values associated with CAT	Extreme values associated with non-CAT
Statistical Analysis	≥ 12	≤ 3
Discriminant Function Analysis	5	0
Curvature Analysis	$\geq 4.5 \times 10^{-7} \text{ m}^{-2}$	$\leq -4.5 \times 10^{-7} \text{ m}^{-2}$

The verification procedure began by determining, for each day, the total distance the aircraft encountered CAT and the total distance the aircraft experienced smooth flight. The total distance the aircraft flew through CAT was determined by summing the distances of all the CAT encounters. The total distance of non-CAT was estimated from the flight tracks. The non-CAT portions and the CAT encounters were separated by a distance of at least 150 km. This was done in consideration of the resolution of the synoptic data employed.

The CAT forecast maps were then compared to the flight track maps containing CAT encounters. The distances of CAT and non-CAT encounters and those forecasted were determined for each day. For both samples, the verification rates of the forecasting procedure were determined by the ratios of the summation of the distances of all the verified CAT encounters $\left(\sum_i (T_v)_i\right)$ and the summation of the distances of all the verified non-CAT portions $\left(\sum_i (NT_v)_i\right)$ each divided by the summation of the distance of the actual CAT encounters $\left(\sum_i T_i\right)$ and non-CAT portions $\left(\sum_i (NT)_i\right)$, respectively. In equation form:

$$\text{CAT Verification Percentage} = \frac{\sum_i (T_v)_i}{\sum_i (T)_i} \quad (16)$$

$$\text{Non-CAT Verification Percentage} = \frac{\sum_i (NT_v)_i}{\sum_i (NT)_i} \quad (17)$$

The results are presented in the following section.

In addition, the verification percentages were determined for the forecasting procedure for each of the five, 2.1-km (7000-ft) thick sub-layers of the stratosphere. These rates would indicate the sub-layer where the forecasting procedure most accurately predicted the occurrence of CAT.

The CAT encounters were categorized into groups determined by the altitude of the aircraft at the time CAT was encountered. The CAT verification rates were then determined for each sub-layer from the CAT encounters in that particular sub-layer and Eq. 16. The results are discussed in the following section.

This verification procedure was not performed for the non-CAT portions of the flight tracks, due to the definition of the non-CAT portions. According to the definition established, non-CAT portions were portions of the flight track where the aircraft did not encounter CAT within a distance of approximately 150 km. The non-CAT sample sizes in some of the sub-layers were insufficient since, in most cases, the aircraft did not fly through the lowest sub-layers for long distances.

D. RESULTS

The verification rates for the CAT and non-CAT areas of the first sample (comprised of 23 XB-70 flight tracks) are presented in Table 15. Those for the second sample (comprised of 10 XB-70 and 3 YF-12A flight tracks) are presented in Table 16. In addition, the CAT and non-CAT verification percentages are presented for each day.

In the first sample, 3910 km of CAT was encountered, 3120 km of which was correctly forecasted. The aircraft experienced smooth flights totaling approximately 25,600 km, 15,050 km of which was correctly forecasted. In the second sample, 2900 km of CAT was encountered and 2290 km were forecasted correctly. The aircraft experienced smooth flights totaling approximately 17,000 km in this sample and 7825 km were forecasted correctly.

When the non-CAT portions above 18.3 km (60,000 ft) were not considered, the non-CAT verification rates for both samples were improved. The improved non-CAT verification rates for the two samples are presented in Tables 17 and 18. The verification percentages increased by 7.5% and 9.1% for the first and second samples, respectively. This improvement in the non-CAT verification rate may have resulted from inadequate data above 18.3 km, or CAT patches were not encountered even though they existed, or CAT existed at altitudes below 18.3 km.

The CAT verification percentages for the five, 2.1-km (7000-ft) thick sub-layers of the larger sample are presented in Table 19. Most of the CAT encountered occurred in the 15.2-17.4-km (50,000-57,000-ft) and the 16.8-18.9-km (55,000-62,000-ft) sub-layers. The CAT verification percentages for these two sub-layers (91.9% and 82.7%, respectively) were higher than those for the remaining sub-layers. The lowest CAT verification percentage resulted for the lowest sub-layer (12.2-14.3-km or 40,000-47,000-ft sub-layer), which contained the least CAT (see Table 19), and is also more subject to variation between the stratosphere and troposphere.

Table 15. Verification rates of the forecasting procedure for the first sample of 23 flight tracks.

Date	no. of turbulent km correctly forecasted	total no. of turbulent km	no. of non-turb. km correctly forecasted	total no. of non-turb. km
March 4, 1965	52.6	209.5	0.0	0.0
April 20, 1965	296.2	306.6	0.0	0.0
April 28, 1965	0.0	14.0	1550.0	1550.0
May 7, 1965	170.9	170.9	0.0	0.0
June 16, 1965	93.4	177.5	100.0	250.0
July 1, 1965	0.0	17.0	650.0	1850.0
July 27, 1965	0.0	4.1	2250.0	2250.0
September 22, 1965	33.0	129.0	100.0	450.0
October 14, 1965	23.7	42.6	1200.0	1500.0
October 16, 1965	194.5	194.5	500.0	1100.0
October 26, 1965	0.0	1.7	1350.0	1900.0
November 2, 1965	0.0	28.8	1500.0	1500.0
November 30, 1965	0.0	3.7	700.0	1700.0
December 1, 1965	14.4	14.4	950.0	1900.0
December 2, 1965	94.5	116.6	500.0	550.0
December 11, 1965	15.0	24.6	1250.0	1800.0
January 3, 1966	374.6	489.6	0.0	750.0
January 12, 1966	205.0	205.0	100.0	850.0
February 9, 1966	171.2	171.2	1400.0	1750.0
March 10, 1966	39.8	151.5	300.0	750.0
March 15, 1966	425.3	467.7	550.0	1200.0
March 17, 1966	254.7	257.1	100.0	750.0
March 19, 1966	662.0	712.7	0.0	1100.0
Totals	3120.8	3910.3	15,050.0	25,600.0
	% correctly forecasted	79.8%		58.8%

Table 16. Verification rates of the forecasting procedure for the second sample of 13 flight tracks.

Date	no. of turbulent km correctly forecasted	total no. of turbulent km	no. of non-turb. km correctly forecasted	total no. of non-turb. km
March 24, 1966	0.0	104.1	1000.0	1000.0
March 31, 1966	68.0	117.4	1275.0	2250.0
April 4, 1966	79.6	96.5	850.0	2200.0
April 5, 1966	18.7	41.9	700.0	1200.0
April 8, 1966	37.0	139.5	600.0	1050.0
April 12, 1966	326.1	339.8	50.0	1000.0
April 13, 1966	14.5	185.0	425.0	1150.0
April 26, 1966	1105.5	1105.5	350.0	500.0
October 11, 1967	112.6	203.7	325.0	325.0
November 2, 1967	200.8	200.8	0.0	1025.0
March 26, 1970	317.3	317.3	0.0	150.0
May 7, 1970	8.4	8.4	800.0	2975.0
May 27, 1970	0.0	39.7	950.0	950.0
Totals	2288.5	2899.6	7325.0	15,775.0
% correctly forecasted		78.9%	46.4%	

Table 17. Verification rates of the forecasting procedure for the non-CAT portions of the first sample excluding the non-CAT portions above 18.3 km (60,000 ft).

Date	no. of non-turbulent km, 18.3 km (60 k ft) or below, correctly forecasted	total no. of non-turb. km, 18.3 km (60 k ft) or below
March 4, 1965	0.0	0.0
April 20, 1965	0.0	0.0
April 28, 1965	1550.0	1550.0
May 4, 1965	0.0	0.0
June 16, 1965	0.0	0.0
July 1, 1965	350.0	750.0
July 27, 1965	950.0	950.0
September 22, 1965	0.0	0.0
October 14, 1965	250.0	250.0
October 16, 1965	550.0	1100.0
October 26, 1965	1350.0	1900.0
November 2, 1965	1500.0	1500.0
November 30, 1965	700.0	1700.0
December 1, 1965	950.0	1900.0
December 2, 1965	500.0	550.0
December 11, 1965	300.0	450.0
January 3, 1966	0.0	0.0
January 12, 1966	0.0	0.0
February 9, 1966	50.0	450.0
March 10, 1966	150.0	450.0
March 15, 1966	0.0	0.0
March 17, 1966	0.0	300.0
March 19, 1966	0.0	0.0
Totals	9150.0	13,800.0
% correctly forecasted		66.3%

Table 18. Verification rates of the forecasting procedure for the non-CAT portions of the second sample excluding the non-CAT portion above 18.3 km (60,000 ft).

Date	no. of non-turbulent km, 18.3 km (60 k ft) or below, correctly forecasted	total no. of non-turb. km, 18.3 km (60 k ft) or below
March 24, 1966	1000.0	1000.0
March 31, 1966	200.0	300.0
April 4, 1966	450.0	550.0
April 5, 1966	700.0	1200.0
April 8, 1966	300.0	300.0
April 12, 1966	0.0	300.0
April 13, 1966	425.0	700.0
April 26, 1966	0.0	150.0
October 11, 1966	325.0	325.0
November 2, 1970	0.0	375.0
March 26, 1970	0.0	150.0
May 7, 1970	800.0	2975.0
May 27, 1970	950.0	950.0
Totals	5150.0	9275.0
% correctly forecasted		55.5%

Table 19. CAT verification rates for the five, 2.1-km (7000-ft) thick sub-layers of the first sample.

Date	Altitude layer (km)									
	12.2-14.3		13.7-15.9		15.2-17.4		16.8-18.9		18.3-20.4	
Mar 4 1965	52.6	187.1	27.4	68.0	0.0	0.0	0.0	0.0	0.0	0.0
May 7 1965	92.7	92.7	39.3	39.3	51.5	51.5	31.3	31.3	0.0	0.0
April 20 1965	67.1	77.5	62.8	62.8	131.1	131.1	107.5	107.5	0.0	0.0
April 28 1965	0.0	0.0	0.0	0.0	0.0	0.0	0.0	14.0	0.0	0.0
June 16 1965	12.3	12.3	7.1	7.1	42.2	42.2	31.1	115.2	38.9	38.9
July 1 1965	0.0	0.0	0.0	14.4	0.0	15.7	0.0	0.0	0.0	0.0
July 27 1965	0.0	0.0	0.0	0.0	0.0	0.0	0.0	0.0	0.0	4.0
Sept 22 1965	0.0	9.1	0.0	0.0	0.0	29.0	33.0	55.6	33.0	90.9
Oct 14 1965	0.0	0.0	0.0	15.0	23.7	39.8	0.0	2.8	0.0	0.0
Oct 16 1965	24.0	24.0	54.1	54.1	103.6	103.6	107.1	107.1	0.0	0.0
Oct 26 1965	0.0	1.7	0.0	1.7	0.0	0.0	0.0	0.0	0.0	0.0
Nov 2 1965	0.0	0.0	0.0	2.2	0.0	25.6	0.0	26.6	0.0	0.0
Nov 30 1965	0.0	1.1	0.0	3.7	0.0	2.6	0.0	0.0	0.0	0.0
Dec 1 1965	2.8	2.8	5.2	5.2	0.0	0.0	6.4	6.4	0.0	0.0
Dec 2 1965	0.0	38.4	82.9	94.8	18.3	25.9	2.0	12.2	0.0	0.0
Dec 11 1965	0.0	4.8	0.0	1.9	0.0	0.0	0.0	4.8	13.1	13.1
Jan 3 1966	0.0	0.0	56.5	56.5	40.4	40.4	252.6	367.6	155.5	180.5
Jan 12 1966	43.7	43.7	4.1	4.1	43.2	43.2	5.9	5.9	67.2	67.2
Feb 9 1966	29.1	29.1	73.4	73.4	97.8	97.8	92.5	92.5	0.0	0.0
Mar 3 1966	18.9	20.9	0.0	14.3	0.0	12.4	9.4	20.1	20.9	107.6
Mar 15 1966	40.1	40.1	0.0	0.0	139.7	139.7	223.0	223.0	102.8	145.2
Mar 17 1966	0.0	0.0	0.0	0.0	9.6	9.6	38.9	38.9	210.8	214.9
Mar 19 1966	0.0	0.0	0.0	0.0	530.1	530.1	449.9	449.9	97.4	97.4
Totals	383.3	585.2	412.8	518.5	1231.2	1340.2	1390.6	1681.4	739.6	959.8
% verified	65.9%		79.6%		91.9%		82.7%		77.1%	

CHAPTER VII. SUMMARY AND COMMENTS

The ultimate objective of this research was the development of a method for forecasting clear air turbulence (CAT) over the mountainous regions of the western United States at altitudes of 12-20 km. The only meteorological data available for these altitudes were rawinsonde soundings taken by the National Weather Service at 0000 GMT and 1200 GMT daily. These data were taken from the teletype records and transmitted by the National Weather Service and stored in the Texas A&M University Meteorological Archives.

Information regarding regions of turbulence used in the research was taken from 46 XB-70 and 22 YF-12A flights. Each of these flights originated and terminated at Edwards Air Force Base, California, and most flights covered quite a large area. Turbulence encounters were recorded on VGH recorders from which the horizontal dimensions, maximum vertical accelerations, and the number of the turbulence patches could be determined. From this information turbulent and non-turbulent regions were specified which had horizontal dimensions of approximately 200 km for each flight. Each turbulent region usually consisted of a number of turbulent patches while each non-turbulent region was free of turbulence. There were 94 turbulent and 78 non-turbulent regions defined for the XB-70 data, and 22 turbulent and 18 non-turbulent regions defined for the YF-12A data. These data and the rawinsonde soundings constituted the principal data source for this research.

Synoptic charts were prepared from the rawinsonde data for the 100-, 200-, and 300-mb levels at 0000 and 1200 GMT on each flight day and analyzed in the usual manner. A square grid with grid points spaced at approximately 158 km was superimposed on the synoptic charts and values of height and temperature extracted from the 200- and 300-mb levels, and temperature and wind data from the 100-mb level. These parameters form the basic meteorological data which were used to calculate all parameters considered in the study. A total of 69 parameters classified as measured, derived, or time rate-of-change was used in the research. The measured parameters consisted of wind, temperature, and height; the derived parameters included such items as vorticity and advection, and the time rate-of-change was computed for all measured and derived parameters. Empirical probability distributions were then computed for each parameter associated with the turbulent and non-turbulent regions. The distributions were then analyzed by inspection and limits noted where the distributions differed in a systematic way and included at least 10% or more of the total number of observations. The ranges thus established were used to compute conditional probabilities, and to relate parameters and combinations of parameters to regions of CAT and non-CAT.

The meteorological parameters discussed above and associated with regions of CAT and non-CAT were used in a discriminant function analysis to relate CAT and non-CAT areas to meteorological parameters. The atmosphere was divided into 2.1-km (7000-ft) layers between 12.2 and 20.4 km (40,000 and 67,000 ft) altitude and discriminant functions prepared for each layer. A large number of discriminant functions were prepared, and the five best for each layer were chosen and used in combination in the development of the forecasting procedure. This technique differentiated between CAT and

non-CAT areas for approximately 80% of the regions and indicates some possibility for distinguishing probable areas of CAT as a function of altitude.

It is well established that CAT is associated with well-developed mountain waves. Conditions favorable for mountain waves were specified and changes in the Scorer parameter with altitude were related to the turbulent and non-turbulent areas. This method gave results comparable to the discriminant function method and the statistical method in that it distinguished between turbulent and non-turbulent regions for approximately 80% of the cases.

The three methods described above, i.e., empirical probability distributions, discriminant function analysis, and mountain-wave theory were combined to form a CAT forecasting procedure. This procedure utilizes all three methods, and a CAT and non-CAT forecast is based upon the agreement of at least two of the methods, or when one gives a strong indication of the presence or absence of CAT and the others show no clear distinction. The percentage verification for the CAT and non-CAT areas for this combined procedure was approximately the same as the verifications for the individual method; however, it is believed that the statistical confidence of this forecast is far superior to the methods considered individually. With the limited amount of data available it was not possible to perform an adequate and independent evaluation of the techniques. The methods were checked from sub-samples of data drawn from the data available, and the results for individual days appear to confirm the conclusions reached from the total sample.

REFERENCES

- Badgley, F. I., 1969: Large scale processes contributing energy to clear air turbulence. Clear Air Turbulence and Its Detection, Y. H. Pao and A. Goldberg, Eds., New York, Plenum Press, 109-123.
- Ball, J. T., 1970: Cloud and synoptic parameters associated with clear air turbulence. NASA CR-111778.
- Burnham, J., 1968: Atmospheric turbulence and the SST: a review in the light of recent research. Royal Aircraft Establishment Technical Report No. 68096, 38 pp.
- _____, 1969: Atmospheric turbulence at supersonic transport altitudes. Quart. J. Roy. Meteor. Soc., 95, 782-784.
- Clodman, J., G. Morgan, Jr., and J. T. Ball, 1961: High level turbulence. Final Report, AF19(604)-5208, College of Engineering, New York University, New York, 73-75.
- Colquhoun, J. R. and V. L. Bourke, 1967: Clear air turbulence analysis over the South Pacific Region for a five-day period in December 1964. Australian Meteorological Journal, 15, No. 2, 47-72.
- _____, 1967: A summary of four, five-day clear air turbulence reporting periods. Australian Meteorological Journal, 15, No. 2, 131-132.
- Colson, D. and H. A. Panofsky, 1965: An index of clear air turbulence. Quart. J. Roy. Meteor. Soc., 91, No. 390, 507-513.
- _____, 1969: Clear-air turbulence and upper level meteorological patterns. Clear Air Turbulence and Its Detection, Y. H. Pao and A. Goldberg, Eds., New York, Plenum Press, 337-359.
- Corby, G. A. and J. S. Sawyer, 1958: The air flow over a ridge--the effects of the upper boundary and high level conditions. Quart. J. Roy. Meteor. Soc., 84, 5-37.
- _____ and C. E. Wallington, 1956: Air flow over mountains: the lee-wave amplitude. Quart. J. Roy. Meteor. Soc., 82, 266-274.
- Cox, R. E., 1973: Forecasting stratospheric clear-air turbulence by discriminant analysis. M.S. Thesis, Texas A&M University, College Station, Texas, 64 pp.
- Delay, R. D. and J. A. Dutton, 1971: An analysis of conditions associated with an occurrence of stratospheric CAT. Journal of Atmospheric Science, 28, No. 7, 1272-1279.
- Dutton, J. A., 1969: An energy budget for a layer of stratospheric CAT. Radio Science, 4, No. 12, 1137-1142.

REFERENCES (Continued)

- _____ and H. A. Panofsky, 1970: Clear air turbulence: a mystery may be unfolding, Science, 167, No. 3920, 937-944.
- Ehernberger, L. J., 1968: Atmospheric conditions associated with turbulence encountered by the XB-70 airplane above 40,000 feet altitude. NASA TN D-4768, Washington, D. C., 47 pp.
- Eliassen, A. and E. Palm, 1961: On the transfer of energy in stationary mountain waves. Geofys. Publikasjoner, 22, No. 3, 1-23.
- Endlich, R. M., 1964: The mesoscale structure of some regions of CAT. J. Appl. Meteor., 3, 261-276.
- _____ and R. L. Mancuso, 1964: Clear-air turbulence and its analysis by use of rawinsonde data. Final Report, Project No. 4521, Stanford Research Institute, Menlo Park, California, 55 pp.
- _____, 1967: Forecasting clear-air turbulence by computer techniques. Final Report, Project No. 153-002-01A, Stanford Research Institute, Menlo Park, California, 86 pp.
- Fisher, R. A., 1936: The use of multiple measurements in taxonomic problems. Ann. Eugenics, 7, Part II, 179-188.
- Foltz, H. P., 1967: Prediction of clear air turbulence. Atmospheric Science Paper No. 106, Colorado State University, Fort Collins, Colorado, 145 pp.
- Fulton, F. L., 1968: Lessons from the XB-70 as applied to the supersonic transport. NASA TMX-56014.
- Gazzola, A., 1964: The effects of mountains on air currents (translation). Redstone Scientific Information Center-131, U.S. Army Missile Command, Redstone Arsenal, Alabama, 21 pp.
- Gotaas, Y., 1961: Mother of pearl clouds over Southern Norway, February 21, 1959, Geofys. Publikasjoner, 22, No. 4, 13 pp.
- Haltiner, G. J. and F. L. Martin, 1957: Dynamical and Physical Meteorology. McGraw-Hill, New York, 470 pp.
- Harrison, H. T., 1959: The uses of horizontal wind shear in forecasting high level clear-air turbulence. United Air Lines Meteorology Circular No. 49, Denver, Colorado, 22 pp.
- _____ and D. F. Sowa, 1966: Mountain wave exposure on jet routes of Northwest Airlines and United Air Lines. UAL Meteorology Circular No. 60, Denver, 66 pp.

REFERENCES (Continued)

- Hicks, J. J. and J. K. Angell, 1968: Radar observations of breaking gravitational waves in the visually clear atmosphere. J. Appl. Meteor., 7, 114-121.
- Hines, C. O., 1960: Internal atmospheric gravity waves at ionospheric heights. Can. J. Physics, 38, 1441-1481.
- _____ and C. A. Reddy, 1967: On the propagation of atmospheric gravity waves through regions of wind shear. J. Geophys. Res., 72, 1015-1034.
- Holmboe, J., 1963: Instability of stratospheric shear flow. Final Report, AF 19(604)-7999, University of California at Los Angeles.
- _____ and J. Klieforth, 1957: Investigations of mountain lee-waves and the air flow over the Sierra Nevada. Final Report, Contract No. AF 19(064)-728, Dept. of Meteorology, Univ. of California, Los Angeles, California, 290 pp.
- Kordes, E. E. and B. J. Love, 1967: Preliminary evaluation of XB-70 airplane encounters with high-altitude turbulence. NASA TN D-4209.
- Kronebach, G. W., 1964: An automated procedure for forecasting clear air turbulence. Jour. of Applied Meteor., 3, No. 2, 119-125.
- Kuettner, J. P., 1952: On the possibility of soaring on traveling waves in the jet stream. Aero. Eng. Rev., 11, 1-7.
- Lumley, J. L. and H. A. Panofsky, 1964: The Structure of Atmospheric Turbulence. John Wiley and Sons, New York, 239 pp.
- Mancuso, R. L., R. M. Endlich, and J. W. Davies, 1966: Techniques for determining a world-wide climatology of turbulence through use of meteorological data. Final Report, Project No. 8624, AF 19(628)-5173, Stanford Research Institute, Menlo Park, California, 62 pp.
- Miller, R. G., 1962: Statistical prediction by discriminant analysis. Meteor. Monogr., 4, No. 25, 54 pp.
- Mitchell, F. A. and D. T. Prophet, 1969: Meteorological analysis of clear air turbulence in the stratosphere. Clear Air Turbulence and Its Detection, Y. H. Pao and A. Goldberg, Eds., New York, Plenum Press, 144-182.
- Moore, R. L. and T. N. Krishnamurti, 1966: A theory of generation of clear air turbulence. Proceedings of ION/SAE Conference on Clear Air Turbulence, 13-27.

REFERENCES (Continued)

- Palm, E. and A. Foldvik, 1960: Contribution to the theory of two-dimensional mountain waves. Geofys. Publikasjoner, 21, No. 6, 1-30.
- Panofsky, H. A. and G. W. Brier, 1958: Some Applications of Statistics to Meteorology. Pennsylvania State University, University Park, Pennsylvania, 118-122.
- Pao, Y. H. and A. Goldberg, Editors, 1969: Clear Air Turbulence and Its Detection, Plenum Press, New York.
- Powell, F. A., 1968: An evaluation of stratospheric CAT forecasts for mid-latitudes. Australian Meteorological Journal, 16, No. 2, 35-46.
- Reiter, E. R., 1969: The nature of clear air turbulence: a review. Clear Air Turbulence and Its Detection. Y. H. Pao and A. Goldberg, Eds., New York, Plenum Press, 542 pp.
- _____ and H. P. Foltz, 1967: The prediction of clear-air turbulence over mountainous terrain. Jour. of Applied Meteor., 6, 549-556.
- Robinson, G. D., 1967: Some current projects for global meteorological observation and experiment. Quart. J. Roy. Meteor. Soc., 93, 409-418.
- Sawyer, J. S., 1960: Numerical calculation of the displacements of a stratified air stream crossing a ridge of small height. Quart. J. Roy. Meteor. Soc., 86, 326-345.
- Scoggins, J. R., J. E. Wood, H. E. Fuelberg, and W. L. Read, 1972: An investigation of relationships between meso- and synoptic-scale phenomena. Final Report, NASA Contract NAS8-25400, Dept. of Meteorology, Texas A&M University, College Station, Texas, 179 pp.
- _____ and T. P. Incrocci, 1973: Mountain waves and CAT encountered by the XB-70 in the stratosphere. Jour. of Aircraft, 10, 172-180.
- Scorer, R. S., 1949: Theory of waves in the lee of mountains. Quart. J. Roy. Meteor. Soc., 75, 41-56.
- _____, 1954: Theory of airflow over mountains - III airstream characteristics. Quart. J. Roy. Meteor. Soc., 75, 417-428.
- _____, 1969: Mechanisms of clear air turbulence. Clear Air Turbulence and Its Detection, Y. H. Pao and A. Goldberg, Eds., Plenum Press, New York, 34-50.
- Starch, S., 1968: Flying in turbulence. Combat Crew, October, 8-12.
- Thompson, G. J., 1973: The nature of the mesoscale wind and temperature structure during a case of CAT. AFCRL-TR-73-0222, Air Force Cambridge Research Laboratories, Bedford, Massachusetts, 13 pp.

REFERENCES (Continued)

- Veazey, D. R., 1970: A literature survey of clear-air turbulence. Report No. 1, NGR-44-001-081, Department of Meteorology, Texas A&M University, College Station, Texas, 101 pp.
- Waco, D. E., 1970: A statistical analysis of wind and temperature variables associated with high altitude clear-air turbulence (HICAT). J. Appl. Meteor., 9, 300-308.
- Wilson, R. J., B. J. Love, and R. R. Larson, 1971: Evaluation of effects of high-altitude turbulence encounters on the XB-70 airplane. TN D-6457.

APPENDIX A

Computer Program for the Computation of Synoptic Meteorological Parameters

Most of the flight altitudes for the 46 XB-70 flights considered in this report were between the 300- and 100-mb levels. Synoptic charts were analyzed for the 300-, 200-, and 100-mb constant-pressure surfaces in the usual manner and data obtained from the analyzed charts or by interpolation for each grid point.

The computer program presented here was used to compute the following parameters at each grid point shown in Fig. 1 in the text.

1. Richardson number (Ri)
2. Horizontal wind shear ($\partial \vec{v}_n / \partial n$)
3. Lapse rate of temperature ($\partial T / \partial z$)
4. Advection of relative vorticity ($-\vec{v} \cdot \vec{\nabla} \zeta$)
5. Advection of temperature ($-\vec{v} \cdot \vec{\nabla} T$)
6. Temperature (T)
7. CAT Index (I)
8. Zonal wind component (u)
9. Meridional wind component (v)
10. Scalar wind speed (V)
11. Relative vorticity (ζ)
12. Absolute vorticity (η)
13. Product (βv)
14. Contour heights (H) (200 and 300 mb only)
15. Vertical vector wind shear ($\partial \vec{v} / \partial z$)
16. Advection of absolute vorticity ($-\vec{v} \cdot \vec{\nabla} (\zeta + f)$)
17. Time rate-of-change of each of the above parameters over the 12-hr period encompassing each flight.

In addition to the parameters listed above, the horizontal gradient of temperature on each constant-pressure surface also was computed; however, the computation of this parameter was accomplished separately and is not included in the computer program.

For those familiar with FORTRAN programming, it is not difficult to follow the procedures employed in the computations. Each of the above items is referred to as an equation in the computer program and each equation is referred to in the coding. The finite-difference equations will not be presented for each parameter, however, the following example will be given.

Consider the advection of temperature ($-\vec{v} \cdot \vec{\nabla} T$) referred to as Eq. 5 in the computer program. By definition of a vector dot product

$$-\vec{v} \cdot \vec{\nabla} T = -u \frac{\partial T}{\partial x} - v \frac{\partial T}{\partial y} \quad (\text{A-1})$$

where u and v are the zonal (W-E) and meridional (S-N) wind components, respectively, and x and y are the orthogonal horizontal coordinates with x positive toward the east and y positive toward the north. Assuming u and v as components of the geostrophic wind (this assumption was made for the 200- and 300-mb levels but not for the 100-mb level where the wind components were taken from analyzed charts), Eq. A-1 may be written

$$-\vec{v} \cdot \vec{\nabla} T = -\frac{g}{f} \frac{\partial H}{\partial y} \frac{\partial T}{\partial x} - \frac{g}{f} \frac{\partial H}{\partial x} \frac{\partial T}{\partial y} \quad (\text{A-2})$$

where H represents the geopotential height of the constant-pressure surface, g is the acceleration due to gravity, and f is the coriolis parameter. Equation A-2 written in finite-difference form, where the finite differences are over an interval of $2\Delta x$ (Δx is the distance between points in Fig. 1 (see text) in either the x - or y -direction), becomes

$$-\vec{v} \cdot \vec{\nabla} T = \frac{-g}{4f(\Delta x)^2} (H_{i,j+1} - H_{i,j-1})(T_{i+1,j} - T_{i-1,j}) + (H_{i+1,j} - H_{i-1,j})(T_{i,j+1} - T_{i,j-1}). \quad (\text{A-3})$$

The computed value of advection is associated with the mid-point of the array of points used in Eq. A-3. The subscripts i and j refer to points in the array shown in Fig. 1 with i beginning with one in the lower left-hand corner and increasing toward the right (along the x -axis), and j beginning with one at the same place and increasing toward the top of the figure (along the y -axis).

COMPUTER PROGRAM

C 100, 200 & 300 MBS. PROGRAMS COMBINED TO COMPUTE PARTIAL OF A PARAMETER
 C WITH RESPECT TO TIME.
 C TEXAS A&M UNIVERSITY ... METEOROLOGY DEPT. ... DAVID LINE/PROGRAMMER
 C N.B. LAST CARD OF DATA DECK MUST HAVE AN ASTIK IN COLUMN 2

C THE EQUATIONS USED IN THIS PROGRAM AS THEY ARE NUMBERED
 C EQ. 01 RICHARDSON NUMBER (RI)
 C EQ. 02 HORIZONTAL WIND SHEAR (DV/DN)
 C EQ. 03 PARTIAL OF TEMPERATURE WITH RESPECT TO HEIGHT (TZ)
 C EQ. 04 ADVECTION OF RELATIVE VORTICITY (-V .NABLA(ZETA))
 C EQ. 05 ADVECTION OF TEMPERATURE (-V .NABLA T)
 C EQ. 06 TEMPERATURE
 C EQ. 07 CAT INDEX (IX)
 C EQ. 08 ZONAL WIND COMPONENT (U)
 C EQ. 09 MERIDIONAL WIND COMPONENT (V)
 C EQ. 10 SCALAR WIND SPEED (|V|)
 C EQ. 11 RELATIVE VORTICITY (ZETA)
 C EQ. 12 ABSOLUTE VORTICITY (ETA)
 C EQ. 13 PRODUCT BV
 C EQ. 14 CONTOUR HEIGHTS (200 & 300 MBS. ONLY)
 C EQ. 15 VERTICAL WIND SHEAR (DV/DZ)
 C EQ. 16 ADVECTION OF (ZETA+F)

C .. DIMENSION STATEMENTS ..

REAL
 . RI(11,11) , RIP(11,11) , VN1(11,11) , VN1P(11,11)
 . , VN2(11,11) , VN2P(11,11) , VN3(11,11) , VN3P(11,11)
 . , TZ(11,11) , TZP(11,11) , AZ1(11,11) , AZ1P(11,11)
 . , AZ2(11,11) , AZ2P(11,11) , AZ3(11,11) , AZ3P(11,11)
 . , AT1(11,11) , AT1P(11,11) , AT2(11,11) , AT2P(11,11)
 REAL
 . AT3(11,11) , AT3P(11,11) , T1(11,11) , T1P(11,11)
 . , T2(11,11) , T2P(11,11) , T3(11,11) , T3P(11,11)
 . , IX(11,11) , IXP(11,11) , U1(11,11) , U1P(11,11)
 . , U2(11,11) , U2P(11,11) , U3(11,11) , U3P(11,11)
 . , V1(11,11) , V1P(11,11) , V2(11,11) , V2P(11,11)
 REAL
 . V3(11,11) , V3P(11,11) , VS1(11,11) , VS1P(11,11)
 . , VS2(11,11) , VS2P(11,11) , VS3(11,11) , VS3P(11,11)
 . , ZETA1(11,11) , ZETA1P(11,11) , ZETA2(11,11) , ZETA2P(11,11)
 . , ZETA3(11,11) , ZETA3P(11,11) , ETA1(11,11) , ETA1P(11,11)
 . , ETA2(11,11) , ETA2P(11,11) , ETA3(11,11) , ETA3P(11,11)
 REAL
 . BV1(11,11) , BV1P(11,11) , BV2(11,11) , BV2P(11,11)
 . , BV3(11,11) , BV3P(11,11) , H2(11,11) , H2P(11,11)
 . , H3(11,11) , H3P(11,11) , VZ(11,11) , VZP(11,11)
 . , E1(11,11) , E1P(11,11) , E2(11,11) , E2P(11,11)
 . , E3(11,11) , E3P(11,11) , OZ(11,11) , OV2(11,11)

```

REAL
.   AUX(11,11) , AUX1(11,11) , F(11)
INTEGER
.   LABEL(7,40) , LABELP(7,40) , NAME1(26) , NAME2(26)
.   , NAME3(26) , NAME4(26) , KAUX(11,11) , ASTRIK
DATA ASTRIK /'*' /
COMMON AUX1
CONSTANTS
IE = 11
JE = 11
IS = IF - 1
JS = JE - 1
B39 = 1.78E-11
DX = 1.6272E05
F35 = 0.835E-04
G = 9.80616
CDX = 1.0/(4.0*DX*DX)
CDX1 = 1.0/(2.0*DX)
KOUNT = 0
100 CONTINUE
KOUNT = KOUNT + 1
IF(KOUNT.GT.2) KOUNT = 1
C .. READ ALL DATA AT ONE REFERENCE TIME ..
C IF(KOUNT.EQ.1) TIME REFERENCE = 00
C IF(KOUNT.EQ.2) TIME REFERENCE = +12
C
C -- 100 MB. LEVEL --
101 READ(5,10) INDEX, (LABEL(1,I),I=1,40)
10 FORMAT(11,40A1)
IF(LABEL(1,1).EQ.ASTRIK) GO TO 9999
CALL READX(KAUX,IE,JE)
DO 105 J = 1, JE
DO 105 I = 1, IE
105 KAUX(I,J) = -KAUX(I,J)
CALL SMOOTH(KAUX,T1,IE,JE)
WRITE(6,11) INDEX, (LABEL(1,I),I=1,40)
11 FORMAT(/1H1,11,7X,40A1///)
CALL PRINT(T1,AUX,IF,JE)
READ(5,10) INDEX, (LABEL(2,I),I=1,40)
CALL READX(KAUX,IE,JE)
CALL SMOOTH(KAUX,U1,IE,JE)
WRITE(6,11) INDEX, (LABEL(2,I),I=1,40)
READ(5,10) INDEX, (LABEL(3,I),I=1,40)
CALL READX(KAUX,IE,JE)
CALL SMOOTH(KAUX,V1,IE,JE)
DO 110 I = 1, IE
DO 110 J = 1, JE
UI(I,J) = U1(I,J)/1.94254

```

```

110      VI(I,J) = VI(I,J)/1.94254
      CALL PRINT(U1,AUX,IE,JE)
      WRITE(6,11) INDEX, (LABEL(3,I),I=1,40)
      CALL PRINT(V1,AUX,IE,JE)
C
C      --200 MB. LEVEL.
C
      READ(5,10) INDEX, (LABEL(4,I),I=1,40)
      CALL READX(KAUX,IE,JE)
      CALL SMOOTH(KAUX,H2,IE,JE)
      CALL SMOO(H2,AUX,IE,JE)
      WRITE(6,12) INDEX, (LABEL(4,I),I=1,40)
      CALL PRINT(H2,AUX,IE,JE)
12  FORMAT(/1H1,I1,7X,40A1,5X,' HEIGHT GIVEN IN TENS OF METERS'///)
      READ(5,10) INDEX, (LABEL(5,I),I=1,40)
      CALL RFADX(KAUX,IE,JE)
      DO 115 I = 1, IE
          DO 115 J = 1, JE
115      KAUX(I,J) = -KAUX(I,J)
      CALL SMOOTH(KAUX,T2,IE,JE)
      WRITE(6,11) INDEX, (LABEL(5,I),I=1,40)
      CALL PRINT(T2,AUX,IE,JE)
C
C      --300 MB. LEVEL
C
      READ(5,10) INDEX, (LABEL(6,I),I=1,40)
      CALL READX(KAUX,IE,JE)
      CALL SMOOTH(KAUX,H3,IE,JE)
      CALL SMOO(H3,AUX,IE,JE)
      WRITE(6,12) INDEX, (LABEL(6,I),I=1,40)
      CALL PRINT(H3,AUX,IE,JE)
      READ(5,10) INDEX, (LABEL(7,I),I=1,40)
      CALL READX(KAUX,IE,JE)
      DO 120 I = 1, IE
          DO 120 J = 1, JE
120      KAUX(I,J) = -KAUX(I,J)
      CALL SMOOTH(KAUX,T3,IE,JE)
      WRITE(6,11) INDEX, (LABEL(7,I),I=1,40)
      CALL PRINT(T3,AUX,IE,JE)
C
C      COMPUTATION OF THE FIELDS
C
      DO 125 J = 2, JS
125  F(J) = F35 + B39*(FLOAT(J-1) * DX)
C
C      --100 MB. LEVEL--

```

```

C
150 C = 1.0/(2.0 * DX )
DO 200 J = 2, JS
  DO 200 I = 2, IS
    TX = T1(I+1,J) - T1(I-1,J)
    TY = T1(I,J+1) - T1(I,J-1)
    VX = V1(I+1,J) - V1(I-1,J)
    UY = U1(I,J+1) - U1(I,J-1)
    AT1(I,J) = C * (-U1(I,J)*TX - V1(I,J)*TY)
    ZETA1(I,J) = C * (VX - UY)
    ETA1(I,J) = ZETA1(I,J) + F(J)
    BV1(I,J) = 839 * V1(I,J)
200  VS1(I,J) = SQRT(U1(I,J)**2 + V1(I,J)**2)
    CALL EXTRAP(VS1,IE,JE)
    CALL EXTRAP(BV1,IE,JE)
    CALL EXTRAP(ETA1,IE,JE)
    CALL EXTRAP(ZETA1,IE,JE)
    CALL EXTRAP(AT1,IE,JE)
    DO 250 J = 2, JS
      DO 250 I = 2, IS
        ETAX = ETA1(I+1,J) - ETA1(I-1,J)
        ETAY = ETA1(I,J+1) - ETA1(I,J-1)
        ZETAX = ZETA1(I+1,J) - ZETA1(I-1,J)
        ZETAY = ZETA1(I,J+1) - ZETA1(I,J-1)
        VX = VS1(I+1,J) - VS1(I-1,J)
        VY = VS1(I,J+1) - VS1(I,J-1)
        E1(I,J) = C * (-U1(I,J)*ETAX - V1(I,J)*ETAY)
        AZ1(I,J) = C * (-U1(I,J)*ZETAX - V1(I,J)*ZETAY)
250  VNI(I,J) = C * (V1(I,J)*VX - U1(I,J)*VY)/VS1(I,J)
    CALL EXTRAP(E1,IE,JE)
    CALL EXTRAP(AZ1,IE,JE)
    CALL EXTRAP(VNI,IE,JE)
    DO 275 I = 1, 26
275  NAME1(I) = LABEL(1,I+14)
    WRITE(6,17) NAME1
17  FORMAT('1ADVECTION FROM -VEC V.NABLA T',5X,26A1///)
    CALL PRINT(AT1,AUX,IE,JE)
    WRITE(6,18) NAME1
18  FORMAT('1ZETA',5X,26A1///)
    CALL PRINT(ZETA1,AUX,IE,JE)
    WRITE(6,19) NAME1
19  FORMAT('1ETA',5X,26A1///)
    CALL PRINT(ETA1,AUX,IE,JE)
    WRITE(6,20) NAME1
20  FORMAT('1BV',5X,26A1///)
    CALL PRINT(BV1,AUX,IE,JE)
    WRITE(6,21) NAME1
21  FORMAT('1VS ,WIND SCALAR',5X,26A1///)

```

EQ. 5
EQ. 11
EQ. 12
EQ. 13
EQ. 10

EQ. 16
EQ. 4
EQ. 2

```

CALL PRINT(VS1,AUX,IE,JE)
WRITE(6,22) NAME1
22 FORMAT('IE ,FROM -VEC V.NABLA(ZETA+F)',5X,26A1///)
CALL PRINT(E1,AUX,IE,JE)
WRITE(6,23) NAME1
23 FORMAT('IAZ ,FROM -VEC V.NABLA(ZETA)',5X,26A1///)
CALL PRINT(AZ1,AUX,IE,JE)
WRITE(6,24) NAME1
24 FORMAT('IVN ,GRAD(SPEED), DV/DN',5X,26A1///)
CALL PRINT(VN1,AUX,IE,JE)
C
C --200 MB LEVEL--
C
DO 300 J = 2, JS
C = G/(4.0*F(J) * DX**2) * 10.0
C1 = G/(F(J)*DX**2) * 10.0
C2 = B39 * G/(2.0*F(J)*DX)*10.0
C3 = G/(2.0*F(J)*DX)*10.0
DO 300 I = 2, IS
ZY = H2(I,J+1) - H2(I,J-1)
ZX = H2(I+1,J) - H2(I-1,J)
TX = T2(I+1,J) - T2(I-1,J)
TY = T2(I,J+1) - T2(I,J-1)
AT2(I,J) = C * (-ZY*TX - ZX*TY) EQ. 5
ZETA2(I,J) = C1 * (H2(I+1,J) + H2(I-1,J) + H2(I,J+1) + H2(I,J
-1) - 4.0 * H2(I,J)) EQ. 11
ETA2(I,J) = ZETA2(I,J) + F(J) EQ. 12
BV2(I,J) = C2 * ZX EQ. 13
U2(I,J) = -C3 * ZY EQ. 8
V2(I,J) = C3 * ZX EQ. 09
300 VS2(I,J) = SQRT( U2(I,J)**2 + V2(I,J)**2) EQ. 10
CALL EXTRAP(VS2,IE,JE)
CALL EXTRAP(AT2,IE,JE)
CALL EXTRAP(ZETA2,IE,JE)
CALL EXTRAP(ETA2,IE,JE)
CALL EXTRAP(BV2,IE,JE)
CALL EXTRAP(U2,IE,JE)
CALL EXTRAP(V2,IE,JE)
349 DO 350 J = 2, JS
C = G/(4.0 * F(J) * DX**2) * 10.0
DO 350 I = 2, IS
ZX = H2(I+1,J) - H2(I-1,J)
ZY = H2(I,J+1) - H2(I,J-1)
ETAX = ETA2(I+1,J) - ETA2(I-1,J)
ETAY = ETA2(I,J+1) - ETA2(I,J-1)
ZETAX = ZETA2(I+1,J) - ZETA2(I-1,J)
ZETAY = ZETA2(I,J+1) - ZETA2(I,J-1)
VX = VS2(I+1,J) - VS2(I-1,J)

```

```

      VY = VS2(I,J+1) - VS2(I,J-1)
      E2(I,J) = C * ( ZY*ETAX - ZX*ETAY )
      A22(I,J) = C * ( ZY*ZETAX - ZX*ZETAY )
      VABS = SQRT( ZX**2 + ZY**2 )
350  VN2(I,J) = ((ZX*VX + ZY*VY)/VABS) * CDX1
      CALL EXTRAP(VN2,IE,JE)
      CALL EXTRAP(E2,IE,JE)
      CALL EXTRAP(A22,IE,JE)
370  DO 375 I = 1, 26
375  NAME1(I) = LABEL(4,I+14)
      WRITE(6,17) NAME1
      CALL PRINT(AT2,AUX,IE,JE)
      WRITE(6,18) NAME1
      CALL PRINT(ZETA2,AUX,IE,JE)
      WRITE(6,19) NAME1
      CALL PRINT(ETA2,AUX,IE,JE)
      WRITE(6,20) NAME1
      CALL PRINT(BV2,AUX,IE,JE)
      WRITE(6,25) NAME1
25  FORMAT( '1U BY GEOSTROPHIC WIND FORMULA',5X,26A1//)
      CALL PRINT(U2,AUX,IE,JE)
      WRITE(6,26) NAME1
26  FORMAT( '1V BY GEOSTROPHIC WIND FORMULA',5X,26A1//)
      CALL PRINT(V2,AUX,IE,JE)
      WRITE(6,21) NAME1
      CALL PRINT(VS2,AUX,IE,JE)
      WRITE(6,22) NAME1
      CALL PRINT(E2,AUX,IE,JE)
      WRITE(6,23) NAME1
      CALL PRINT(A22,AUX,IE,JE)
      WRITE(6,24) NAME1
      CALL PRINT(VN2,AUX,IE,JE)

C
C  --300 MB. LEVEL--
C
390  DO 400 J = 2, JS
      C = G/(4.0 * F(J) * DX**2) * 10.0
      C1 = G/(F(J) * DX**2) * 10.0
      C2 = B39 * G/(2.0 * F(J) * DX) * 10.0
      C3 = G/(2.0 * F(J) * DX) * 10.0
      DO 400 I = 2, IS
          ZY = H3(I,J+1) - H3(I,J-1)
          ZX = H3(I+1,J) - H3(I-1,J)
          TX = T3(I+1,J) - T3(I-1,J)
          TY = T3(I,J+1) - T3(I,J-1)
          AT3(I,J) = C * (-ZY*TX - ZX*TY)
          ZETA3(I,J) = C1 * (H3(I+1,J) + H3(I-1,J) + H3(I,J+1) + H3(I,J
          -1) - 4.0 * H3(I,J))

```

EQ. 16

EQ. 4

EQ. 2

EQ. 5

EQ. 11

	ETA3(I,J) = ZETA3(I,J) + F(J)	EQ. 12
	BV3(I,J) = C2 * ZX	EQ. 13
	U3(I,J) = -C3 * ZY	EQ. 8
	V3(I,J) = C3 * ZX	EQ. 9
400	VS3(I,J) = SQRT(U3(I,J)**2 + V3(I,J)**2)	EQ. 10
	CALL EXTRAP(VS3,IE,JE)	
	CALL EXTRAP(AT3,IE,JE)	
	CALL EXTRAP(ZETA3,IE,JE)	
	CALL EXTRAP(ETA3,IE,JE)	
	CALL EXTRAP(BV3,IE,JE)	
	CALL EXTRAP(U3,IE,JE)	
	CALL EXTRAP(V3,IE,JE)	
449	DO 450 J = 2, JS	
	C = G/(4.0 * F(J) *DX**2) *10.0	
	DO 450 I = 2, IS	
	ZX = H3(I+1,J) - H3(I-1,J)	
	ZY = H3(I,J+1) - H3(I,J-1)	
	ETAX = ETA3(I+1,J) - ETA3(I-1,J)	
	ETAY = ETA3(I,J+1) - ETA3(I,J-1)	
	ZETAX = ZETA3(I+1,J) - ZETA3(I-1,J)	
	ZETAY = ZETA3(I,J+1) - ZETA3(I,J-1)	
	VX = VS3(I+1,J) - VS3(I-1,J)	
	VY = VS3(I,J+1) - VS3(I,J-1)	
	E3(I,J) = C * (ZY*ETAX - ZX*ETAY)	EQ. 16
	AZ3(I,J) = C * (ZY*ZETAX - ZX*ZETAY)	EQ. 4
	VABS = SQRT(ZX**2 + ZY**2)	
450	VN3(I,J) = ((ZX*VX + ZY*VY) / VABS) * CDX1	EQ. 2
	CALL EXTRAP(VN3,IE,JE)	
	CALL EXTRAP(E3,IE,JE)	
	CALL EXTRAP(AZ3,IE,JE)	
470	DO 475 I = 1, 26	
475	NAME1(I) = LABEL(6,I+14)	
	WRITE(6,17) NAME1	
	CALL PRINT(AT3,AUX,IE,JE)	
	WRITE(6,18) NAME1	
	CALL PRINT(ZETA3,AUX,IE,JE)	
	WRITE(6,19) NAME1	
	CALL PRINT(ETA3,AUX,IE,JE)	
	WRITE(6,20) NAME1	
	CALL PRINT(BV3,AUX,IE,JE)	
	WRITE(6,25) NAME1	
	CALL PRINT(U3,AUX,IE,JE)	
	WRITE(6,26) NAME1	
	CALL PRINT(V3,AUX,IE,JE)	
	WRITE(6,21) NAME1	
	CALL PRINT(VS3,AUX,IE,JE)	
	WRITE(6,22) NAME1	
	CALL PRINT(E3,AUX,IE,JE)	

```

WRITE(6,23) NAME1
CALL PRINT(AZ3,AUX,IE,JE)
WRITE(6,24) NAME1
CALL PRINT(VN3,AUX,IE,JE)
C
C  --100 & 200 MB. LEVELS TOGETHER--
C
499 DO 500 I = 1, IE
      DO 500 J = 1, JE
          DZ(I,J) = 20.3 * ((T1(I,J) + T2(I,J))/2.0 + 273.0)
          TZ(I,J) = (T1(I,J) - T2(I,J))/DZ(I,J) EQ. 3
          UV2(I,J) = (U1(I,J) - U2(I,J))**2 + (V1(I,J)-V2(I,J))**2 EQ. 15
          VZ(I,J) = SQRT(UV2(I,J))/DZ(I,J) EQ. 15
          RI(I,J) = (9.8/(DZ(I,J)/20.3))*((TZ(I,J) + 0.00976)/(UV2(I,J) EQ. 1
            /((DZ(I,J)**2))) EQ. 7
500 IX(I,J) = UV2(I,J) *( 1.0 - 2.0*RI(I,J))
      DO 525 I = 1, 26
          NAME1(I) = LABEL(1,I+14)
525 NAME2(I) = LABEL(4,I+14)
      WRITE(6,27) NAME1, NAME2
27 FORMAT('1DT/DZ DEG. CEL./MX10E-03',5X,26A1,' & ',26A1///)
      CALL PRINT(TZ,AUX,IE,JE)
      WRITE(6,28) NAME1, NAME2
28 FORMAT('1DV/DZ SEC-1 X 10E-03',3X,26A1,' & ',26A1/// )
      CALL PRINT(VZ,AUX,IE,JE)
      WRITE(6,29) NAME1, NAME2
29 FORMAT('1RICHARDSON NUMBER',3X,26A1,' & ',26A1/// )
C .. BOUND RICHARDSON NUMBER FIELD BY 99.0
      DO 535 I = 1, IF
          DO 535 J = 1, JE
              AUX1(I,J) = RI(I,J)
              IF(ABS(AUX1(I,J)).LT.99.0) GO TO 535
              IF(AUX1(I,J).GT.0.0) AUX1(I,J) = 99.0
              IF(AUX1(I,J).LT.0.0) AUX1(I,J) = -99.0
535 CONTINUE
      CALL PRINT(AUX1,AUX,IE,JE)
      WRITE(6,30) NAME1, NAME2
30 FORMAT('1CAT INDEX',3X,26A1,' & ',26A1 /// )
      CALL PRINT(IX,AUX,IE,JE)
C
C  --TRANSFER OF STORAGE IF KOUNT = 1--
C
      IF(KOUNT.EQ.2) GO TO 600
549 DO 550 I = 1, IE
      DO 550 J = 1, JE
          RIP(I,J) = RI(I,J)
          VN1P(I,J) = VN1(I,J)
          VN2P(I,J) = VN2(I,J)

```

```

VN3P(I,J) = VN3(I,J)
TZP(I,J) = TZ(I,J)
AZ1P(I,J) = AZ1(I,J)
AZ2P(I,J) = AZ2(I,J)
AZ3P(I,J) = AZ3(I,J)
AT1P(I,J) = AT1(I,J)
AT2P(I,J) = AT2(I,J)
AT3P(I,J) = AT3(I,J)
T1P(I,J) = T1(I,J)
T2P(I,J) = T2(I,J)
T3P(I,J) = T3(I,J)
IXP(I,J) = IX(I,J)
U1P(I,J) = U1(I,J)
U2P(I,J) = U2(I,J)
U3P(I,J) = U3(I,J)
V1P(I,J) = V1(I,J)
V2P(I,J) = V2(I,J)
V3P(I,J) = V3(I,J)
VS1P(I,J) = VS1(I,J)
VS2P(I,J) = VS2(I,J)
VS3P(I,J) = VS3(I,J)
ZETA1P(I,J) = ZETA1(I,J)
ZETA2P(I,J) = ZETA2(I,J)
ZETA3P(I,J) = ZETA3(I,J)
ETA1P(I,J) = ETA1(I,J)
ETA2P(I,J) = ETA2(I,J)
ETA3P(I,J) = ETA3(I,J)
BV1P(I,J) = BV1(I,J)
BV2P(I,J) = BV2(I,J)
BV3P(I,J) = BV3(I,J)
H2P(I,J) = H2(I,J)
H3P(I,J) = H3(I,J)
VZP(I,J) = VZ(I,J)
E1P(I,J) = E1(I,J)
E2P(I,J) = E2(I,J)
550 E3P(I,J) = E3(I,J)
555 DO 560 I = 1, 7
      DO 560 J = 1, 40
560 LABELP(I,J) = LABEL(I,J)
      GO TO 100

C
C   --COMPUTATION OF RATE OF CHANGE OF PARAMETERS--
C
600 CONTINUE
C   --100 MBS.--
      DO 610 I = 1, 26
        NAME1(I) = LABELP(1,I+14)
610 NAME2(I) = LABEL(1,I+14)

```

```

WRITE(6,40) NAME1, NAME2
40 FORMAT('1D TEMP/DT',5X,26A1,' & ',26A1 /// )
CALL DIFF(T1,T1P)
CALL PRINT(AUX1,AUX,IE,JE)
WRITE(6,41) NAME1, NAME2
41 FORMAT('1D U/DT',5X,26A1,' & ',26A1 /// )
CALL DIFF(U1,U1P)
CALL PRINT(AUX1,AUX,IE,JE)
WRITE(6,42) NAME1, NAME2
42 FORMAT('1D V/DT',5X,26A1,' & ',26A1 /// )
CALL DIFF(V1,V1P)
CALL PRINT(AUX1,AUX,IE,JE)
WRITE(6,43) NAME1, NAME2
43 FORMAT('1D WIND SCALAR/DT',5X,26A1,' & ',26A1 /// )
CALL DIFF(VS1,VS1P)
CALL PRINT(AUX1,AUX,IE,JE)
WRITE(6,44) NAME1, NAME2
44 FORMAT('1D BV/DT',5X,26A1,' & ',26A1 ///)
CALL DIFF(BV1,BV1P)
CALL PRINT(AUX1,AUX,IE,JE)
WRITE(6,45) NAME1, NAME2
45 FORMAT('1D HCRIZONTAL WIND SHEAR/DT',5X,26A1,' & ',26A1 /// )
CALL DIFF(VN1,VN1P)
CALL PRINT(AUX1,AUX,IE,JE)
WRITE(6,46) NAME1, NAME2
46 FORMAT('1D ZETA/DT',5X,26A1,' & ',26A1 /// )
CALL DIFF(ZETA1,ZETA1P)
CALL PRINT(AUX1,AUX,IE,JE)
WRITE(6,47) NAME1, NAME2
47 FORMAT('1 D ETA/DT',5X,26A1,' & ',26A1 /// )
CALL DIFF(ETA1,ETA1P)
CALL PRINT(AUX1,AUX,IE,JE)
WRITE(6,48) NAME1, NAME2
48 FORMAT('1D ADVECTION OF ZETA/DT',5X,26A1,' & ',26A1 ///)
CALL DIFF(AZ1,AZ1P)
CALL PRINT(AUX1,AUX,IE,JE)
WRITE(6,49) NAME1, NAME2
49 FORMAT('1D ADVECTION OF ETA/DT',5X,26A1,' & ',26A1 ///)
CALL DIFF(E1,E1P)
CALL PRINT(AUX1,AUX,IE,JE)
WRITE(6,50) NAME1, NAME2
50 FORMAT('1D ADVECTION OF TEMP./DT',5X,26A1,' & ',26A1 /// )
CALL DIFF(AT1,AT1P)
CALL PRINT(AUX1,AUX,IE,JE)

```

C
C
C

--200 MBS.--

DD 620 I = 1, 26

```

NAME1(I) = LABELP(4, I+14)
620 NAME2(I) = LABEL(4, I+14)
WRITE(6,40) NAME1, NAME2
CALL DIFF(T2, T2P)
CALL PRINT(AUX1, AUX, IE, JE)
WRITE(6,51) NAME1, NAME2
51 FORMAT('1 D HEIGHT/DT', 5X, 26A1, ' & ', 26A1 /// )
CALL DIFF(H2, H2P)
C .. CONVERT HEIGHT FROM TENS OF METERS TO METERS ..
DO 625 I = 1, IE
DO 625 J = 1, JE
625 AUX1(I, J) = AUX1(I, J) * 10.0
CALL PRINT(AUX1, AUX, IE, JE)
WRITE(6,41) NAME1, NAME2
CALL DIFF(U2, U2P)
CALL PRINT(AUX1, AUX, IE, JE)
WRITE(6,42) NAME1, NAME2
CALL DIFF(V2, V2P)
CALL PRINT(AUX1, AUX, IE, JE)
WRITE(6,43) NAME1, NAME2
CALL DIFF(VS2, VS2P)
CALL PRINT(AUX1, AUX, IE, JE)
WRITE(6,44) NAME1, NAME2
CALL DIFF(BV2, BV2P)
CALL PRINT(AUX1, AUX, IE, JE)
WRITE(6,45) NAME1, NAME2
CALL DIFF(VN2, VN2P)
CALL PRINT(AUX1, AUX, IE, JE)
WRITE(6,46) NAME1, NAME2
CALL DIFF(ZETA2, ZETA2P)
CALL PRINT(AUX1, AUX, IE, JE)
WRITE(6,47) NAME1, NAME2
CALL DIFF(ETA2, ETA2P)
CALL PRINT(AUX1, AUX, IE, JE)
WRITE(6,48) NAME1, NAME2
CALL DIFF(AZ2, AZ2P)
CALL PRINT(AUX1, AUX, IE, JE)
WRITE(6,49) NAME1, NAME2
CALL DIFF(E2, E2P)
CALL PRINT(AUX1, AUX, IE, JE)
WRITE(6,50) NAME1, NAME2
CALL DIFF(AT2, AT2P)
CALL PRINT(AUX1, AUX, IE, JE)
C
C --300 MBS.--
C
DO 630 I = 1, 26
NAME1(I) = LABELP(6, I+14)

```

```

630 NAME2(I) = LABEL(6,I+14)
    WRITE(6,40) NAME1, NAME2
    CALL DIFF(T3,T3P)
    CALL PRINT(AUX1,AUX,IE,JE)
    WRITE(6,51) NAME1, NAME2
    CALL DIFF(H3,H3P)
C    .. CONVERT HEIGHT FROM TENS OF METERS TO METERS ..
    DO 635 I = 1, IE
    DO 635 J = 1, JE
635 AUX1(I,J) = AUX1(I,J) * 10.0
    CALL PRINT(AUX1,AUX,IE,JE)
    WRITE(6,41) NAME1, NAME2
    CALL DIFF(U3,U3P)
    CALL PRINT(AUX1,AUX,IE,JE)
    WRITE(6,42) NAME1, NAME2
    CALL DIFF(V3,V3P)
    CALL PRINT(AUX1,AUX,IE,JE)
    WRITE(6,43) NAME1, NAME2
    CALL DIFF(VS3,VS3P)
    CALL PRINT(AUX1,AUX,IE,JE)
    WRITE(6,44) NAME1, NAME2
    CALL DIFF(BV3,BV3P)
    CALL PRINT(AUX1,AUX,IE,JE)
    WRITE(6,45) NAME1, NAME2
    CALL DIFF(VN3,VN3P)
    CALL PRINT(AUX1,AUX,IE,JE)
    WRITE(6,46) NAME1, NAME2
    CALL DIFF(ZETA3,ZETA3P)
    CALL PRINT(AUX1,AUX,IE,JE)
    WRITE(6,47) NAME1, NAME2
    CALL DIFF(ETA3,ETA3P)
    CALL PRINT(AUX1,AUX,IE,JE)
    WRITE(6,48) NAME1, NAME2
    CALL DIFF(AZ3,AZ3P)
    CALL PRINT(AUX1,AUX,IE,JE)
    WRITE(6,49) NAME1, NAME2
    CALL DIFF(E3,E3P)
    CALL PRINT(AUX1,AUX,IE,JE)
    WRITE(6,50) NAME1, NAME2
    CALL DIFF(AT3,AT3P)
    CALL PRINT(AUX1,AUX,IE,JE)
C
C    --100 & 200 MB LEVELS TOGETHER--
C
    DO 640 I = 1, 26
    NAME1(I) = LABELP(1,I+14)
    NAME2(I) = LABELP(4,I+14)
    NAME3(I) = LABEL(1,I+14)

```

```

640 NAME4(I) = LABEL(4,I+14)
WRITE(6,53) NAME1, NAME2, NAME3, NAME4
53 FORMAT('1D VERT. WIND SHEAR/DT',3X,' FROM ',26A1,2X,26A1/ 28X,' &
.,26A1,2X,26A1/// )
CALL DIFF(VZ,VZP)
CALL PRINT(AUX1,AUX,IE,JE)
WRITE(6,54) NAME1, NAME2, NAME3, NAME4
54 FORMAT('1D LAPSE RATE OF TEMP./DT',3X,' FROM ',26A1,2X,26A1/28X,'
& ',26A1,2X,26A1 /// )
CALL DIFF(TZ,TZP)
CALL PRINT(AUX1,AUX,IE,JE)
WRITE(6,55) NAME1, NAME2, NAME3, NAME4
55 FORMAT('1D RICHARDSON NUMBER/DT',3X,' FROM ',26A1,2X,26A1/28X,' & ',26
.A1,2X,26A1 /// )
CALL DIFF(RI,RIP)
C .. BOUND D RI/DT BY 99.0
DO 650 I = 1, IE
DO 650 J = 1, JE
IF(ABS(AUX1(I,J)).LT.99.0) GO TO 650
IF(AUX1(I,J).GT.0.0) AUX1(I,J) = 99.0
IF(AUX1(I,J).LT.0.0) AUX1(I,J) = -99.0
650 CONTINUE
CALL PRINT(AUX1,AUX,IE,JE)
WRITE(6,56) NAME1, NAME2, NAME3, NAME4
56 FORMAT('1 D CAT INDEX/DT',3X,' FROM ',26A1,2X,26A1/28X,' & ',26A1,2X
.,26A1 /// )
CALL DIFF(IX,IXP)
CALL PRINT(AUX1,AUX,IE,JE)
GO TO 100
9999 WRITE(6,60)
60 FORMAT( /1H1,60X,'END OF FILE'/1H1 )
STOP
END

```

```

SUBROUTINE SMOO( A, B, IE, JE )
DIMENSION A(IE,JE), B(IE,JE)
DO 400 I = 1, IE
DO 400 J = 1, JE
B(I,J) = 0.0
K = 0
IF( I.EQ.1 ) GO TO 100
B(I,J) = B(I,J) + A(I,J) + A(I-1,J)
K = K + 2
100 IF( I.EQ.IE ) GO TO 200
B(I,J) = B(I,J) + A(I,J) + A(I+1,J)
K = K + 2
200 IF( J.EQ.1 ) GO TO 300
B(I,J) = B(I,J) + A(I,J) + A(I,J-1)
K = K + 2
300 IF( J.EQ.JE ) GO TO 400
B(I,J) = B(I,J) + A(I,J) + A(I,J+1)
K = K + 2
400 B(I,J) = B(I,J)/FLOAT(K)
DO 500 I = 1, IE
DO 500 J = 1, JE
500 A(I,J) = B(I,J)
RETURN
END

```

```

SUBROUTINE EXTRAP( A, IE, JE )
DIMENSION A(IE,JE)
IS = IF - 1
JS = JE - 1
DO 20 I = 2, IS
  A(I,1) = (3.0 * A(I,2) - A(I,3))/2.0
20 A(I,JE) = (3.0 * A(I,JS) - A(I,JE-2))/2.0
DO 30 J = 2, JS
  A(1,J) = (3.0 * A(2,J) - A(3,J))/2.0
30 A(IE,J) = (3.0 * A(IS,J) - A(IE-2,J))/2.0
  A(1,1) = 0.5 * ( A(1,2) + A(2,1) )
  A(1,JE) = 0.5 * ( A(2,JE) + A(1,JS) )
  A(IE,1) = 0.5 * ( A(IS,1) + A(IE,2) )
  A(IE,JE) = 0.5 * ( A(IS,JE) + A(IE,JS) )
RETURN
END

```

```

SUBROUTINE DIFF(A,AP)
REAL A(11,11) , AP(11,11) , AUX1(11,11)
COMMON AUX1
IE = 11
JE = 11
DO 10 I = 1, IE
DO 10 J = 1, JF
10 AUX1(I,J) = ( A(I,J) - AP(I,J))/43200.00
RETURN
END

```

```

SUBROUTINE READX(L, IE, JE)
DIMENSION L(IE,JE)
JE1 = JE + 1
DO 10 J = 1, JE
JA = JE1 - J
10 READ(5,1) ( L(I,JA),I=1,IE)
1 FORMAT(11I4)
RETURN
END

```

```

SUBROUTINE SMOOTH( L, A, IE, JE )
DIMENSION L(IE,JE), A(IE,JE)
DO 400 I = 1, IE
DO 400 J = 1, JE
  A(I,J) = 0.0
  IDIV = 0
  IF( I.EQ.1 ) GO TO 100
  A(I,J) = A(I,J) + FLOAT( L(I,J) + L(I-1,J) )
  IDIV = IDIV + 2
100 IF( I.EQ.IE ) GO TO 200
  A(I,J) = A(I,J) + FLOAT( L(I,J) + L(I+1,J) )
  IDIV = IDIV + 2
200 IF( J.EQ.1 ) GO TO 300
  A(I,J) = A(I,J) + FLOAT( L(I,J) + L(I,J-1) )
  IDIV = IDIV + 2
300 IF( J.EQ.JE ) GO TO 400
  A(I,J) = A(I,J) + FLOAT( L(I,J) + L(I,J+1) )
  IDIV = IDIV + 2
400 A(I,J) = A(I,J)/FLOAT(IDIV)
RETURN
END

```



```

SUBROUTINE SCALE( A, II, JJ, R )
C, SEARCH THE EXTREMA AND REDUCE TO THE SCALE 100 - 0.
  DIMENSION A(II, JJ)
  AMAX = -1.E+19
  AMIN = 1.E+19
  DO 5 I = 1, II
    DO 5 J = 1, JJ
      IF( A(I, J) - AMAX ) 2, 2, 1
1     AMAX = A(I, J)
      I1 = I
      J1 = J
      IF( A(I, J) - AMIN ) 3, 4, 4
2     AMIN = A(I, J)
3     I2 = I
      J2 = J
4     CONTINUE
5  CONTINUE
  R = ( AMAX - AMIN )
  IF( AMAX ) 30, 8, 9
  8 IF( AMIN ) 30, 32, 35
  9 IF( AMIN ) 20, 10, 10
10 C = AMAX
  GO TO 40
20 IF( AMAX + AMIN ) 30, 10, 10
30 C = ABS(AMIN)
  GO TO 40
32 WRITE(6, 33)
33 FORMAT( ' ----- NO SCALING PERFORMED ' )
  GO TO 55
35 MA = 1
  WRITE(6, 37)
37 FORMAT( ' WARNING. AMAX .LE. AMIN' )
  GO TO 42
40 IF( C.LT.1.0 ) C = C/10.0
  ALO = ALOG10(C)
  MA = INT(ALO)
42 IX = 1 - MA
  IY = -IX
  FACTOR = 10.0**IX
  IF( FACTOR.EQ.1.0 ) GO TO 32
  DO 50 I = 1, II
  DO 50 K = 1, JJ
50 A(I, K) = A(I, K) * FACTOR
55 WRITE(6, 60) AMAX, I1, J1, AMIN, I2, J2, R
60 FORMAT( ' MAXIMUM I K MINIMUM I K RANGE' /
. , 1P E16.8, 2I3, E16.8, 2I3, OP F16.8 )
  WRITE(6, 65) IY
65 FORMAT( ' UNITS OF F', I3 )
  RETURN
  END

```

```

SUBROUTINE PRINT( P, A, II, JJ )
C, PRINTING OF SCALAR FIELDS
  DIMENSION A(II, JJ), P(II, JJ)
  DO 1 I = 1, II
    DO 1 J = 1, JJ
1     A(I, J) = P(I, J)
  R = 1.0
  CALL SCALE( A, II, JJ, R )
  DO 2 J = 1, JJ
  J1 = JJ + 1 - J
  WRITE(6, 3) ( A(I, J1), I = 1, II )
2  CONTINUE
3  FORMAT( //1X, 11F5.1 )
  RETURN
  END

```

APPENDIX B

Frequency Distributions for Synoptic Meteorological Parameters

The synoptic meteorological parameters were classified as measured, derived, or time rate-of-change. Empirical frequency distributions and a brief discussion of these for each parameter are presented below. The number of cases in each distribution associated with turbulent areas is 94 and the number associated with non-turbulent areas is 78. Percentages of the total number of cases in each class interval are given in parentheses.

1. Measured Parameters

a. Height. Frequency distributions for the height of the 300- and 200-mb levels are shown in Table 1. When the height of the 300-mb

Table 1. Empirical frequency distributions of the height of the 300- and 200-mb surfaces associated with turbulent and non-turbulent areas.

		(a) 300 mb										
		$H_{300} \times 10^2 \text{ m}$										
Areas		≤ 87.9	88.0-88.9	89.0-89.9	90.0-90.9	91.0-91.9	92.0-92.9	93.0-93.9	94.0-94.9	95.0-95.9	96.0-96.9	≥ 97.0
Turbulent		0(0)	3(3)	4(4)	9(10)	20(21)	13(14)	20(21)	16(17)	8(9)	1(1)	0(0)
Non-turbulent		0(0)	2(3)	1(1)	6(8)	13(17)	14(18)	8(10)	19(24)	12(15)	3(4)	0(0)

		(b) 200 mb									
		$H_{200} \times 10^2 \text{ m}$									
Areas		≤ 114.9	115.0-115.9	116.0-116.9	117.0-117.9	118.0-118.9	119.0-119.9	120.0-120.9	121.0-121.9	≥ 122.0	
Turbulent		1(1)	6(6)	8(9)	16(17)	14(15)	20(21)	16(17)	8(9)	5(5)	
Non-turbulent		2(3)	2(3)	4(5)	10(13)	17(22)	7(9)	16(21)	11(14)	9(12)	

level is low, the frequency of areas with and without turbulence is about the same, but as the height increases to a value of 9.4 km and higher there were nearly twice as many areas without turbulence as there were with turbulence. In this range of heights, 44 percent of the total number of areas without turbulence occurred while only 27 percent of those with turbulence occurred in this range. The height of the 200-mb level is associated with areas with and without turbulence in about the same way as the 300-mb level. When the 200-mb level is below 12 km there is no significant difference between the areas with and without turbulence; however, 46 percent of the cases without turbulence occurred

when the height was 12 km or greater as compared to 31 percent of the cases with turbulence in this height range. Thus, when the height of these pressure levels exceeds the stated values, there are more cases without turbulence than there are with turbulence.

b. Temperature. The frequency distributions of temperature at the 300-, 200-, and 100-mb levels are presented in Table 2. Temperature does not distinguish between areas with and without turbulence at the 300- and 200-mb levels, and not in a clear way at the 100-mb level. At 100 mb, a range of temperature between -55 and -65°C contain 74 percent of the cases with turbulence as compared to 58 percent without turbulence. When the temperature was lower than -65°C , 33 percent of the cases were associated with non-turbulent areas while only 17 percent were associated with turbulent areas. From these distributions, the temperature at 100 mb can be used to a limited extent as a predictor of CAT.

Table 2. Empirical frequency distributions of temperature at 300, 200, and 100 mb associated with turbulent and non-turbulent areas.

		(a) 300 mb							
		$T_{300}^{\circ}\text{C}$							
Areas		≤ -35.0	-37.9 to -36.0	-39.9 to -38.0	-41.9 to -40.0	-43.9 to -42.0	-45.9 to -44.0	-47.9 to -46.0	≥ -48.0
		Turbulent		0(0)	3(3)	7(7)	13(14)	19(20)	13(14)
Non-turbulent		5(6)	4(5)	1(1)	15(19)	15(19)	10(13)	9(12)	19(24)

		(b) 200 mb				
		$T_{200}^{\circ}\text{C}$				
Areas		≤ -65.1	-65.0 to -60.1	-60.0 to -55.1	-55.0 to -50.1	≥ -50.0
		Turbulent		4(4)	38(40)	22(23)
Non-turbulent		3(6)	25(32)	18(23)	23(29)	7(9)

		(c) 100 mb				
		$T_{100}^{\circ}\text{C}$				
Areas		≤ -65.1	-65.0 to -60.1	-60.0 to -55.1	-55.0 to -50.1	≥ -50.0
		Turbulent		16(17)	42(45)	28(30)
Non-turbulent		26(33)	28(36)	17(22)	7(9)	0(0)

c. Wind. Frequency distributions for the zonal wind component associated with turbulent and non-turbulent areas are presented in Table 3 for the 300-, 200-, and 100-mb levels. At 300 mb, 73 percent of all the cases without turbulence occurred when the wind component was between 0 and 19 m s^{-1} (a turbulence toward the east). Forty-three percent of the cases with turbulence occurred when the zonal wind component was 20 m s^{-1} or greater as compared to only 22 percent of the non-turbulent cases. Very few cases with or without turbulence occurred when the zonal wind component was negative. At 200 mb, 61 percent of the non-turbulent cases occurred when the wind component was between 0 and 19 m s^{-1} while only 37 percent of the turbulent cases occurred in this

range. The trend was reversed for the higher wind speeds as indicated by the fact that 55 percent of the turbulent cases occurred when the wind speed was 20 m s^{-1} or greater as compared to only 33 percent of the non-turbulent cases. A trend similar to that shown by the distributions at the 300- and 200-mb levels is present also at the 100-mb level. Fifty-four percent of the non-turbulent cases occurred when the wind component was between 0 and 12 m s^{-1} as compared with 39 percent of the cases with turbulence. Fifty-six percent of the cases with turbulence were associated with a wind speed of 12 m s^{-1} and greater while only 40 percent of the non-turbulent cases were associated with this range.

Table 3. Empirical frequency distributions of the zonal wind component at 300, 200, and 100 mb associated with turbulent and non-turbulent areas.

		(a) 300 mb								
		$u_{300} \text{ m s}^{-1}$								
Areas		-40 to -31	-30 to -21	-20 to -11	-10 to -1	0-9	10- 19	20- 29	30- 39	≥ 40
Turbulent		0(0)	1(1)	4(4)	7(7)	14(15)	27(29)	23(24)	17(18)	1(1)
Non-turbulent		0(0)	0(0)	1(1)	3(4)	27(35)	30(38)	14(18)	3(4)	0(0)

		(b) 200 mb								
		$u_{200} \text{ m s}^{-1}$								
Areas		≤ -31	-30 to -21	-20 to -11	-10 to -1	0-9	10- 19	20- 29	30- 39	≥ 40
Turbulent		0(0)	1(1)	2(2)	5(5)	12(13)	23(24)	31(33)	19(20)	1(1)
Non-turbulent		0(0)	0(0)	0(0)	5(6)	13(17)	34(44)	18(23)	8(10)	0(0)

		(c) 100 mb							
		$u_{100} \text{ m s}^{-1}$							
Areas		< -4.0	-4.0 to 0.0	0.0- 4.0	4.1 8.0	8.0 12.0	12.1- 16.0	16.1- 20.0	> 20.0
Turbulent		2(2)	4(4)	10(11)	11(12)	15(16)	24(26)	14(15)	14(15)
Non-turbulent		0(0)	5(6)	15(19)	7(9)	20(26)	16(21)	10(13)	5(6)

Frequency distributions of the meridional wind component at the 300-, 200-, and 100-mb levels are presented in Table 4. Only the distribution for 200 mb shows a preferred range in speed of this component for the areas with or without turbulence. Thirty-one percent of the cases with turbulence were associated with wind speeds less than -10 m s^{-1} , while 21 percent were associated with non-turbulence. A large range in the magnitude of this wind component was observed and, as might be expected, the frequency distributions show a predominance of cases for areas with, as well as those without, turbulence with a magnitude within 10 m s^{-1} of zero meridional wind speed.

The percentage frequencies of scalar wind speed associated with turbulent and non-turbulent areas at the 300-, 200-, and 100-mb levels are shown in Table 5. At 300 mb, 58 percent of the non-turbulent cases occurred when the wind speed was less than 19 m s^{-1} while only 32 percent

Table 4. Empirical frequency distributions of the meridional wind component at 300, 200, and 100 mb associated with turbulent and non-turbulent areas.

		(a) 300 mb								
		$v_{300} \text{ m s}^{-1}$								
Areas		-40 to -31	-30 to -21	-20 to -11	-10 to - 1	0-9	10- 19	20- 29	30- 39	≥ 40
Turbulent		9(10)	8(9)	15(16)	22(23)	25(27)	6(6)	6(6)	1(1)	2(2)
Non-turbulent		2(3)	5(6)	11(14)	25(32)	21(27)	12(15)	1(1)	1(1)	0(0)

		(b) 200 mb								
		$v_{200} \text{ m s}^{-1}$								
Areas		≤ 31	-30 to -21	-20 to -11	-10 to - 1	0-9	10- 19	20- 29	30- 39	≥ 40
Turbulent		5(5)	6(6)	22(23)	20(21)	26(28)	8(9)	5(5)	2(2)	0(0)
Non-turbulent		1(1)	5(6)	11(14)	30(38)	17(22)	9(12)	4(5)	1(1)	0(0)

		(c) 100 mb								
		$v_{100} \text{ m s}^{-1}$								
Areas		≤ 31	-30 to -21	-20 to -11	-10 to - 1	0-9	10- 19	20- 29	≥ 30	
Turbulent		4(4)	5(5)	13(14)	28(30)	28(30)	5(5)	3(3)	8(9)	
Non-turbulent		1(1)	1(1)	10(13)	28(36)	24(31)	4(5)	4(5)	6(8)	

of the cases with turbulence occurred in this range. Wind speeds in excess of 30 m s^{-1} at the 300-mb level were associated with 41 percent of the cases with turbulence as compared to only 13 percent without turbulence. Similar results were observed at the 200-mb level where 52 percent of the cases without turbulence were associated with wind speeds less than 19 m s^{-1} as compared to only 24 percent with turbulence. Forty-two percent of the cases with turbulence were associated with wind speeds of 30 m s^{-1} and greater as compared to only 14 percent of the non-turbulent cases. At the 100-mb level, 30 percent of the non-turbulent cases were associated with wind speeds less than 9 m s^{-1} as compared to 16 percent of the turbulent cases. Fifty percent of the cases with turbulence occurred when the wind speed was greater than 15 m s^{-1} as compared to 35 percent of the cases without turbulence.

There appears to be little doubt that the zonal wind component and the scalar wind speed are associated with turbulent and non-turbulent areas. When the magnitude of either of these becomes great, turbulence is more likely, and when the scalar wind speed, in particular, is below 20 m s^{-1} the flight is more likely to be smooth at the levels examined.

Table 5. Empirical frequency distributions of the scalar wind speed at 300, 200, and 100 mb associated with turbulent and non-turbulent areas.

(a) 300 mb

Areas	$V_{300} \text{ m s}^{-1}$						
	0-9	10-19	20-29	30-39	40-49	50-59	≥ 60
Turbulent	3(3)	27(29)	27(29)	18(19)	10(11)	7(7)	2(2)
Non-turbulent	14(18)	31(40)	23(29)	6(8)	4(5)	0(0)	0(0)

(b) 200 mb

Areas	$V_{200} \text{ m s}^{-1}$					
	0-9	10-19	20-29	30-39	40-49	≥ 50
Turbulent	3(3)	20(21)	32(34)	28(30)	9(10)	2(2)
Non-turbulent	9(12)	31(40)	27(35)	9(12)	1(1)	1(1)

(c) 100 mb

Areas	$V_{100} \text{ m s}^{-1}$								
	0-3.1	3.1-6.0	6.1-9.0	9.1-12.0	12.1-15.0	15.1-18.0	18.1-21.0	21.1-24.0	≥ 24.0
Turbulent	0(0)	4(4)	11(12)	15(16)	17(18)	18(19)	14(15)	10(11)	5(5)
Non-turbulent	0(0)	13(17)	10(13)	12(15)	16(21)	11(14)	10(13)	2(3)	4(5)

2. Derived Parameters

a. Relative vorticity. Frequency distributions of relative vorticity at the 300-, 200-, and 100-mb levels are shown in Table 6. There are no clear distinctions between turbulent and non-turbulent areas at 200 mb, although a large percentage (78%) of the non-turbulent areas at 300 mb had values of relative vorticity between -5 and $5 \times 10^{-5} \text{ s}^{-1}$ compared with 61 percent of the turbulent cases in this range. Nineteen percent of the turbulent and 9 percent of the non-turbulent cases were associated with values $< -5 \times 10^{-5} \text{ s}^{-1}$. The distributions at 100 mb show 52 percent of the non-turbulent areas to be associated with values of relative vorticity below $-5 \times 10^{-6} \text{ s}^{-1}$ (anticyclonic vorticity) as compared to 35 percent of the areas with turbulence in this range. When the relative vorticity was cyclonic (positive), 42 percent of the turbulent areas were associated with values $> 10^{-5} \text{ s}^{-1}$ as compared to 24 percent of the non-turbulent areas. Thus, relative vorticity at 100 and 300 mb is associated with turbulent and non-turbulent areas and may be useful as a predictor, but at 200 mb the association is poor or non-existent.

b. Absolute vorticity. Frequency distributions of absolute vorticity at the 300-, 200-, and 100-mb levels are shown in Table 7. This variable does not distinguish clearly between the turbulent and non-turbulent areas at 300 and 200 mb, but does at 100 mb. Sixty-nine percent of the non-turbulent areas were associated with values of the absolute vorticity $\leq 10^{-4} \text{ s}^{-1}$, while 41 percent of the turbulent areas were associated with these values. A comparison of Tables 6 and 7 shows that absolute vorticity at 100 mb is a better indicator of turbulence than relative vorticity.

Table 6. Empirical frequency distributions of relative vorticity at 300, 200, and 100 mb associated with turbulent and non-turbulent areas.

(a) 300 mb

Areas	$\zeta_{300} \times 10^{-5} \text{ s}^{-1}$						
	≤ -10.1	-10.0 to -5.1	-5.0 to -0.0	0.0 to 5.0	5.1 to 10.0	10.1 to 15.0	≥ 15.1
Turbulent	1(1)	17(18)	37(39)	21(22)	7(7)	4(4)	7(7)
Non-turbulent	0(0)	7(9)	36(46)	25(32)	5(6)	3(4)	2(3)

(b) 200 mb

Areas	$\zeta_{200} \times 10^{-5} \text{ s}^{-1}$					
	≤ -10.0	-10.0 to -5.1	-5.0 to -0.0	0.0 to 5.0	5.1 to 10.0	≥ 10.0
Turbulent	2(2)	13(14)	36(38)	25(27)	12(13)	6(6)
Non-turbulent	1(1)	12(15)	29(37)	23(29)	7(9)	6(8)

(c) 100 mb

Areas	$\zeta_{100} \times 10^{-6} \text{ s}^{-1}$					
	≤ -5.1	-5.0 to -0.0	0.0 to 5.0	5.1 to 10.0	10.1 to 15.0	≥ 15.1
Turbulent	21(22)	12(13)	13(14)	9(10)	11(12)	28(30)
Non-turbulent	24(31)	16(21)	9(12)	10(13)	4(5)	15(19)

Table 7. Empirical frequency distributions of absolute vorticity at 300, 200, and 100 mb associated with turbulent and non-turbulent areas.

(a) 300 mb

Areas	$\eta_{300} \times 10^{-5} \text{ s}^{-1}$					
	≤ 0.0	0.0 to 3.0	3.1 to 6.0	6.1 to 9.0	9.1 to 12.0	≥ 12.1
Turbulent	2(2)	9(10)	13(14)	28(30)	12(13)	30(32)
Non-turbulent	0(0)	4(5)	14(18)	23(29)	15(19)	22(28)

(b) 200 mb

Areas	$\eta_{200} \times 10^{-5} \text{ s}^{-1}$					
	≤ 0.0	0.0 to 5.0	5.1 to 10.0	10.1 to 15.0	15.1 to 20.0	≥ 20.0
Turbulent	3(4)	14(15)	33(35)	26(28)	10(11)	8(9)
Non-turbulent	1(1)	13(17)	29(37)	23(29)	7(9)	5(6)

(c) 100 mb

Areas	$\eta_{100} \times 10^{-5} \text{ s}^{-1}$					
	≤ 6.1	6.0 to 8.0	8.1 to 10.0	10.1 to 12.0	12.1 to 14.0	≥ 14.0
Turbulent	1(1)	12(13)	24(26)	36(38)	21(22)	0(0)
Non-turbulent	0(0)	10(13)	36(46)	25(32)	7(9)	0(0)

c. Advection of temperature. Frequency distributions of the advection of temperature at the 300-, 200-, and 100-mb levels are shown in Table 8. This table shows that the advection of temperature is not strongly related to the turbulent or non-turbulent areas at the 200-mb level, and at the 300- and 100-mb levels only for strong cold advection. At 300 mb, 15 percent of the turbulent and 4 percent of the non-turbulent cases were associated with values $< -10^{-4} \text{ }^\circ\text{C s}^{-1}$, and at 100 mb, 24 percent of the turbulent and 13 percent of the non-turbulent cases were associated with values $< -4 \times 10^{-5} \text{ }^\circ\text{C s}^{-1}$.

Table 8. Empirical frequency distributions of the advection of temperature at 300, 200, and 100 mb associated with turbulent and non-turbulent areas.

(a) 300 mb							
Areas	$(-\vec{V} \cdot \vec{\nabla}T)_{300} \times 10^{-5} \text{ }^\circ\text{C s}^{-1}$						
	≤ -20.1	-20.0 to -10.1	-10.0 to -0.0	0.0 to 10.0	10.1 to 20.0	20.1 to 30.0	≥ 30.1
Turbulent	6(6)	8(9)	24(26)	46(49)	8(9)	1(1)	1(1)
Non-turbulent	1(1)	2(3)	33(42)	34(44)	5(6)	2(3)	1(1)

(b) 200 mb							
Areas	$(-\vec{V} \cdot \vec{\nabla}T)_{200} \times 10^{-5} \text{ }^\circ\text{C s}^{-1}$						
	≤ -30.1	-30.0 to -20.1	-20.0 to -10.1	-10.0 to 0.0	0.1 to 10.0	10.1 to 20.0	≥ 20.1
Turbulent	3(3)	4(4)	16(17)	24(26)	29(31)	12(13)	6(7)
Non-turbulent	1(1)	4(5)	4(5)	22(28)	31(40)	10(13)	6(8)

(c) 100 mb						
Areas	$(-\vec{V} \cdot \vec{\nabla}T)_{100} \times 10^{-5} \text{ }^\circ\text{C s}^{-1}$					
	≤ -8.1	-8.0 to -4.1	-4.0 to -0.0	0.0 to 4.0	4.1 to 8.0	≥ 8.1
Turbulent	5(5)	18(19)	34(36)	26(28)	7(7)	4(4)
Non-turbulent	3(4)	7(9)	32(41)	25(32)	7(9)	4(5)

d. Advection of relative vorticity. Frequency distributions of the advection of relative vorticity at the 300-, 200-, and 100-mb levels are shown in Table 9. The distributions do not show a clear relationship between this variable and areas with or without turbulence at the 200-mb level, although there is a tendency for strong negative advection to be associated with turbulence. At 300 mb, 18 percent of the cases with turbulence were associated with values $< -3 \times 10^{-9} \text{ s}^{-2}$, while there was only 6 percent of the non-turbulent cases observed in this range. At the 100-mb level, there is a tendency for positive advection to be associated with turbulent areas. Seventeen percent of the turbulent cases were associated with values of the advection of relative vorticity $> 4 \times 10^{-9} \text{ s}^{-2}$ as compared to only five percent of the non-turbulent cases in this range. Hence, the advection of relative vorticity at any of the levels considered does not clearly distinguish between turbulent and non-turbulent areas.

Table 9. Empirical frequency distributions of the advection of relative vorticity at 300, 200, and 100 mb associated with turbulent and non-turbulent areas.

		(a) 300 mb								
		$(-\vec{v} \cdot \vec{\nabla} \zeta)_{300} \times 10^{-9} \text{ s}^{-2}$								
Areas		≤ -9.1	-9.0 to -6.1	-6.0 to -3.1	-3.0 to -0.0	0.0-3.0	3.1-6.0	6.1-9.0	9.1-12.0	≥ 12.1
Turbulent		3(3)	5(5)	9(10)	40(43)	27(29)	6(6)	1(1)	2(2)	1(1)
Non-turbulent		0(0)	1(1)	4(5)	40(51)	28(36)	4(5)	0(0)	0(0)	1(1)

		(b) 200 mb								
		$(-\vec{v} \cdot \vec{\nabla} \zeta)_{200} \times 10^{-9} \text{ s}^{-2}$								
Areas		≤ -12.1	-12.0 to -9.1	-9.0 to -6.1	-6.0 to -3.1	-3.0 to -0.0	0.0-3.0	3.1-6.0	6.1-9.0	≥ 9.1
Turbulent		0(0)	4(4)	6(6)	6(6)	38(40)	28(30)	7(7)	4(4)	1(1)
Non-turbulent		0(0)	0(0)	4(5)	4(5)	31(40)	29(37)	7(9)	3(4)	0(0)

		(c) 100 mb								
		$(-\vec{v} \cdot \vec{\nabla} \zeta)_{100} \times 10^{-10} \text{ s}^{-2}$								
Areas		≤ -16.0	-16.0 to -12.1	-12.0 to -8.1	-8.0 to -4.1	-4.0 to -0.0	0.0-4.0	4.1-8.0	8.1-12.0	≥ 12.1
Turbulent		0(0)	0(0)	7(7)	14(15)	31(33)	26(28)	8(9)	7(7)	1(1)
Non-turbulent		0(0)	2(3)	1(1)	7(9)	42(54)	22(28)	4(5)	0(0)	0(0)

e. Horizontal wind shear. Frequency distributions of horizontal wind shear at the 300-, 200-, and 100-mb levels are shown in Table 10. These distributions do not show a strong relationship between horizontal wind shear and turbulence, although at 300 mb 18 percent of the turbulent as compared with 9 percent of the non-turbulent areas occurred when the magnitude of the shear equalled or exceeded $45 \times 10^{-6} \text{ s}^{-1}$. At 100 mb, 29 percent of the turbulent and 16 percent of the non-turbulent areas were associated with values $\geq 16 \times 10^{-6} \text{ s}^{-1}$ (cyclonic shear).

f. Vertical wind shear. Frequency distributions of vertical wind shear computed from 200- and 100-mb data are shown in Table 11. The percentages for turbulent and non-turbulent cases for values less than $3.0 \times 10^{-3} \text{ s}^{-1}$ are 38 and 56, respectively. Twenty-nine percent of the turbulent areas were associated with vertical vector wind shears that exceeded $5 \times 10^{-3} \text{ s}^{-1}$ as compared to only 13 percent for the non-turbulent areas.

g. Lapse rate of temperature. Frequency distributions for the lapse rate of temperature between the 200- and 100-mb levels are presented in Table 12. These distributions do not show any strong differences between turbulent and non-turbulent conditions.

h. CAT Index. Frequency distributions of the Colson-Panofsky CAT Index are shown in Table 13. There are no significant differences between the distributions for turbulent and non-turbulent areas. Based on this data sample, this index does not distinguish well between turbulent and non-turbulent areas.

Table 10. Empirical frequency distributions of horizontal wind shear at 300, 200, and 100 mb associated with turbulent and non-turbulent areas.

		(a) 300 mb							
		$(\partial \bar{V} / \partial n)_{300} \times 10^{-6} \text{ s}^{-1}$							
Areas		≤ -45.0	-44.5 to -30.0	-29.9 to -15.0	-14.9 to 0.0	0.1-15.0	15.1-30.0	30.1-45.0	≥ 45.1
Turbulent		8(9)	9(10)	21(22)	21(22)	17(18)	3(3)	7(7)	8(9)
Non-turbulent		2(3)	6(8)	17(22)	21(27)	17(22)	9(12)	1(1)	5(6)

		(b) 200 mb							
		$(\partial \bar{V} / \partial n)_{200} \times 10^{-6} \text{ s}^{-1}$							
Areas		≤ -45.0	-44.9 to -30.0	-29.9 to -15.0	-14.9 to 0.0	0.1-15.0	15.1-30.0	30.1-45.0	≥ 45.1
Turbulent		3(3)	9(10)	16(17)	18(19)	22(23)	14(15)	8(9)	4(4)
Non-turbulent		5(6)	4(5)	14(18)	15(19)	14(18)	15(19)	6(8)	5(6)

		(c) 100 mb								
		$(\partial \bar{V} / \partial n)_{100} \times 10^{-6} \text{ s}^{-1}$								
Areas		≤ -12	-11 to -7	-6 to -1	0-5	6-10	11-15	16-20	21-25	≥ 26
Turbulent		6(6)	5(5)	12(13)	14(15)	18(19)	11(12)	16(17)	7(7)	5(5)
Non-turbulent		4(5)	6(8)	10(13)	19(24)	14(18)	13(17)	7(9)	3(4)	2(3)

Table 11. Empirical frequency distributions of vertical vector wind shear between 200 and 100 mb associated with turbulent and non-turbulent areas.

		$(\partial \bar{V} / \partial z)_{200-100} \times 10^{-4} \text{ s}^{-1}$						
Areas		0-9.9	10.0-19.9	20.0-29.9	30.0-39.9	40.0-49.9	50.0-59.9	≥ 60.0
Turbulent		5(5)	23(24)	8(9)	21(22)	10(11)	9(10)	18(19)
Non-turbulent		8(10)	21(27)	15(19)	15(19)	9(12)	3(4)	7(9)

Table 12. Empirical frequency distributions of the lapse rate of temperature between 200 and 100 mb associated with turbulent and non-turbulent areas.

		$(\partial T / \partial z)_{200-100} \times 10^{-4} \text{ } ^\circ\text{C m}^{-1}$					
Areas		≤ -20.1	-20.0 to -10.1	-10.0 to -0.0	0.0 to 10.0	10.1 to 20.0	≥ 20.1
Turbulent		20(21)	20(21)	21(22)	28(30)	3(3)	2(2)
Non-turbulent		22(28)	18(23)	17(22)	15(19)	6(8)	0(0)

Table 13. Empirical frequency distributions of the CAT Index associated with turbulent and non-turbulent areas.

Areas	CAT Index ($\times 10^3$)						
	≤ -20.1	-20.0 to -18.1	-18.0 to -16.1	-16.0 to -14.1	-14.0 to -12.1	-12.0 to -10.1	≥ -10.0
Turbulent	0(0)	11(12)	23(24)	27(29)	18(19)	12(13)	3(3)
Non-turbulent	1(1)	5(6)	20(26)	19(24)	16(21)	12(15)	5(6)

i. Richardson number. Frequency distributions of the Richardson number are shown in Table 14. This parameter was computed from the wind shear and temperature lapse rate computed from the 200- and 100-mb data. The Richardson number distinguishes turbulent and non-turbulent areas only when the Richardson number is small or large. When its value is below 20, more cases with turbulence were observed than without (32 and 21 percent, respectively). When its value exceeded 40, more areas without turbulence were observed than with turbulence (62 and 44 percent, respectively). In the range between 20 and 40, turbulent and non-turbulent areas occurred with about the same frequency.

Table 14. Empirical frequency distributions of the Richardson number associated with turbulent and non-turbulent areas.

Areas	Ri						
	0.0- 10.0	10.1- 20.0	20.1- 30.0	30.1- 40.0	40.1- 60.0	60.1- 80.0	80.1- 100.0
Turbulent	15(16)	15(16)	16(17)	7(7)	3(9)	7(7)	26(28)
Non-turbulent	7(9)	9(12)	9(12)	5(6)	10(13)	10(13)	28(36)

3. Time Rate-of-Change of Parameters

The time rate-of-change of parameters was computed from rawinsonde data measured before and after each flight of the XB-70. The rawinsonde times were 1200 GMT on the day of each flight, and 0000 GMT the following day. Most of the flights occurred between 1600 and 2100 GMT.

a. Height of constant-pressure surfaces. Frequency distributions of the time rate-of-change of height of the 300- and 200-mb surfaces are shown in Table 15. The height of the 100-mb surface is not included in the table since it was not included in the computations. The frequency distributions do not show any preferred values of changes in height at the 300-mb level associated with turbulent or non-turbulent areas. At 200 mb, 18 percent of the turbulent areas were associated with values $< -5 \times 10^{-4} \text{ m s}^{-1}$ as compared with 7 percent of the non-turbulent areas in this range.

Table 15. Empirical frequency distributions of the time rate-of-change of height of the 300- and 200-mb surfaces associated with turbulent and non-turbulent areas.

		(a) 300 mb								
		$(\partial H/\partial t)_{300} \times 10^{-4} \text{ m s}^{-1}$								
Areas		-21.0 to -17.0	-16.0 to -12.0	-11.0 to - 7.0	-6.0 to -1.0	0- 5.0	6.0 10.0	11.0- 15.0	16.0- 20.0	≥ 21.0
Turbulent		4(4)	2(2)	7(7)	12(13)	22(23)	13(14)	13(14)	7(7)	14(15)
Non-turbulent		2(3)	0(0)	6(8)	10(13)	17(22)	15(19)	15(19)	4(5)	9(12)

		(b) 200 mb								
		$(\partial H/\partial t)_{200} \times 10^{-4} \text{ m s}^{-1}$								
Areas		≤ 15.1	-15.1 to -10.1	-10.0 to - 5.1	-5.0 to -0.1	0.0-5.0	5.1- 10.0	10.1- 15.0	15.1- 20.0	≥ 20.1
Turbulent		4(4)	1(1)	12(13)	5(5)	16(17)	17(18)	15(16)	11(12)	13(14)
Non-turbulent		0(0)	1(1)	5(6)	7(9)	13(17)	18(23)	12(15)	15(19)	7(9)

b. Temperature change on constant-pressure surfaces. Frequency distributions for the time rate-of-change of temperature at the 300-, 200-, and 100-mb surfaces are shown in Table 16. At 300 mb, 39 percent of the cases without turbulence were associated with an increase in temperature with time between values of 20 and $40 \times 10^{-6} \text{ }^\circ\text{C s}^{-1}$ as compared with only 16 percent of the areas with turbulence in this range. Twenty-nine percent of the areas with turbulence were associated with a decrease of temperature with time as compared with 14 percent of the areas without turbulence. When the temperature increase was between zero and 20 or greater than $40 \times 10^{-6} \text{ }^\circ\text{C s}^{-1}$, there were no systematic differences in the frequencies associated with turbulent or non-turbulent areas. At the 200-mb level, there were no significant differences in the frequency distributions between the turbulent and non-turbulent areas. At 100 mb, 26 percent of turbulent and 14 percent of non-turbulent cases were associated with values $\geq 4.0 \times 10^{-5} \text{ }^\circ\text{C s}^{-1}$. Thus the local rate-of-change of temperature does not distinguish well between turbulent and non-turbulent areas at the 200- and 100-mb levels, but does within certain intervals at the 300-mb level.

c. Zonal wind component on constant-pressure surfaces. Frequency distributions for the zonal (west to east) wind component are shown in Table 17 for the 300-, 200-, and 100-mb levels. The zonal wind component is positive for a west wind and negative for an east wind. When the local rate-of-change is negative, the component is becoming more westerly or less easterly, (change vector points toward the west) and when it is positive the component is becoming more easterly or less westerly (change vector points toward the east). Although some slight differences are indicated at 100 mb, the distributions in Table 17 do not indicate any significant differences between turbulent and non-turbulent areas. Therefore, this parameter does not appear to distinguish between areas with or without turbulence.

Table 16. Empirical frequency distributions of the time rate-of-change of temperature at 300, 200, and 100 mb associated with turbulent and non-turbulent areas.

(a) 300 mb

Areas	$(\partial T/\partial t)_{300} \times 10^{-6} \text{ } ^\circ\text{C s}^{-1}$						
	≤ -10.1	-10.0 to -0.0	0.0 to 10.0	10.1 to 20.0	20.1 to 30.0	30.1 to 40.0	≥ 40.1
Turbulent	21(22)	7(7)	14(15)	18(19)	8(9)	7(7)	19(20)
Non-turbulent	8(10)	3(4)	14(18)	8(10)	13(17)	17(22)	15(19)

(b) 200 mb

Areas	$(\partial T/\partial t)_{200} \times 10^{-6} \text{ } ^\circ\text{C s}^{-1}$					
	≤ -10.1	-100.0 to -50.0	-50.0 to -00.0	00.0 to 50.0	50.1 to 100.0	≥ 100.1
Turbulent	6(6)	8(9)	26(28)	38(40)	9(10)	7(7)
Non-turbulent	4(5)	4(5)	25(32)	29(37)	11(14)	5(6)

(c) 100 mb

Areas	$(\partial T/\partial t)_{100} \times 10^{-6} \text{ } ^\circ\text{C s}^{-1}$						
	≤ -10.1	-10.0 to -0.0	0.0 to 10.0	10.1 to 20.0	20.1 to 30.0	30.1 to 40.0	≥ 40.1
Turbulent	23(24)	10(11)	5(5)	13(14)	12(13)	7(7)	24(26)
Non-turbulent	20(26)	7(9)	6(8)	13(17)	14(18)	7(9)	11(14)

Table 17. Empirical frequency distributions of the time rate-of-change of the longitudinal wind component at 300, 200, and 100 mb associated with turbulent and non-turbulent areas.

(a) 300 mb

Areas	$(\partial u/\partial t)_{300} \times 10^{-5} \text{ m s}^{-2}$									
	≤ -41	-40 to -31	-30 to -21	-20 to -11	-10 to -1	0-9	10-19	20-29	30-39	≥ 40
Turbulent	5(5)	2(2)	7(7)	12(13)	18(19)	24(26)	14(15)	7(7)	1(1)	4(4)
Non-turbulent	1(1)	3(4)	5(6)	7(9)	17(22)	21(27)	14(18)	7(9)	2(3)	1(1)

(b) 200 mb

Areas	$(\partial u/\partial t)_{200} \times 10^{-5} \text{ m s}^{-2}$								
	≤ -17	-16 to -12	-11 to -7	-6 to -1	0-5	6-10	11-15	16-20	≥ 21
Turbulent	13(14)	7(7)	11(12)	11(12)	11(12)	15(16)	9(10)	4(4)	13(14)
Non-turbulent	13(17)	6(8)	6(8)	8(10)	11(14)	4(5)	9(12)	8(10)	13(17)

(c) 100 mb

Areas	$(\partial u/\partial t)_{100} \times 10^{-5} \text{ m s}^{-2}$								
	≤ -17	-16 to -12	-11 to -7	-6 to -1	0-5	6-10	11-15	16-20	≥ 21
Turbulent	20(21)	2(2)	10(11)	23(24)	17(18)	9(10)	6(6)	1(1)	6(6)
Non-turbulent	8(10)	3(4)	7(9)	15(19)	23(29)	14(18)	1(1)	3(4)	4(5)

d. Meridional wind component on constant-pressure surfaces.

Frequency distributions of the meridional (south to north) wind component for the 300-, 200-, and 100-mb levels are shown in Table 18; negative values indicate the meridional wind component as becoming more northerly (increasing toward the north) while positive values indicate it is becoming more southerly (increasing toward the south). The frequency distributions in Table 18 do not show any systematic differences between turbulent and non-turbulent areas.

Table 18. Empirical frequency distributions of the time rate-of-change of the meridional wind component at 300, 200, and 100 mb associated with turbulent and non-turbulent areas.

(a) 300 mb

Areas	$(\partial v/\partial t)_{300} \times 10^{-5} \text{ m s}^{-2}$									
	≤ -41	-40 to -31	-30 to -21	-20 to -11	-10 to -1	0-9	10-19	20-29	30-39	≥ 40
Turbulent	6(6)	5(5)	5(5)	12(13)	17(18)	16(17)	16(17)	5(5)	4(4)	8(9)
Non-turbulent	6(8)	1(1)	7(9)	11(14)	7(9)	19(24)	15(19)	4(5)	4(5)	4(5)

(b) 200 mb

Areas	$(\partial v/\partial t)_{200} \times 10^{-5} \text{ m s}^{-2}$									
	≤ -17	-16 to -12	-11 to -7	-6 to -1	0-5	6-10	11-15	16-20	≥ 21	
Turbulent	19(20)	6(6)	12(13)	5(5)	16(17)	8(9)	8(9)	4(4)	16(17)	
Non-turbulent	18(23)	7(9)	5(6)	9(12)	12(15)	4(5)	5(6)	4(5)	14(18)	

(c) 100 mb

Areas	$(\partial v/\partial t)_{100} \times 10^{-5} \text{ m s}^{-2}$									
	≤ -17	-16 to -12	-11 to -7	-6 to -1	0-5	6-10	11-15	16-20	≥ 21	
Turbulent	6(6)	6(6)	6(6)	16(17)	22(23)	11(12)	5(5)	4(4)	18(19)	
Non-turbulent	2(3)	3(4)	8(10)	22(28)	13(17)	12(15)	8(10)	2(3)	8(10)	

e. Scalar wind speeds on constant-pressure surfaces. Frequency distributions of the time rate-of-change of scalar wind speed at the 300-, 200-, and 100-mb levels are shown in Table 19. These distributions are similar to those shown in Tables 17 and 18 inasmuch as they do not distinguish between turbulent and non-turbulent areas except possibly for large negative values at 300 and 200 mb. It is clear from Tables 17, 18, and 19 that the local rate-of-change of component or scalar wind speeds does not distinguish between turbulent and non-turbulent areas.

f. Relative vorticity on constant-pressure surfaces. Frequency distributions for the time rate-of-change of relative vorticity at the 300-, 200-, and 100-mb levels are shown in Table 20. The distributions associated with turbulent and non-turbulent areas at the 300- and 200-mb levels do not show any significant differences. At the 100-mb level, 33 percent of the areas with turbulence were associated with rates-of-change less than $-20 \times 10^{-11} \text{ s}^{-2}$ as compared with 20 percent of the non-turbulent areas in this range. There were 53 percent of the non-turbulent areas associated with changes in the relative vorticity between -10 to $+30 \times 10^{-11} \text{ s}^{-2}$ as compared with only 32 percent of the areas with turbulence associated

Table 19. Empirical frequency distributions of the time rate-of-change of the scalar wind speed at 300, 200, and 100 mb associated with turbulent and non-turbulent areas.

(a) 300 mb

Areas	$(\partial V/\partial t)_{300} \times 10^{-5} \text{ m s}^{-2}$								
	≤ -17	-16 to -12	-11 to -7	-6 to -1	0-5	6-10	11-15	16-20	≥ 21
Turbulent	24(26)	6(6)	8(9)	9(10)	9(10)	13(14)	5(5)	8(9)	12(13)
Non-turbulent	9(12)	5(6)	10(13)	9(12)	10(13)	10(13)	7(9)	7(9)	11(14)

(b) 200 mb

Areas	$(\partial V/\partial t)_{200} \times 10^{-5} \text{ m s}^{-2}$								
	≤ -17	-16 to -12	-11 to -7	-6 to -1	0-5	6-10	11-15	16-20	≥ 21
Turbulent	16(17)	8(9)	7(7)	9(10)	18(19)	11(12)	10(11)	4(4)	11(12)
Non-turbulent	8(10)	8(10)	3(4)	9(12)	16(21)	10(13)	6(8)	5(6)	13(17)

(c) 100 mb

Areas	$(\partial V/\partial t)_{100} \times 10^{-5} \text{ m s}^{-2}$									
	≤ -12.1	-12.0 to -9.1	-9.0 to -6.1	-6.0 to -3.1	-3.0 to -0.0	0.0-3.0	3.1-6.0	6.1-9.0	9.1-12.0	≥ 12.0
Turbulent	4(5)	5(5)	7(7)	14(15)	23(24)	11(12)	12(13)	8(9)	3(3)	7(7)
Non-turbulent	3(4)	5(6)	5(6)	5(6)	18(23)	16(21)	12(15)	7(9)	4(5)	3(4)

Table 20. Empirical frequency distributions of the time rate-of-change of relative vorticity at 300, 200, and 100 mb associated with turbulent and non-turbulent areas.

(a) 300 mb

Areas	$(\partial \zeta/\partial t)_{300} \times 10^{-10} \text{ s}^{-2}$					
	≤ -30.1	-20.1 to -30.0	-10.1 to -20.0	-0.0 to -10.0	0.0 to 10.0	≥ 10.1
Turbulent	1(1)	10(11)	5(5)	30(32)	35(37)	13(14)
Non-turbulent	3(4)	2(3)	10(13)	28(36)	27(35)	8(10)

(b) 200 mb

Areas	$(\partial \zeta/\partial t)_{200} \times 10^{-10} \text{ s}^{-2}$					
	≤ -30.1	-20.1 to -30.0	-10.1 to -20.0	-0.0 to -10.0	0.0 to 10.0	≥ 10.1
Turbulent	0(0)	5(5)	12(13)	35(37)	29(31)	13(14)
Non-turbulent	2(3)	4(5)	14(18)	25(32)	25(32)	8(10)

(c) 100 mb

Areas	$(\partial \zeta/\partial t)_{100} \times 10^{-11} \text{ s}^{-2}$							
	≤ -30.1	-20.1 to -30.0	-10.1 to -20.0	-0.0 to -10.0	0.0-10.0	10.1-20.0	20.1-30.0	≥ 30.1
Turbulent	21(22)	10(11)	13(14)	12(13)	8(9)	8(9)	1(1)	21(22)
Non-turbulent	9(12)	6(8)	11(14)	18(23)	10(13)	7(9)	6(8)	11(14)

with this range. The frequency distributions associated with turbulent and non-turbulent areas are quite different at 100 mb, but do not show any significant difference at the 300- and 200-mb levels.

g. Vorticity due to the coriolis force on constant-pressure surfaces. Frequency distributions of the rate-of-change of vorticity due to the coriolis force at the 300-, 200-, and 100-mb levels are shown in Table 21. These distributions do not distinguish between turbulent and non-turbulent areas at 300 or 100 mb, but at 200 mb there were 43 percent and 29 percent of turbulent and non-turbulent cases, respectively, for values $< -1.6 \times 10^{-10} \text{ s}^{-2}$, and 20 percent and 35 percent for turbulent and non-turbulent cases, respectively, for values between zero and $-1.6 \times 10^{-10} \text{ s}^{-2}$.

Table 21. Empirical frequency distributions of the time rate-of-change of vorticity due to the coriolis force at 300, 200, and 100 mb associated with turbulent and non-turbulent areas.

(a) 300 mb

Areas	$Bv_{300} \times 10^{-11} \text{ s}^{-2}$								
	≤ -17	-16 to -12	-11 to -7	-6 to -1	0-5	6- 10	11- 15	16- 20	≥ 21
Turbulent	32(34)	6(6)	8(9)	9(10)	11(12)	7(7)	6(6)	7(7)	8(9)
Non-turbulent	19(24)	8(6)	12(15)	9(12)	7(9)	9(12)	4(5)	2(3)	10(13)

(b) 200 mb

Areas	$Bv_{200} \times 10^{-11} \text{ s}^{-2}$								
	≤ -17	-16 to -12	-11 to -7	-6 to -1	0-5	6- 10	11- 15	16- 20	≥ 21
Turbulent	40(43)	6(6)	8(9)	4(4)	11(12)	5(5)	8(9)	4(4)	8(9)
Non-turbulent	23(29)	8(10)	9(12)	10(13)	4(5)	4(5)	5(5)	8(10)	7(9)

(c) 100 mb

Areas	$Bv_{100} \times 10^{-11} \text{ s}^{-2}$								
	≤ -17	-16 to -12	-11 to -7	-6 to -1	0-5	6- 10	11- 15	16- 20	≥ 21
Turbulent	13(14)	8(9)	12(13)	15(16)	18(19)	15(16)	7(7)	1(1)	5(5)
Non-turbulent	8(10)	8(10)	8(10)	15(19)	17(22)	10(13)	4(5)	5(6)	3(4)

h. Advection of temperature on constant-pressure surfaces. Frequency distributions for the time rate-of-change of the advection of temperature at the 300-, 200-, and 100-mb levels are shown in Table 22. Negative values indicate a decrease in the rate of advection (less warm or more cold) while positive values indicate an increase in the rate of advection (less cold or more warm). At 300 mb, there are more turbulent than non-turbulent areas associated with magnitudes exceeding $\pm 20 \times 10^{-10} \text{ }^\circ\text{C s}^{-2}$. In addition, 56 percent of the cases without turbulence occurred between $\pm 10^{-9} \text{ }^\circ\text{C s}^{-2}$ as compared to 40 percent of the areas with turbulence in this range. Thus at 300 mb the distributions show definite differences between turbulent and non-turbulent areas. These differences are not reflected as clearly in the distributions at 200 and 100 mb although there

Table 22. Empirical frequency distributions of the time rate-of-change of the advection of temperature at 300, 200, and 100 mb associated with turbulent and non-turbulent areas.

		(a) 300 mb					
		$\partial(-\vec{V} \cdot \vec{\nabla}T)/\partial t_{300} \times 10^{-10} \text{ } ^\circ\text{C s}^{-2}$					
Areas		≤ -20.1	-20.0 to -10.1	-10.0 to - 0.0	0.0 to 10.0	10.1 to 20.0	≥ 20.1
Turbulent		22(23)	10(11)	19(20)	19(20)	9(10)	15(16)
Non-turbulent		11(14)	10(13)	22(28)	23(29)	6(8)	6(8)

		(b) 200 mb							
		$\partial(-\vec{V} \cdot \vec{\nabla}T)/\partial t_{200} \times 10^{-10} \text{ } ^\circ\text{C s}^{-2}$							
Areas		≤ -30.1	-30.0 to -20.1	-20.0 to -10.1	-10.0 to - 0.0	0.0 to 10.0	10.1 to 20.0	20.1 to 30.0	≥ 30.1
Turbulent		18(19)	12(13)	7(7)	13(14)	10(11)	15(16)	4(4)	15(16)
Non-turbulent		13(17)	6(8)	6(8)	15(19)	13(17)	11(14)	8(10)	6(8)

		(c) 100 mb					
		$\partial(-\vec{V} \cdot \vec{\nabla}T)/\partial t_{100} \times 10^{-10} \text{ } ^\circ\text{C s}^{-2}$					
Areas		≤ -10.1	-10.0 to - 5.1	-5.0 to -0.0	0.0 to 5.0	5.1 to 10.0	≥ 10.1
Turbulent		18(19)	15(16)	17(18)	14(15)	10(11)	20(21)
Non-turbulent		10(13)	11(14)	24(31)	12(15)	10(13)	11(14)

is, in general, a tendency for a greater percentage of the turbulence cases to be associated with large values in the rate-of-change of advection, both positive and negative, than for the areas without turbulence. In summary, at the 200- and 100-mb levels the time rate-of-change of the advection of temperature does not appear to distinguish between turbulent and non-turbulent areas except for large magnitudes.

i. Advection of relative vorticity on constant-pressure surfaces. Frequency distributions of the time rate-of-change of the advection of relative vorticity at the 300-, 200-, and 100-mb levels are shown in Table 23. None of these distributions shows any features which distinguish between turbulent and non-turbulent areas.

j. Horizontal wind shear on constant-pressure surfaces. Frequency distributions of the time rate-of-change of horizontal wind shear at the 300-, 200-, and 100-mb levels are shown in Table 24. Fifty-four percent of the cases without turbulence were associated with values between zero and $-9.9 \times 10^{-10} \text{ s}^{-2}$, while 41 percent of the cases with turbulence occurred in this range. There were no apparent differences at 200 mb. At the 100-mb level, 32 percent of the turbulent areas were associated with changes in the horizontal wind shear $\leq 20 \times 10^{-10} \text{ s}^{-2}$ as compared with only 13 percent of the areas without turbulence. For values between -10 and $1 \times 10^{-11} \text{ s}^{-2}$, 26 percent of the cases without turbulence fell in this range compared with only 6 percent of the areas with turbulence. In Table 24, negative values indicate that the horizontal wind shear is becoming more anti-cyclonic with time while positive values indicate that it is becoming more cyclonic with time. Thus the occurrence of turbulence,

Table 23. Empirical frequency distributions of the time rate-of-change of the advection of relative vorticity at 300, 200, and 100 mb associated with turbulent and non-turbulent areas.

(a) 300 mb

Areas	$\partial(-\bar{v} \cdot \bar{v}_c) / \partial t_{300} \times 10^{-14} \text{ s}^{-3}$									
	≤ -20.1	-20.0 to -15.1	-15.0 to -10.1	-10.0 to -5.1	-5.0 to -0.0	0.0-5.0	5.1-10.0	10.0-15.0	15.1-20.0	≥ 21.0
Turbulent	1(1)	2(2)	4(4)	8(9)	30(32)	26(28)	9(10)	8(9)	3(3)	3(3)
Non-turbulent	3(4)	0(0)	6(8)	4(5)	25(32)	24(31)	7(9)	6(8)	1(1)	2(3)

(b) 200 mb

Areas	$\partial(-\bar{v} \cdot \bar{v}_c) / \partial t_{200} \times 10^{-14} \text{ s}^{-3}$							
	≤ -20.1	-21.0 to -14.1	-14.0 to -7.1	-7.0 to -0.0	0.0-7.0	7.1-14.0	14.1-21.0	≥ 21.1
Turbulent	6(6)	2(2)	9(10)	35(37)	18(19)	14(15)	3(3)	7(7)
Non-turbulent	4(5)	5(6)	11(14)	21(27)	21(27)	10(13)	3(4)	3(4)

(c) 100 mb

Areas	$\partial(-\bar{v} \cdot \bar{v}_c) / \partial t_{100} \times 10^{-15} \text{ s}^{-3}$							
	≤ -15.1	-15.0 to -10.1	-10.0 to -5.1	-5.0 to -0.0	0.0-5.0	5.1-10.0	10.1-15.0	≥ 15.1
Turbulent	9(10)	4(4)	12(13)	19(20)	20(21)	15(16)	7(7)	8(9)
Non-turbulent	6(8)	3(4)	7(9)	17(22)	23(29)	6(8)	9(12)	7(9)

Table 24. Empirical frequency distributions of the time rate-of-change of the horizontal wind shear at 300, 200, and 100 mb associated with turbulent and non-turbulent areas.

(a) 300 mb

Areas	$(\partial \bar{v}_n / \partial t)_{300} \times 10^{-10} \text{ s}^{-2}$							
	≤ -15.0	-14.9 to -10.0	-9.9 to -5.0	-4.9 to 0.0	0.1-5.0	5.1-10.0	10.1-15.0	≥ 15.1
Turbulent	4(4)	4(4)	11(12)	27(29)	30(32)	11(12)	5(5)	2(2)
Non-turbulent	2(3)	2(3)	14(18)	28(36)	20(26)	11(14)	1(1)	0(0)

(b) 200 mb

Areas	$(\partial \bar{v}_n / \partial t)_{200} \times 10^{-10} \text{ s}^{-2}$							
	≤ -15.0	-14.9 to -10.0	-9.9 to -5.0	-4.9 to 0.0	0.1-5.0	5.1-10.0	10.1-15.0	≥ 15.1
Turbulent	3(3)	4(4)	17(18)	23(24)	36(38)	7(7)	4(4)	0(0)
Non-turbulent	4(5)	5(6)	15(19)	22(28)	22(28)	9(12)	1(1)	0(0)

(c) 100 mb

Areas	$(\partial \bar{v}_n / \partial t)_{100} \times 10^{-11} \text{ s}^{-2}$									
	≤ -41	-40 to -31	-30 to -21	-20 to -11	-10 to -1	0-9	10-19	20-29	30-39	≥ 40
Turbulent	8(9)	8(9)	13(14)	16(17)	6(6)	16(17)	9(10)	8(9)	3(3)	7(7)
Non-turbulent	3(4)	3(4)	4(5)	14(18)	20(26)	14(18)	11(14)	4(5)	3(4)	2(3)

particularly at the 100-mb level, is associated with conditions which lead to larger anti-cyclonic horizontal wind shear, while areas without turbulence occur more frequently for small negative changes in the horizontal wind shear which do not exceed 10^{-11} s^{-2} .

k. Vertical wind shear. Frequency distributions of the rate-of-change of vertical wind shear between the 200- and 100-mb levels are shown in Table 25. Sixteen percent of the turbulent areas are associated with a rate-of-change which exceeds 10^{-7} s^{-2} as compared with only 4 percent of the cases without turbulence. Thus, when the vertical wind shear is increasing rapidly with time, turbulence may be expected to occur more frequently than smooth conditions.

Table 25. Empirical frequency distributions of the time rate-of-change of vertical wind shear between 200 and 100 mb associated with turbulent and non-turbulent areas.

Areas	$(\partial \bar{v}_H / \partial t)_{200-100} \times 10^{-8} \text{ s}^{-2}$									
	≤ -20.0	-20.0 to -15.1	-15.0 to -10.1	-10.0 to -5.1	-5.0 to 0.0	0.0-5.0	5.1-10.0	10.1-15.0	15.1-20.0	≥ 21.0
Turbulent	1(1)	0(0)	3(3)	5(5)	31(33)	26(28)	13(14)	8(9)	5(5)	2(2)
Non-turbulent	0(0)	1(1)	0(0)	4(5)	33(42)	27(35)	10(13)	2(3)	0(0)	1(1)

l. Lapse rate of temperature. Frequency distributions for the time rate-of-change of the lapse rate of temperature between 200 and 100 mb are shown in Table 26. Forty-nine percent of the non-turbulent cases were associated with negative values between 0 and $-2 \times 10^{-8} \text{ }^\circ\text{C m}^{-1} \text{ s}^{-1}$ as compared with 29 percent of the turbulent cases. The trend is reversed for large positive values ($\geq 2.0 \times 10^{-8} \text{ }^\circ\text{C m}^{-1} \text{ s}^{-1}$) where 15 percent and 6 percent, respectively, are associated with turbulent and non-turbulent conditions. Thus, the occurrence of turbulence is associated with conditions leading to a more stable lapse rate of temperature, and less turbulence to conditions leading to a larger lapse rate of temperature. The lapse rate was defined previously as dT/dz which differs in sign from the usual definition. The time rate-of-change of the lapse rate of temperature is related to the occurrence of turbulence and should be a useful parameter for the determination of areas where turbulence would be expected.

Table 26. Empirical frequency distributions of the time rate-of-change of the lapse rate of temperature between 200 and 100 mb associated with turbulent and non-turbulent areas.

Areas	$(\partial \gamma / \partial t)_{200-100} \times 10^{-9} \text{ }^\circ\text{C m}^{-1} \text{ s}^{-1}$					
	≤ -20.1	-20.0 to -10.1	-10.0 to -0.0	0.0 to 10.0	10.1 to 20.0	≥ 20.0
Turbulent	7(7)	9(10)	18(19)	37(39)	9(10)	14(15)
Non-turbulent	3(4)	13(17)	25(32)	24(31)	8(10)	5(6)

m. CAT Index. Frequency distributions of the rate-of-change of the CAT Index are shown in Table 27. This index was computed from vertical wind shear and the lapse rate of temperature each computed from the 200- and 100-mb data. Twenty-five percent of the turbulent areas are associated with values $\leq -20 \times 10^{-3} \text{ s}^{-1}$, while 14 percent of the areas without turbulence are associated with these values of the CAT Index. Fifty-two percent of the non-turbulent areas are associated with positive values between zero and $4.0 \times 10^{-2} \text{ s}^{-1}$ as compared with 31 percent of the turbulent areas in this range.

Table 27. Empirical frequency distributions of the time rate-of-change of the CAT Index associated with turbulent and non-turbulent areas.

Areas	$\partial(\text{CAT Index})/\partial t \times 10^{-3} \text{ s}^{-1}$							
	≤ -60.1	-60.0 to -40.1	-40.0 to -20.1	-20.0 to -0.0	0.0 to 20.0	20.1 to 40.0	40.1 to 60.0	≥ 60.1
Turbulent	3(3)	5(5)	16(17)	28(30)	25(27)	4(4)	7(7)	6(6)
Non-turbulent	1(1)	1(1)	9(12)	23(29)	24(31)	16(21)	2(3)	2(3)

n. Richardson number. Frequency distributions of the time rate-of-change of the Richardson number are shown in Table 28. The Richardson number was computed from vertical wind shear and lapse rate of temperature taken from the 200- and 100-mb levels. The distributions do not show any significant differences and hence local changes in the Richardson number on this thickness scale cannot be used to distinguish between turbulent and non-turbulent areas.

Table 28. Empirical frequency distributions of the time rate-of-change of the Richardson number associated with turbulent and non-turbulent areas.

Areas	$\partial Ri/\partial t \times 10^{-2} \text{ s}^{-1}$							
	≤ -0.8	-0.8 to -0.6	-0.5 to -0.3	-0.2 to -0.0	0.0- 0.2	0.3- 0.5	0.6- 0.8	≥ 0.8
Turbulent	5(5)	4(4)	9(10)	35(37)	29(31)	5(5)	0(0)	7(7)
Non-turbulent	8(10)	1(1)	2(3)	27(35)	28(36)	5(6)	0(0)	7(9)

APPENDIX C

Computer Program for Combined Forecasting Procedure

The computer program presented here provides combined results from each forecasting technique presented in the text. An example of the product (output) of the program also is given in the text.

A block (flow) diagram is given in Fig. B-1 followed by the FORTRAN program. After reading the text it should not be difficult to follow the program logic.

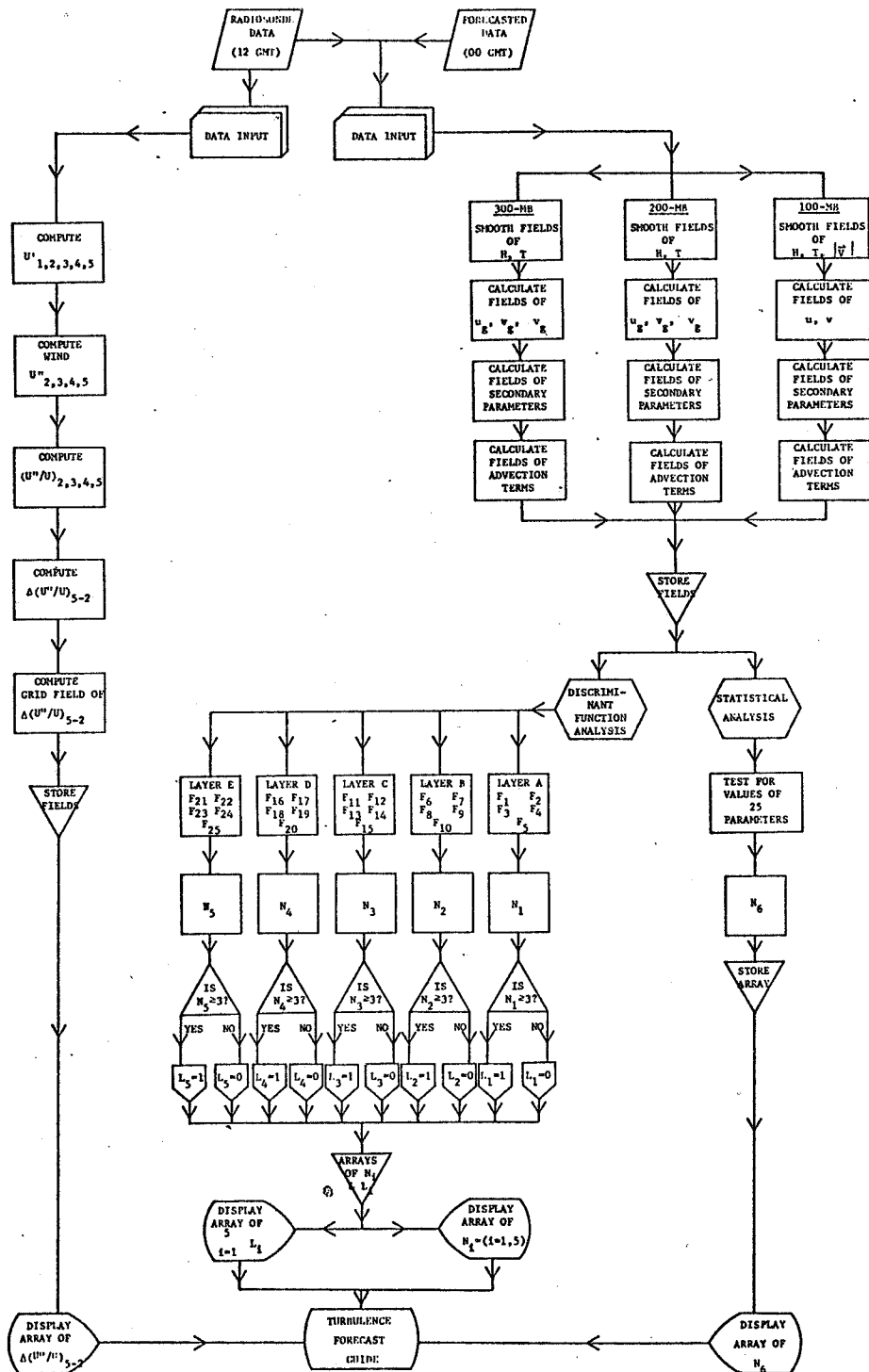


Fig. B-1. Block diagram of computer program.

COMPUTER PROGRAM

FORTRAN IV G LEVEL 21 MAIN DATE = 75205 14/57/30

```

0001                      DIMENSION DLAT(26),DLON(26),R(18,18),ND(26),DCURV(18,18)
0002                      DIMENSION Z(26,6),U(26,6),UP(26,6),UDP(26,6),TWO(26,6),DIFF(26)
0003                      DIMENSION AP(18,18,36),ZETA(18,18,6),ETA(18,18),DZETA1(18,18)
0004                      DIMENSION F(18,18),RD(26,22),KS(22),VN(4),AT(6),AZ(6),BV(6)
0005                      DIMENSION R1(18,18),R2(18,18),R3(18,18)
0006                      DIMENSION NPE(18,18),NTL(18,18),NF123(18,18),F45(18,18)
0007                      COMMON DATA(26),FI(26),FJ(26),A(18,18),TC(18,18),TW(18,18),NCNT
0008                      COMMON /GRIDIJ/ ISTART,JSTART,IEND,JEND
0009                      ICAY = 13
0010                      I4 = 2
0011                      I5 = 12
0012                      J4 = 3
0013                      J5 = 13
0014                      I6 = I4 - 1
0015                      I7 = I5 + 1
0016                      J6 = J4 - 1
0017                      J7 = J5 + 1
0018                      INRPTS = 26
0019                      NRPT = 25
0020                      ISTART = 1
0021                      IEND = 18
0022                      JSTART = 1
0023                      JEND = 18
0024                      I1 = ISTART + 1
0025                      I2 = IEND - 1
0026                      J1 = JSTART + 1
0027                      J2 = JEND - 1
0028                      DTINF=4.32E 04
0029                      CD=0.017453
0030                      DX=1.58PE 05
0031                      CP= 1./(2.*DX)
0032                      READ(5,727) Q,R,S,T
0033                      727 FORMAT (4A4)
C
C                      READ STATION #, LATITUDE, AND LONGITUDE
0034                      DO 9 I = 1,INRPTS
0035                      READ(5,100) NG(I),DLAT(I),DLON(I)
0036                      100 FORMAT(13,2F6,2)
0037                      CALL DEGRID(DLAT(I),DLON(I),FI(I),FJ(I))
0038                      9 CONTINUE
0039                      READ(5,6) (KS(K),K=1,22)
0040                      6 FORMAT(22I3)
0041                      DO 747 NDAY = 1,ICAY
C
C                      *****
C                      CURVATURE TERM METHOD -- POSSIEL
C                      *****
C

```

```

0042      DO 4000 J=1,18
0043      DO 4000 I=1,18
0044      A(I,J) = 0.
0045      B(I,J) = 0.
0046      4000 CONTINUE
      C
      C      READ HEIGHT - WIND VALUES
0047      DO 110 I=1,INRPTS
0048      READ (5,707) C,O,E,H,G
0049      707 FORMAT (5A4)
0050      READ (5,717) (Z(I,J), J=1,6),(U(I,J), J=1,6)
0051      717 FORMAT (6F7.1,6F6.1)
0052      110 CONTINUE
0053      DO 199 I = 1,INRPTS
      C
      C      CALCULATES WIND SHEAR
0054      DO 200 J=1,5
0055      IF(U(I,J).EQ.0.0) GO TO 198
0056      IF(U(I,J+1).EQ.0.0) GO TO 198
0057      200 UP(I,J) = (U(I,J+1)-U(I,J))/(Z(I,J+1)-Z(I,J))
      C
      C      CALCULATES CURVATURE
0058      DO 201 J=1,4
0059      201 UDP(I,J+1) = (UP(I,J+1)-UP(I,J))/((Z(I,J+2)+Z(I,J+1))/2.-(Z(I,J+1)
      * +Z(I,J))/2.)
      C
      C      CALCULATES CURVATURE TERM
0060      DO 202 J=1,4
0061      202 TWO(I,J+1) = UDP(I,J+1)/U(I,J+1)
      C
      C      CALCULATES VERT. GRAD. OF CURVATURE TERM = NABLA (U**/U)
0062      DIFF(I) = TWO(I,5)-TWO(I,2)
0063      GO TO 197
0064      198 DIFF(I) = 0.0
0065      197 CONTINUE
0066      199 CONTINUE
      C
      C      NABLA (U**/U) ON GRID
0067      DO 175 I = 1,INRPTS
0068      175 DATA(I) = DIFF(I)
0069      CALL ANAL (INRPTS,3.0,6.1)
0070      CALL SMOOTH (A,B,0.01)
      C
      C      DCURV = NABLA (U**/U)
0071      DO 203 I = 1,18
0072      DO 204 J = 1,18
0073      B(I,J) = B(I,J)*1.0E08
0074      IF (B(I,J).GT.99.0) B(I,J) = 99.

```



```

0075      IF (B(I,J).LT.-99.0) B(I,J) = -99.
0076      204 DCURV(I,J) = B(I,J)
0077      203 CONTINUE
      C
      C      CALCULATE PARAMETER FIELDS
      C
      C      READ 00 GMT FORECASTED VALUES OF THE VARIABLES FOR EACH INPUT STATION
0078      DO 10 I=1,NRPT
0079      READ(5,1102) (RD(I,K),K=1,8)
0080      1102 FORMAT(F7.0,F6.1,7X,F7.0,F6.1,7X,F7.0,F6.1,F4.0,F3.0)
      C      CALCULATE THE 00 GMT 100-MB WIND COMPONENTS FOR EACH INPUT STATION
0081      CALL UVCMP(RD(I,7),RD(I,8),RD(I,9),RD(I,10))
0082      10 CONTINUE
0083      DO 11 I=1,NRPT
      C      READ 12 GMT VALUES OF THE VARIABLES FOR EACH INPUT STATION
0084      READ(5,1102) (RD(I,K),K=11,18)
      C      CALCULATE THE 12 GMT 100-MB WIND COMPONENTS FOR EACH INPUT STATION
0085      CALL UVCMP(RD(I,17),RD(I,18),RD(I,19),RD(I,20))
0086      11 CONTINUE
      C      CALCULATE HEIGHT FIELDS
0087      DO 4002 J=1,18
0088      DO 4002 I=1,18
0089      A(I,J)=0.
0090      B(I,J)=0.
0091      4002 CONTINUE
0092      DO 39 K= 1,13,2
0093      IF(K.EQ.7) GO TO 39
0094      DO 15 I=1,NRPT
0095      15 DATA(I)=RD(I,K)
0096      CALL ANAL(NRPT,4.0,4.1)
0097      CALL SMOOTH(A,B,0.2)
0098      DO 40 I=16,17
0099      DO 40 J=16,17
0100      AD(I,J,K5(K)) = B(I,J)
0101      40 CONTINUE
0102      39 CONTINUE
      C      CALCULATE TEMPERATURE FIELDS
0103      DO 4001 J=1,18
0104      DO 4001 I=1,18
0105      A(I,J) =0.
0106      B(I,J)=0.
0107      4001 CONTINUE
0108      DO 38 K=2,14,2
0109      IF(K.EQ. 8) GO TO 38
0110      DO 16 I=1,NRPT
0111      16 DATA(I)=RD(I,K)
0112      CALL ANAL(NRPT,4.0,4.1)
0113      CALL SMOOTH(A,B,0.2)

```

```

0114      DO 41 I=16,I7
0115      DO 41 J=J6,J7
0116      AP(I,J,K5(K)) = B(I,J)
0117      41 CONTINUE
0118      38 CONTINUE
      C    CALCULATE THE VALUE OF THE CORIOLIS PARAMETER FOR EACH GRID POINT
0119      DO 70 I=I4,I5
0120      DO 70 J=J4,J5
0121      BI = I
0122      BJ = J
0123      CALL GRIDEG(BI,BJ,FLAT,FLON,F,I,J)
0124      70 CONTINUE
      C    CALCULATE GEOSTROPHIC WIND FIELDS AT 300 AND 200 MB
0125      CALL GEOCMP(AP,F)
      C    CALCULATE 100 MB WIND FIELDS
0126      M=1
0127      DO 42 KK=8,I3
0128      K=KK
0129      IF(KK.GE.11) K=KK+7
0130      M=KK+9
0131      DO 17 I=1,NRPT
0132      17 DATA(I)=RD(I,K)
0133      CALL ANAL(NRPT,4,0,4,1)
0134      CALL SMOOTH(A,B,0,2)
0135      DO 44 I=16,I7
0136      DO 44 J=J6,J7
0137      44 AP(I,J,K5(M)) = B(I,J)
0138      42 CONTINUE
      C    CALCULATE THE VORTICITY FOR EACH GRID POINT
0139      CALL VORT(AP,ZETA,ETA,DZETA1,F)
      C    CALCULATE THE VALUES OF THE REMAINING VARIABLES FOR EACH GRID POINT
0140      DO 23 I=I4,I5
0141      DO 23 J=J4,J5
      C    CALCULATES HORIZONTAL WIND SHEAR AT 100 MB AT 00 Z AND AT 300 AND
      C    100 MB AT 12 Z AND STORES THEM IN VN ARRAY
0142      DO 1 M=1,4
0143      MM=2*M+28
0144      NN=4*M+8
0145      IF(M.EQ.3) GO TO 1
0146      DYX=AP(I+1,J,MM) - AP(I-1,J,MM)
0147      DYY=AP(I,J-1,MM) - AP(I,J+1,MM)
0148      1 VN(M) = CP*(AP(I,J,MM)*DYX - AP(I,J,MM-1)*DYY)/AP(I,J,NN)
0149      DVN1 = (VN(1) - VN(4))/DTIME
      C    CALCULATES ADVECTION OF TEMPERATURE AND RELATIVE VORTICITY FOR ALL
      C    LEVELS AND BOTH TIME PERIODS AND STORES THEM IN AT AND AZ ARRAYS
0150      DO 2 M=1,6
0151      MM=2*M+24
0152      MMM=4*(M-1)+2

```

```

0153      TX=AP(I+1,J,MMM) - AP(I-1,J,MMM)
0154      TY=AP(I,J-1,MMM) - AP(I,J+1,MMM)
0155      AT(M)=CP*(-AP(I,J,MM-1)*TX - AP(I,J,MM)*TY)
0156      ZFTAX = ZETA(I+1,J,M) - ZETA(I-1,J,M)
0157      ZFTAY = ZETA(I,J-1,M) - ZETA(I,J+1,M)
0159      2 AZ(M) = CP*(-AP(I,J,MM-1)*ZETAX - AP(I,J,MM)*ZETAY)
0159      CAT2 = (AT(2)-AT(5))/DTIME
0160      CAT3 = (AT(1)-AT(4))/DTIME
0161      DAZ1 = (AZ(3)-AZ(6))/DTIME
0162      DAZ3 = (AZ(1)-AZ(4))/DTIME
C      CALCULATES BETA,V AT 200 MB AT 00 Z AND ALL LEVELS AT 12 Z AND
C      STORES THEM IN BV ARRAY
0163      DO 3 M=2,6
0164      MM=2*M+24
0165      IF(M.EQ.3) GO TO 3
0166      BV(M) = (1.78E-11)*AP(I,J,MM)
0167      3 CONTINUE
0168      FBV2 = (BV(2)-BV(5))/DTIME
C      CALCULATES TEMPERATURE LAPSE RATE, VERTICAL SHEAR, RICHARDSON NUMBER
C      AND CAT INDEX FOR 200-100 MB LAYER FOR BOTH TIME PERIODS
0169      CH121 = AP(I,J,5) - AP(I,J,9)
0170      CH12 = AP(I,J,17) - AP(I,J,21)
0171      VXVY1 = (AP(I,J,29)-AP(I,J,27))*2 + (AP(I,J,30)-AP(I,J,28))*2
0172      VXVY = (AP(I,J,35)-AP(I,J,33))*2 + (AP(I,J,36)-AP(I,J,34))*2
0173      DTDZ1 = (AP(I,J,6)-AP(I,J,10))/DH121
0174      DTDZ = (AP(I,J,18)-AP(I,J,22))/DH12
0175      DCTDZ = (CTCZ1-DTDZ)/DTIME
0176      DVDZ1 = (AP(I,J,8)-AP(I,J,12))/DH121
0177      DVDZ = (AP(I,J,20)-AP(I,J,24))/DH12
0178      DVDZ7 = (DVDZ1-DVDZ)/DTIME
0179      R1 = 20.3 * ((AP(I,J,10)+AP(I,J, 6))/2.0 + 273.0)
0180      R2 = (AP(I,J,10)-AP(I,J, 6))/R1
0181      R3 = (AP(I,J,29)-AP(I,J,27))*2 + (AP(I,J,30)-AP(I,J,28))*2
0182      R11 = 9.8 * 20.3 * (R2 + 0.00976) * R1/R3
0183      R1 = 20.3 * ((AP(I,J,22)+AP(I,J,18))/2.0 + 273.0)
0184      R2 = (AP(I,J,22)-AP(I,J,18))/R1
0185      R3 = (AP(I,J,35)-AP(I,J,33))*2 + (AP(I,J,36)-AP(I,J,34))*2
0186      R1 = 9.8 * 20.3 * (R2 + 0.00976) * R1/R3
0187      C11 = VXVY1*(1.0-2.0*R11)
0188      C1 = VXVY*(1.0-2.0*R1)
0189      DC1 = (C11-C1)/DTIME
C      CALCULATES TIME CHANGES OF TEMPERATURE FOR 100 AND 300 MB LEVELS,
C      SCALAR WIND AT 200 AND 300 MB LEVELS, AND HEIGHT OF 200 MB LEVEL
0190      DT1 = (AP(I,J,10)-AP(I,J,22))/DTIME
0191      DT3 = (AP(I,J,2)-AP(I,J,14))/DTIME
0192      DV2 = (AP(I,J,8)-AP(I,J,20))/DTIME
0193      DV3 = (AP(I,J,4)-AP(I,J,16))/DTIME
0194      DH2 = (AP(I,J,5)-AP(I,J,17))/DTIME

```

```

C      CALCULATES THE VALUES OF THE DISCRIMINANT FUNCTIONS
0195      N1=0
0196      N2=0
0197      N3=0
0198      N4=0
0199      N5=0
0200      N6=0
0201      NTL(I,J) = 0

C
C      *****
C      DISCRIMINANT FUNCTION METHOD -- CLARK
C      *****
C
C      CALCULATE THE DISCRIMINANT FUNCTION VALUES FOR EACH GRID POINT
C      40,000-47,000 FT SUB-LAYER
0202      F1 = 1.430 - 2.077E-02*AP(I,J,36) + 2.305E-02*AP(I,J,22) + 1.835E
          011*DAZ3
0203      IF(F1.GT.0.) N1=N1+1
0204      F2 = 6.191 - 5.896E-04*AP(I,J,17) + 1.942E-04*AP(I,J,20)**2 - 1.55
          01E-02*AP(I,J,36)
0205      IF(F2.GT.0.) N1=N1+1
0206      F3 = -0.108 + 3.710E-03*AP(I,J,33) - 9.847E-03*AP(I,J,34) - 6.785E
          + 0A*DAT2
0207      IF(F3.GT.0.) N1=N1+1
0208      F4 = 6.969 - 5.959E-04*AP(I,J,17) + 8.573E-02*AP(I,J,35) - 1.533E
          2CR*BV(4)
0209      IF(F4.GT.0.) N1=N1+1
0210      F5 = 8.656 - 9.394E-04*AP(I,J,13) + 8.746E-03*AP(I,J,35) + 1.152E
          714*DDTDZ**2
0211      IF(F5.GT.0.) N1=N1+1
C      45,000-52,000 FT SUB-LAYER
0212      F1 = 1.656 - 3.662E-04*AP(I,J,13) + 2.902E-02*AP(I,J,24) + 1.386E
          874*ETA(I,J)
0213      IF(F1.GT.0.) N2=N2+1
0214      F2 = 7.307 - 6.413E-04*AP(I,J,17) + 1.498E-02*AP(I,J,20) - 2.941E-
          207*AP(I,J,34)
0215      IF(F2.GT.0.) N2=N2+1
0216      F3 = 8.725 - 7.153E-04*AP(I,J,17) + 2.281E 18*RV(61)**2 - 3.558E-03
          2*RI
0217      IF(F3.GT.0.) N2=N2+1
0218      F4 = 1.840 + 1.230E-02*AP(I,J,20) + 3.445E-02*AP(I,J,22) + 4.439E
          312*DAZ1
0219      IF(F4.GT.0.) N2=N2+1
0220      F5 = 2.242 + 3.373E-02*AP(I,J,22) - 2.671E-03*RI + 2.296E 13*DBV2
0221      IF(F5.GT.0.) N2=N2+1
C      50,000-57,000 FT SUB-LAYER
0222      F1 = -0.548 + 2.379E-02*AP(I,J,16) - 4.828E-03*AP(I,J,18) - 6.731E
          01*DVZ
    
```

```

0223      IF(F1.GT.0.) N3=N3+1
0224      F2 = -0.318 + 1.395E-02*AP(I,J,16) - 1.547E 08*DZETA1(I,J) + 8.229
           @E 05*DDVDZ
0225      IF(F2.GT.0.) N3=N3+1
0226      F3 = -1.461 + 9.413E-05*AP(I,J,17) + 1.470E-02*AP(I,J,20) - 3.385E
           @-02*AP(I,J,34)
0227      IF(F3.GT.0.) N3=N3+1
0228      F4 = 1.110 + 2.685E-02*AP(I,J,24) + 2.2323E-02*AP(I,J,22) + 6.758E
           @ 02*ZETA(I,J,5)
0229      IF(F4.GT.0.) N3=N3+1
0230      F5 = 1.395 + 2.498E-02*AP(I,J,24) + 2.740E-02*AP(I,J,22) + 6.029E
           *24*DAZ1**2
0231      IF(F5.GT.0.) N3=N3+1
           C      55,000-62,000 FT SUB-LAYER
0232      F1 = -0.294 + 2.173E-02*AP(I,J,24) + 4.041E 03*VN(4) + 1.198E 02*
           @ZETA(I,J,5)
0233      IF(F1.GT.0.) N4=N4+1
0234      F2 = -0.227 + 1.969E-02*AP(I,J,24) + 4.870E 02*AT(4) + 3.628E 01*0
           @TDZ
0235      IF(F2.GT.0.) N4=N4+1
0236      F3 = -0.252 + 2.053E-02*AP(I,J,24) + 4.217E 01*0TDZ + 4.660E 06*ZE
           @TA(I,J,5)**2
0237      IF(F3.GT.0.) N4=N4+1
0238      F4 = -0.316 + 3.575E-02*AP(I,J,24) - 1.563E-02*AP(I,J,35) + 1.073E
           @ 02*ZETA(I,J,5)
0239      IF(F4.GT.0.) N4=N4+1
0240      F5 = -6.297 + 2.721E 03*DT1 -3.198*DCI - 2.829E 03*AT(6)
0241      IF(F5.GT.0.) N4=N4+1
           C      60,000-67,000 FT SUR-LAYER
0242      F1 = -0.568 + 3.855E-02*AP(I,J,24) + 4.598E 03*VN(4) + 9.611E 02*Z
           @ETA(I,J,5)
0243      IF(F1.GT.0.) N5=N5+1
0244      F2 = -0.565 + 3.915E-02*AP(I,J,24) - 4.348E-03*AP(I,J,36) + 1.271E
           @ 03*ZETA(I,J,5)
0245      IF(F2.GT.0.) N5=N5+1
0246      F3 = 4.643 - 5.067E-04*AP(I,J,13) + 5.170E 03*DT1 + 5.142E 01*0TDZ
0247      IF(F3.GT.0.) N5=N5+1
0248      F4 = 6.171 - 5.206E-04*AP(I,J,17) - 5.892*DCI + 2.493E 02*AT(6)
0249      IF(F4.GT.0.) N5=N5+1
0250      F5 = 3.204 - 1.130E-02*AP(I,J,24) - 5.609E 01 *DVDZ
0251      IF(F5.GT.0.) N5=N5+1
           C
0252      COUNT THE NUMBER OF TURBULENT LAYERS ABOVE EACH GRID POINT
           IF(N1.GE.4) NTL(I,J) = NTL(I,J) + 1
0253      IF(N2.GE.4) NTL(I,J) = NTL(I,J) + 1
0254      IF(N3.GE.4) NTL(I,J) = NTL(I,J) + 1
0255      IF(N4.GE.4) NTL(I,J) = NTL(I,J) + 1
0256      IF(N5.GE.4) NTL(I,J) = NTL(I,J) + 1
           C      STORE THE NUMBER OF POSITIVE FUNCTIONAL VALUES IN EACH LAYER AT EACH POINT

```

```

0257      NF123(I,J) = N1 * 100 + N2 * 10 + N3
0258      F45(I,J) = N4 * .15/10.
      C
      C *****
      C CRITICAL VALUE METHOD -- SCOGGINS
      C *****
      C
      C COUNT THE NUMBER OF PARAMETERS WHICH HAVE CRITICAL VALUES
0259      IF(AP(I,J,31).GE.20.) N6=N6+1
0260      IF(AP(I,J,16).GE.30.) N6=N6+1
0261      IF(ZETA(I,J,4).LT.-5.0E-05) N6=N6+1
0262      IF(AT(4).LT.1.0E-04) N6=N6+1
0263      IF(AZ(4).LT.-3.0E-09) N6=N6+1
0264      IF(VN(2).GE.4.5E-05) N6=N6+1
0265      IF(DT3.LT.0.) N6=N6+1
0266      IF(DV3.LT.-1.6E-04) N6=N6+1
0267      IF(DAT3.GT.2.0E-09) N6=N6+1
0268      IF(AP(I,J,33).GE.20.) N6=N6+1
0269      IF(AP(I,J,34).LT.-10.) N6=N6+1
0270      IF(AP(I,J,20).GE.30.) N6=N6+1
0271      IF(DH2.LT.-5.0E-04) N6=N6+1
0272      IF(DV2.LT.-1.6E-04) N6=N6+1
0273      IF(BV(5).LT.-1.6E-10) N6=N6+1
0274      IF(AP(I,J,35).GT.12.) N6=N6+1
0275      IF(ETA(I,J).GT.1.2E-04) N6=N6+1
0276      IF(VN(4).GT.1.5E-05) N6=N6+1
0277      IF(DVN1.LT.-2.0E-10) N6=N6+1
0278      IF(DZETA1(I,J).GE.3.0E-10) N6=N6+1
0279      IF(HI.LE.30.) N6=N6+1
0280      IF(DVDZ1.GE.5.0E-03) N6=N6+1
0281      IF(DVDZ2.GT.1.0E-07) N6=N6+1
0282      IF(DOTDZ.GE.2.0E-08) N6=N6+1
0283      IF(DCI.GT.4.0E-02) N6=N6+1
0284      NPE(I,J) = N6
0285      23 CONTINUE
0286      CALL OUTPUT(DCURV,NTL,NPE,NF123,F45, IDAY,Q,R,D,E,H,G)
0287      747 CONTINUE
0288      WRITE (6,69)
0289      59 FORMAT('1')
0290      RETURN
0291      END

```

```

0001      SUBROUTINE SMOOTH(A,B,C)
0002      DIMENSION A(18,18),B(18,18)
0003      COMMON /GRIDIJ/ ISTART,JSTART,IEND,JEND
          C      SMOOTH INTERIOR POINTS
0004      J1 = JSTART + 1
0005      J2 = JEND - 1
0006      I1 = ISTART + 1
0007      I2 = IEND - 1
0008      C2 = C*(1.-C)/2.
0009      C3 = C*C/4.
0010      C4 = 1. - 4.*C2 - 4.*C3
0011      C4 = 1. - 4.*C2 - 4.*C3
0012      DO 1 J=J1,J2
0013      DO 1 I=I1,I2
0014      B(I,J) = C4*A(I,J)+C2*(A(I-1,J)+A(I+1,J))+A(I,J-1)+A(I,J+1)
          * +C3*(A(I-1,J-1)+A(I-1,J+1)+A(I+1,J+1)+A(I+1,J-1))
0015      1 CONTINUE
          C      SMOOTH BORDER PCINTS
0016      C1 = (1.0 - C)/2.0
0017      K = JSTART
0018      L = JEND
0019      M = ISTART
0020      N = IEND
0021      DO 2 I=I1,I2
0022      B(M,K) = A(I,K)*C + C1*(A(I-1,K) + A(I+1,K))
0023      2 B(I,L) = A(I,L)*C + C1*(A(I-1,L) + A(I+1,L))
0024      DO 3 J=J1,J2
0025      B(M,J) = A(M,J)*C + C1*(A(M,J-1) + A(M,J+1))
0026      3 B(N,J) = A(N,J)*C + C1*(A(N,J-1) + A(N,J+1))
          C      SMOOTH CORNERS
0027      B(M,K) = A(M,K)*C + C1*(A(M,K+1) + A(M+1,K))
0028      B(N,K) = A(N,K)*C + C1*(A(N-1,K) + A(N,K+1))
0029      B(M,L) = A(M,L)*C + C1*(A(M,L-1) + A(M+1,L))
0030      B(N,L) = A(N,L)*C + C1*(A(N-1,L) + A(N,L-1))
0031      RETURN
0032      END

```

```

0001      SUBROUTINE EXTRAP(A,IB,JB,IE,JE)
0002      DIMENSION A(18,18)
0003      ID=IB+1
0004      JD=JB+1
0005      IS=IE-1
0006      JS=JE-1
0007      DO 20 I=ID,IS
0008      A(I,JB) = (3.0*A(I,JD)-A(I,JD+1))/2.0
0009      20 A(I,JE) = (3.0 * A(I,JS) - A(I,JE-2))/2.0
0010      DO 30 J=JD,JS
0011      A(IB,J) = (3.0*A(ID,J)-A(ID+1,J))/2.0
0012      30 A(IE,J) = (3.0 * A(IS,J) - A(IE-2,J))/2.0
0013      A(IB,JB) = 0.5*(A(IB,JD)+A(ID,JB))
0014      A(IB,JE) = 0.5*(A(ID,JE)+A(IB,JS))
0015      A(IE,JB) = 0.5*(A(IS,JB)+A(IE,JD))
0016      A(IE,JE) = 0.5*(A(IS,JE)+A(IE,JS))
0017      RETURN
0018      END

```

```

FORTRAN IV G LEVEL 21          UVCMP          DATE = 75205          14/57/30

0001          SUBROUTINE UVCMP(DIR,SPD,VX,VY)
              C      CALCULATES U AND V COMPONENTS OF THE WIND AT EACH STATION FOR ALL
              C      LEVFLS AND BOTH TIME PERIODS AND STORES THEM INTO PD ARRAYS.
0002          DIMENSION PD(25,20)
0003          M=1
0004          IF(DIR.LT.180..AND.DIR.GE.90.) M=2
0005          IF(DIR.LT.270..AND.DIR.GE.180.) M=3
0006          IF(DIR.GE.270.) M=4
0007          GO TO (1,2,3,4),M
0008          1 DIR=DIR*(3.14/180.)
0009          VX=-SPD*SIN(DIR)
0010          VY=-SPD*CCS(DIR)
0011          RETURN
0012          2 DIR=(DIR-90.)*(3.14/180.)
0013          VX=-SPD*COS(DIR)
0014          VY=SPD*SIN(DIR)
0015          RETURN
0016          3 DIR=(DIR-180.)*(3.14/180.)
0017          VX=SPD*SIN(DIR)
0018          VY=SPD*CCS(DIR)
0019          RETURN
0020          4 DIR=(DIR-270.)*(3.14/180.)
0021          VX=SPD*COS(DIR)
0022          VY=-SPD*SIN(DIR)
0023          RETURN
0024          END

```

```

FORTRAN IV G LEVEL 21          INTRP          DATE = 75205          14/57/30

0001          SUBROUTINE INTRP(A,FI,FJ,DINT)
0002          DIMENSION A(18,18)
0003          II = FI
0004          JJ = FJ
0005          DI=FI - FLOAT(II)
0006          DJ=FJ - FLOAT(JJ)
0007          Z1=A(II,JJ)
0008          Z2=A(II+1,JJ)
0009          Z3=A(II,JJ+1)
0010          Z4=A(II+1,JJ+1)
0011          Z5=Z1 + (Z2-Z1)*DI
0012          Z6=Z3 + (Z4-Z3)*DI
0013          DINT=Z5 + (Z6-Z5)*DJ
0014          RETURN
0015          END

```

```

FORTRAN IV G LEVEL 21          DEGRID          DATE = 75205          14/57/30

0001          SUBROUTINE DEGRID(DLAT,DLON,FI,FJ)
0002          CNST = .2679492
0003          FAC2 = .3487812E02
0004          FAC1 = .2802625E02
0005          ALAT = (90. - DLAT)/57.29578
0006          R = FAC1*(TAN(ALAT/2.)/CNST)**0.716
0007          ALON = (125. - DLON)*0.715/57.29578
0008          FI = 1.0 + R*SIN(ALON)
0009          FJ = 1.0 + R*COS(ALON) - FAC2
0010          RETURN
0011          END

```



```

0001      SUBROUTINE ANAL(NRPTS,SRAD,NSCAN,IGO)
C          THIS ROUTINE ANALYZES THE REPORTED DATA AND PUTS THE ADJUSTED
C          VALUES AT GRID POINTS.
0002      DIMENSION A(18,18),TC(18,18),TW(18,18),DATA(26),
          * FI(26),FJ(26)
0003      COMMON DATA,FI,FJ,A,TC,TW,NCNT
0004      COMMON /GRIDIJ/ ISTART,JSTART,IEND,JEND
C
0005      DO 100 NSCAN=1,NCSCAN
0006      DO 15 J=JSTART,JEND
0007      DO 15 I=ISTART,IEND
0008      TC(I,J) = 0.0
0009      15 TW(I,J)=0.0
0010      NCNT = 0
0011      DO 30 K=1,NRPTS
0012      M=1
0013      IF(DATA(K).EQ.0.) M=2
0014      IF(M.EQ.2) GO TO 30
0015      I1=FI(K)
0016      J1=FJ(K)
0017      RMAX = SRAD
0018      RMSQ = RMAX**2
0019      NCNT = NCNT + 1
C          THE FOLLOWING SEQUENCE PERFORMS DOUBLE LINEAR INTERPOLATION
C          ON THE GRID POINT VALUES.
0020      GO TO (31,32),M
0021      31 CALL INTRP(A,FI(K),FJ(K),DINT)
0022      ERROR=DATA(K) -DINT
0023      32 CONTINUE
0024      I1=FI(K) - RMAX+0.5
0025      I2=FI(K) + RMAX+0.5
0026      J1=FJ(K) - RMAX+0.5
0027      J2=FJ(K) + RMAX+0.5
0028      IMIN = MAX0(ISTART,I1)
0029      IMAX = MIN0(IEND,I2)
0030      JMIN = MAX0(JSTART,J1)
0031      JMAX = MIN0(JEND,J2)
0032      DO 25 J=JMIN,JMAX
0033      DO 20 I=IMIN,IMAX
0034      R50 = (FLOAT(I)-FI(K))**2 + (FLOAT(J) - FJ(K))**2
0035      IF(R50.GE.RMSQ) GO TO 20
0036      WGT = EXP(-4.*R50/RMSQ)
0037      TW(I,J)=TW(I,J) + WGT
0038      GO TO (34,35),M
0039      34 TC(I,J)=TC(I,J) + WGT*ERROR
0040      35 CONTINUE
0041      20 CONTINUE
0042      25 CONTINUE
0043      30 CONTINUE
0044      DO 50 J=JSTART,JEND
0045      DO 50 I=ISTART,IEND
0046      IF(TW(I,J).LE.0.0) GO TO 50
0047      A(I,J)=A(I,J) + TC(I,J)/TW(I,J)
0048      50 CONTINUE
0049      100 CONTINUE
0050      RETURN
0051      END

```

FORTRAN IV G LEVEL 21

GEOCMP

DATE = 75205

14/57/30

```

0001      SUBROUTINE GEOCMP(AP,F)
0002      DIMENSION AP(18,18,36),F(18,18)
0003      DIMENSION B1(18,18),B2(18,18),B3(18,18),B(18,18)
0004      I4 = 2
0005      I5 = 12
0006      J4 = 3
0007      J5 = 13
0008      I6 = I4 - 1
0009      I7 = I5 + 1
0010      J6 = J4 - 1
0011      J7 = J5 + 1
0012      C1 = -9.80616/(2.0*1.588E 05)
0013      K1 = 23
0014      DO 1 KK=1,17,4
0015      K1=K1+2
0016      IF(KK.EQ.9) GO TO 1
0017      K3 = KK+3
0018      K2 = K1+1
0019      DO 2 I=I4,I5
0020      DO 2 J=J4,J5
0021      C = C1/F(I,J)
0022      B1(I,J) = -C*(AP(I,J+1,KK)-AP(I,J-1,KK))
0023      B2(I,J) = -C*(AP(I+1,J,KK)-AP(I-1,J,KK))
0024      B3(I,J) = SORT(B1(I,J)**2 + B2(I,J)**2)
0025      2 CONTINUE
0026      CALL EXTRAP(B1,I6,J6,I7,J7)
0027      CALL EXTRAP(B2,I6,J6,I7,J7)
0028      CALL EXTRAP(B3,I6,J6,I7,J7)
0029      DO 3 I=I6,I7
0030      DO 3 J=J6,J7
0031      AP(I,J,K1) = B1(I,J)
0032      AP(I,J,K2) = B2(I,J)
0033      AP(I,J,K3) = B3(I,J)
0034      3 CONTINUE
0035      1 CONTINUE
0036      RETURN
0037      END

```

FORTRAN IV G LEVEL 21

GRIDEG

DATE = 75205

14/57/30

```

0001      SUBROUTINE GRIDFG(FI,FJ,DLAT,DLON,F,I,J)
0002      DIMENSION F(18,18)
0003      CMEGA = 7.292 F-05
0004      FAC1 = .2802625F02
0005      FAC2 = .3487812E02
0006      CNST = .2679492
0007      X = FI - 1.0
0008      Y = FJ + FAC2 - 1.0
0009      R = SORT(X**2 + Y**2)
0010      DLAT = 2.0*ATAN(CNST*((R/FAC1)**1.3906))
0011      DLAT = 90. - DLAT*57.29578
0012      SINFAC = SIN(DLAT/57.29578)
0013      DLON = ATAN(X/Y)
0014      DLON = 125. - DLON*57.29578/0.715
0015      F(I,J) = 2.0 * CMEGA * SINFAC
0016      RETURN
0017      END

```

```

0001      SUBROUTINE VORT(AP,ZETA,ETA,DZETA1,F)
          C      CALCULATES RELATIVE VORTICITY FOR EACH GRID POINT FOR EACH LEVEL
          C      FOR BOTH TIME PERIODS AND ABSOLUTE VORTICITY FOR 100-MB LEVEL AND
          C      12 Z TIME PERIOD AND STORES THEM IN ZETA AND ETA ARRAYS
          DIMENSION AP(18,18,36),ZETA(18,18,6),ETA(18,18),DZETA1(18,18)
0002      DIMENSION B1(18,18),F(18,18)
0003      I4 = 2
0004      I5 = 12
0005      J4 = 3
0006      J5 = 13
0007      I6 = I4 - 1
0008      I7 = I5 + 1
0009      J6 = J4 - 1
0010      J7 = J5 + 1
0011      DX=1.588E 05
0012      CP = 1./(2.*DX)
0013      DO 1 M=1,6
0014      DO 1 I=I4,I5
0015      DO 2 J=J4,J5
0016      MM=2*M + 24
0017      DYX = AP(I+1,J,MM)-AP(I-1,J,MM)
0018      DXY = AP(I,J-1,MM-1) - AP(I,J+1,MM-1)
0019      B1(I,J) = CP*(DYX-DXY)
0020      2 CONTINUE
0021      CALL EXTRAP(A1,I6,J6,I7,J7)
0022      DO 3 I=I6,I7
0023      DO 3 J=J6,J7
0024      ZETA(I,J,M) = B1(I,J)
0025      3 CONTINUE
0026      DO 4 I=I4,I5
0027      DO 4 J=J4,J5
0028      ETA(I,J) = ZETA(I,J,6) + F(I,J)
0029      CZETA1(I,J)=ZETA(I,J,6)-ZETA(I,J,3)
0030      4 CONTINUE
0031      RETURN
0032      END
0033

```

```

0001      SUBROUTINE OUTPUT(DCURV,NTL,NPE,NF123,F45,IDAY,O,P,D,E,H,G)
0002      DIMENSION DCURV(18,18),NTL(18,18),NPE(18,18),NF123(18,18),F45(18,1
          8)
0003      I4 = 2
0004      I5 = 12
0005      J4 = 3
0006      J5 = 13
0007      WRITE(6,1) O,P,D,E,H,G
0008      1 FORMAT('1',T47,'TAMU CAG CAT FORECASTING PROCEDURE',2(/),T46,2A
          *4,3X,'DATE - TIME ',4A4,/)
0009      WRITE(6,2)
0010      2 FORMAT('0',4(/))
0011      DO 10 J= J4,J5
0012      WRITE (6,3) (DCURV(I,J),I=I4,I5),(NTL(K,J),NPE(K,J),K = I4,I5)
0013      3 FORMAT ('0',T37,11F5.0,/,T38,11(1X,11,12,1X))
0014      10 CONTINUE
0015      WRITE (6,9)
0016      9 FORMAT (' ',2(/),T60,10('**'),/,T60,'* LEGEND *',/,T60,10('**'),2(/)
          @ ,T60,'X#1 ',/,T60,'X#2 X#3',2(/),T48,'X#1 : VERT. GRAD. OF CUR
          VATURE TERM',/,T48,'X#2 : DISCRIMINANT FUNCTION ANALYSIS',/,T48,
          @ 'X#3 : STATISTICAL ANALYSIS METHOD')
0017      WRITE(6,1) O,P,D,E,H,G
0018      WRITE(6,7)
0019      7 FORMAT('0',T49,'THE NUMBER OF FUNCTIONS EXCEEDING',/,T49,'THE VALU
          DE OF ZERO FOR EACH LAYER',4(/))
0020      DO 5 J=J4,J5
0021      5 WRITE(6,6) (NF123(I,J),I=I4,I5),(F45(I,J),I=I4,I5)
0022      6 FORMAT('0',T37,11(2X,13)/T37,11(2X,F3.1))
0023      WRITE(6,8)
0024      8 FORMAT(' ',2(/),T60,10('**'),/,T60,'* LEGEND *',/,T60,10('**'),2(/),
          @T60,'L#1 L#2 L#3',/,T60,'L#4 ' L#5',2(/),T54,
          @ 'L#1 : 40,000-47,000 FT',/,T54,'L#2 : 45,000-52,000 FT',/,T54
          @,'L#3 : 50,000-57,000 FT',/,T54,'L#4 : 55,000-62,000 FT',/,T54,'L#
          @5 : 60,000-67,000 FT')
0025      RETURN
0026      END

```

**U.S. AIR FORCE
VAFB TECHNICAL LIBRARY**